PRODUCING MEDICAL RADIOISOTOPES WITH CANDU NUCLEAR REACTORS

By ZACHARY SUTHERLAND, HBSc

A Thesis Submitted to the School of Graduate Studies in Partial Fulfillment of the Requirements for the Degree of Master of Applied Science

McMaster University Master OF APPLIED SCIENCE (2017) Hamilton, Ontario (Engineering Physics)

TITLE: Producing Medical Radioisotopes with CANDU Nuclear Reactors AUTHOR: Zachary Sutherland, HBSc (Brock University) SUPERVISOR: Professor D. R. Novog NUMBER OF PAGES: x, 83

Abstract

In the field of nuclear medicine, radioisotopes are used for applications such as diagnostic imaging, treatment, and equipment sterilization. The most commonly used radioisotope in medicine is technetium-99m (Tc-99m). It is used in 80% of all nuclear medicine procedures. Its parent isotope is molybdenum-99 (Mo-99). NRU, which is now closed, formerly produced 40% of the worlds demand for Mo-99. The production capacity of this reactor has been supplemented by a network of cyclotrons and a modified research reactor. This study aims to provide an alternative means of production for Mo-99, as well as other radioisotopes by modifying the center pin of a standard 37-element bundle of a CANDU reactor.

The neutron transport code DRAGON, and the neutron diffusion code DONJON were used to model a CANDU-9 reactor. The lowest, median, and highest power channels were chosen as candidates for the modified bundles. It was found that the reactor parameters were altered by a negligible amount when any one channel was used to house the modified bundles. Significant quantities of the radioisotope lutetium-177 as well as the generating isotopes of the alpha-emitting radioisotopes lead-212/bismuth-212, and radium-223 were produced. However, only minute amounts of molybdenum-99, and the generating isotope of bismuth-213 were produced.

Acknowledgments

I am grateful for the opportunity, expertise, and guidance that Dr. Novog has provided throughout my time at McMaster. I would like to especially thank him for all the time he has taken to help me understand fundamental reactor physics concepts during one-on-one conversations. Without his guidance, this work would not have been possible.

I would also like to thank my beautiful fiancée who has provided me with endless amounts of love, support, and most of all patience throughout my graduate studies.

Contents

List of Figures

List of Tables

Nomenclature

Abbreviations

2-D	two dimensional
3-D	three dimensional
ACR	Advanced CANDU Reactor
AECL	Atomic Energy of Canada Limited
CANDU	Canadian Deuterium Uranium
CP	Collision Probability
ENDF	Evaluated Nuclear Data Files
ENDL	Evaluated Nuclear Data Library
EOP	End of Processing
HEU	High Enriched Uranium
IAEA	International Atomic Energy Agency
JEFF	Joint Evaluated Fission and Fusion File
LANL	Los Alamos National Laboratory
LEU	Low Enriched Uranium
LWR	Light-Water Reactor
LZC	Liquid Zone Controller
MURR	University of Missouri Research Reactor
NEA	Nuclear Energy Agency
NRU	National Research Universal
PHWR	Pressurized Heavy-Water Reactor
PWR	Pressurized Water Reactor
SDS	Shutdown System
SI	International System of Units
TAT	Targeted Alpha Therapy

TENDL	TALYS Evaluated Neutron Data Library
TRT	Targeted Radionuclide Therapy
UOIT	University of Ontario Institute of Technology
WIMS-D	Winfrith Improved Multigroup Scheme-D
WLUP	WIMS library update project

Units

b	(barn) 10^{-24}cm^2
Bq	becquerel
Ci	curie
eV	electron-Volt
GBq	gigabecquerel
MeV	megaelectron-Volt
mk	milli-k
MW	megawatt
MWd/Mg(U)	megawatt days per megagram of uranium
MWe	megawatt electric
n/kb	neutrons per kilo-barn
TBq	terabecquerel
W	watt
w/o	weight percent

Variables

ν	number of neutrons emitted per fission
ϕ	neutron flux
ρ	reactivity
Σ	macroscopic cross-section, (cm^{-1})

σ	microscopic cross-section, (cm^{-2})
E	neutron energy
k_{∞}	infinite lattice neutron multiplication constant
k_{eff}	effective lattice neutron multiplication constant
T	temperature

1 Introduction

In the field of nuclear medicine, radioisotopes are used in a wide array of applications such as research, diagnostic imaging, treatment, and equipment sterilization [1], [2]. Each year, there are over 40 million medical procedures performed using radioisotopes, with an estimated growth rate of 5% per year [2]. Although radioisotopes such as uranium-235, and radium-226 occur naturally, most radioisotopes used in medicine are produced artificially in nuclear reactors or cyclotrons [2]. The most commonly used radioisotope in medicine is technetium-99m (Tc-99m). It is used in 80% of all nuclear medicine procedures, and has a world market share of approximately $500 million USD per year [2]. Because the half-lives of Tc-99m and it's parent, molybdenum-99 (Mo-99), are so short, they cannot be stockpiled. They therefore must be produced and processed daily to meet global demand [3]. Their half-lives are 6 hours, and 66 hours respectively [3].

Until recently (2014), the National Research Universal (NRU) reactor in Chalk River, Ontario produced 40% of the global demand for Mo-99 [4]. The reactor is now on standby, only to produce Mo-99 in the case of a supply shortage [2]. It is scheduled to shut down completely sometime this year (2018) [2]. Most of the supply formerly produced at NRU is set to be produced at the University of Missouri Research Reactor (MURR), with the addition of a network of 11 cyclotrons across Canada [5]. The cyclotrons are only able to provide a local source of Tc-99m, and require Mo-100 as a target which can only be purchased from Russia [5], [2]. The cost of cyclotron produced Tc-99m is estimated to be three to ten times higher than when produced from reactors [2]. The Mo-99 produced at MURR is from low enriched uranium (LEU) targets in a 10 megawatt (MW) pool-type reactor [2]. The Mo-99 is extracted from the fission products and sent to Ottawa, Ontario for final purification and distribution [6]. Mo-99 produced as a fission product is costly (enrichment) and produces many undesirable fission products, that require further processing and containment.

Lutetium-177 (Lu-177) is a radioisotope that is quickly becoming more important. It is a low energy beta-emitter and, in the form of DOTA-TATE, can be attached to the surface of a tumor [2]. It is used in treatments where other methods fail such as neuroendocrine tumors [2]. The demand for Lu-177 is expected to grow as it is considered perhaps the most important radioisotope for targeted radionuclide therapy (TRT) [7]. Though there have been advancements in large scale production of Lu-177, constant, reliable, and cost effective methods of production need to be continuously explored [7].

Alpha-emitters are a class of radioisotopes that are rapidly emerging in nuclear medicine. Targeted alpha therapy (TAT) is especially useful for the control of metastasized cancers. The short range of the alpha particle is beneficial when very targeted doses of radiation are required. The most promising radioisotopes in this field are astatine-211, bismuth-212, bismuth-213, radium-223, terbium-149, and fermium-255. Due to the novelty of TAT, there is at present no standard method for the production of these radioisotopes.

The goal of this thesis is to explore the possibility of producing Mo-99, as well as other radioisotopes

in CANDU reactors by neutron bombardment of non-fissile sources within the fuel channels. Other radioisotopes that will be investigated are lutetium-177 (Lu-177), lead-212 (Pb-212), bismuth-213 (Bi-213), and radium-223 (Ra-223). The non-fissile targets used to produce these radioisotopes will be incorporated into the fuel channels by modifying the center pin of a standard 37-element fuel bundle for a CANDU reactor. These modified fuel bundles will be analyzed using the DRAGON lattice code as well as the DONJON reactor code.

2 Background

2.1 Radioisotopes

Radioisotopes are classified as any species of the same chemical element with a different mass, and unstable nucleus due to excess nuclear energy [8]. This excess energy is released as radiation in the form of alpha, beta, or gamma rays [8]. In order for an element to be of the same species, it must have the same number of protons (p). If an element has the same number of protons but has a different mass then it must have a different number of neutrons (n). For instance Mo-98, and Mo-99 are isotopes of molybdenum. They both have 42 protons, however Mo-99 has 57 neutrons while Mo-98 has 56 neutrons. Since Mo-99 is found to decay with an half-life of 66 hours, it is said to be unstable and is thus a radioisotope, while Mo-98 is a stable isotope [3].

The types of radiation released by radioisotopes can be either alpha, beta, or gamma rays [8]. Alpha radiation is the emission of two protons and two neutrons in the form of a positively charged helium ion. A schematic representation of an alpha decay event can be seen in Fig. (1). Beta radiation is the emission of an electron, and gamma radiation is the emission of a high energy photon. The International System of Units (SI) unit for radioactivity is the becquerel (Bq), and is defined as one decay event (or, one disintegration) per second. Another common unit is the curie (Ci), which is equal to 3.7×10^{10}Bq [9].

The radioisotope selection criteria for a certain medical procedure depends on its specific chemical and radiological requirements. These requirements can vary greatly for different procedures as do the

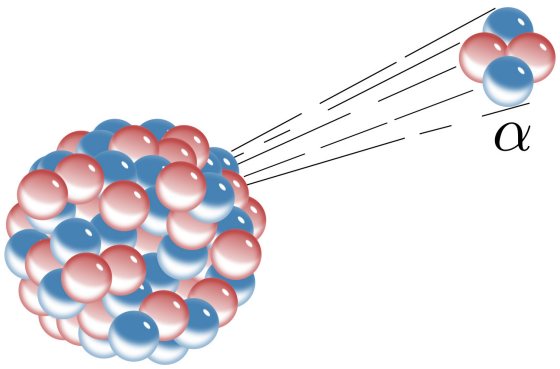

Figure 1: A schematic representation of an alpha decay event.

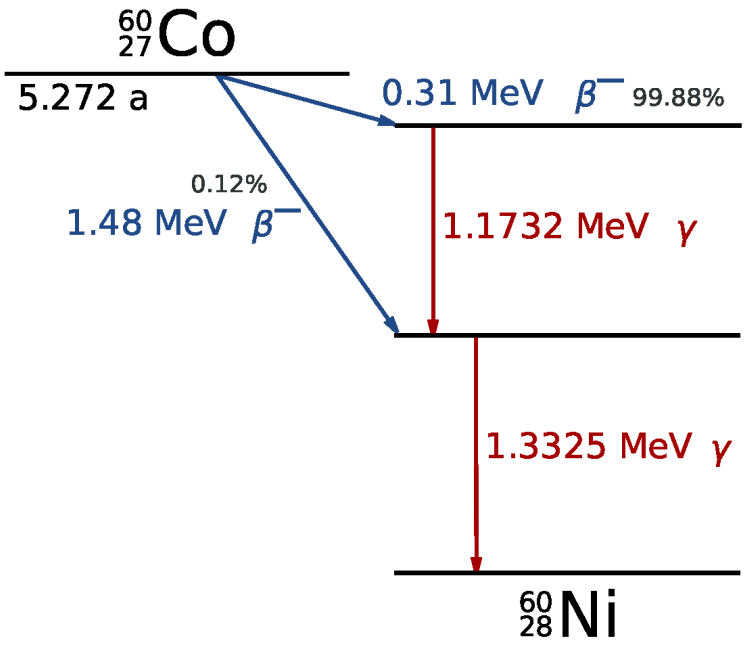

Figure 2: Decay scheme for cobalt-60. The numbers indicate MeV above ground state. The percentages indicate the relative occurrence of the competing decay methods.

radioactive decay processes of the many different radioisotopes. A radioisotope is not strictly limited to one decay path. It can have a multitude of decay paths, whose probabilistic relative occurrences can be measured [9]. The decay scheme of cobalt-60 (Co-60) can be viewed in Fig. (2) where it is shown that the most likely decay event for Co-60 is the emission of an electron, followed by the emission of two photons with an energy of 1.174MeV and 1.332MeV. Diagnostic imaging procedures typically require a high density of high-energy photons in order to achieve the required resolution [10]. On the other hand therapeutic treatments tend to require energy in the form of alpha or beta rays, to be deposited at a local site [10].

2.2 Activity Measurements

The measurement of the amount of radioactivity of substance is referred to as it's activity and is the overall amount of disintegrations that occur per second of a substance. This is typically measured in either becquerels or curies. Specific activity is the amount of activity of a substance per unit-mass, often measured per gram. For instance, the theoretical specific activity of Mo-99 is $17,745$TBq/g [11]. The theoretical specific activity is given by Eq. (1), where a_{th} is the theoretical specific activity of a certain radioisotope, and λ_D is the decay constant of the daughter isotope. The decay constant is the fraction of the number of atoms that decay per second. N_A is Avogadro's constant ($N_A = 6.022 \times 10^{23}\text{mol}^{-1}$), and A_D is the atomic mass number of the daughter isotope. This is the specific activity of a 100% pure

Mo-99 sample, also known as carrier-free. In reality, there is always some isotopic contamination. In other words, whenever a sample of Mo-99 is produced, there will always be some percentage of another isotope (or, carrier) of molybdenum present.

Another unit of measurement commonly used for Mo-99 is the 6-day activity. This is the amount of activity of Mo-99 remaining six days after it leaves the processing facility. This is often called end of processing, or EOP for short.

The amount of specific activity obtained can vary dramatically depending on how the sample is produced. Many factors such as production method, flux, irradiation time, and target purity can all effect the resulting specific activity. The specific activity of Mo-99 produced by the fission of high enriched uranium (HEU) is 185TBq/g, this is lower when low enriched uranium (LEU) targets are used [2]. The specific activity of an isotope produced by neutron capture can be estimated using the neutron saturation model described by Eq. (2), where σ_P is the neutron absorption cross-section of the parent, A_P is the atomic mass of the parent, and ϕ is the neutron flux given in neutrons·cm^{-2} · s^{-1}. Here it is evident that the specific activity is dependent upon the neutron flux in the reactor.

The time required to achieve this amount of specific activity is given by Eq. (3). Where m, called the activation factor, is given by Eq. (4). From Eq. (2), the maximum specific activity of Mo-99 produced from pure Mo-98 targets by neutron capture in a reactor with a neutron flux of 2×10^{14}n·cm^{-2}s^{-1} is 160GBq/g [11]. From Eq. (3), the time it would take to reach this value would be $1,107.2$ hours [11]. The specific activity often achieved through neutron capture is between $3.7 - 74$GBq/g [12]. This specific activity is much lower than that of the fission product method, though it is still high enough to be used in Mo-99/Tc-99m generators.

$$a_{th} = \frac{\lambda_D N_A}{A_D} \tag{1}$$

$$a_{max} = \frac{\sigma_P N_A}{A_P}\phi \tag{2}$$

$$t_{max} = \frac{\ln m}{\lambda_D (m-1)} \tag{3}$$

$$m = \frac{\sigma_P}{\lambda_D}\phi \tag{4}$$

In nuclear physics, the term reaction cross-section (σ) is used to describe an effective area of a nucleus, where an incident particle passing through this area would result in a reaction [11]. In other words, the reaction cross-section is proportional to the probability of a reaction occurring [11]. This is usually measured in barns (b) where $1\text{b} = 10^{-24}\text{cm}^2$. Fig. (3) displays the total, elastic, absorption, and fission cross-sections of incident neutrons on uranium-235 (U-235).

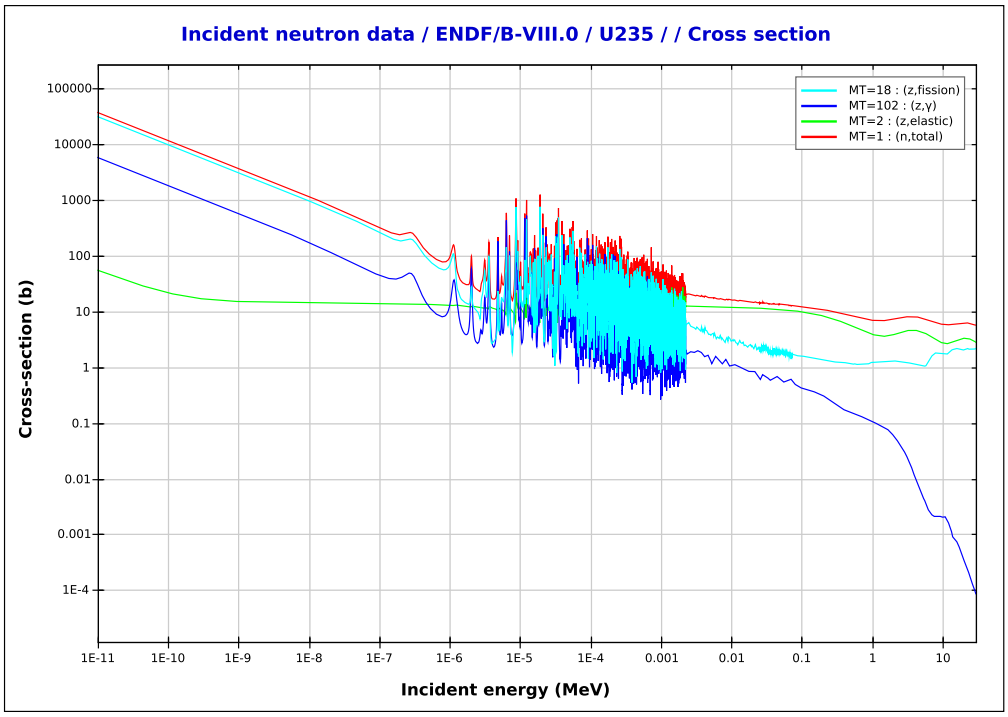

Figure 3: Incident neutron cross-section information for uranium-235.

2.3 Production Methods

There are over 60 radioisotopes commonly used in current medical procedures with several new potential candidates being investigated [2]. There are roughly 45 radioisotopes that are produced in nuclear reactors, with the remaining amount being produced in cyclotrons. Some isotopes can be viably produced through either method [2]. The method of choice for the production of a radioisotope can depend on many factors. For the production of Tc-99m, the cost ratio of cyclotron production versus reactor production can be as much as 10:1 [2]. The downside of reactor-produced Tc-99m is that it requires the fission of enriched uranium. This produces many radioactive by-products that need to be carefully separated. The by-products then require proper disposal, which can be costly. They can also be potentially harmful to both the environment, and human health in the unlikely event of an accident.

Nearly all radioisotopes produced in reactors are done so in specialized research reactors. However there are some that are produced in power reactors. Co-60 is currently produced in the Bruce B and Pickering CANDU reactors. Where specialized adjuster rods containing Co-59 are irradiated for up to three years. This method produces 70% of the worlds supply of Co-60 [2]. The company Areva Med has plans to produce Mo-99, Lu-177, and iridium-192 (Ir-192) in the Bruce-B CANDU power plant in Ontario [13]. Areva intends to use the neutron capture method to produce these radioisotopes through the use of a high-flux viewing port. Another method presented by Areva is the use of an aeroball delivery system whereby Mo-98 is inserted into a guide tube and pneumatically passed through the reactor core [13].

The proposed method of producing Mo-99 through the neutron capture method by modifying the center pin of a fuel bundle with non-fissile sources aims to eliminate the need for enriched uranium and avoid the high cost of building and operating cyclotrons. The cost is mitigated by the fact that the power reactor has already been built and is in operation for the purposes of power production. The inclusion of radioisotope production in a small number of channels is expected to alter the power output of the reactor by an insignificant amount. The benefit of using the fuel channels is to provide yet another potential location to produce radioisotopes within the reactor. If both methods are used then more Mo-98 could be produced. Also the target in the center of the fuel bundle would be subjected to a different flux profile than it would be if it were placed in the moderator region which could potentially be advantageous.

Altering the fuel bundles for the purpose of producing Mo-99 has been previously researched by the University of Ontario Institute of Technology (UOIT). In *Development of a 37-Element Fuel Bundle for the Production of Molybdenum-99 in CANDU Power Reactors* (Haroon, 2014) the fuel bundles were modified to include various amounts of LEU to produce Mo-99 by the fission method. As previously stated, the fission method produces many radioactive by-products, and requires the use of enriched uranium. Also, the inclusion of enriched uranium into the core of a CANDU reactor could be viewed unfavorably by both the utility companies as well as the nuclear regulating agencies.

Many countries are examining the viability of producing Mo-99 domestically, though most seem

to prefer the fission method of LEU [2]. Countries such as India and Kazakhstan, have produced Mo-99 by the bombardment of MoO_3 (natural molybdenum) to produce Mo-99 with a specific activity of 29.6GBq/g [12]. This was done with a thermal neutron flux of $0.9 - 1.1 \times 10^{14} \mathrm{n} \cdot \mathrm{cm}^{-2} \mathrm{s}^{-1}$ for $72 - 200$ hours [12].

Most of the production of Lu-177 and the alpha-emitters are done in research reactors. Lu-177 is typically produced from neutron bombardment of either natural, or enriched Lu_2O_3. The alpha-emitters are produced most often from irradiated thorium though Ac-225 is also produced in cyclotrons by proton bombardment of Ra-226. The demand of these radioisotopes is expected to grow rapidly, and so a wide array of production methods need to be explored. The production of these isotopes within the fuel channels of a CANDU reactor have not be analyzed to any significant degree.

2.4 Generators

Regardless of the production method, Mo-99 has a half-life of 66 hours. In order to supply the hospitals with Tc-99m, Mo-99 is shipped to them in small specialized containers called generators. The post-irradiation molybdenum is chemically treated to produce the molybdate anion (MoO_4^{2-}). Molybdate is then adsorbed onto an alumina column (Al_2O_3), and is placed inside of a radiation shielded container. An example of a Mo-99/Tc-99m generator can be viewed in Fig. (14). As time passes the Mo-99 in the generator decays to Tc-99m. When this happens, the radioactive pertechnetate anion ($^{99m}TcO_4^-$) is formed. Since pertechnetate has a charge of $[1-]$, and molybdate has a charge of $[2-]$, the pertechnetate is less tightly bound to the alumina. Once enough pertechnetate has been formed, a saline solution is passed through the generator, this process is known as elution. The saline solution washes the less tightly bound pertechnetate out of the generator to form sodium pertechnetate ($NaTcO_4$) in solution. The sodium pertechnetate can then be administered to patients. The saline wash does collect some of the molybdenum and is considered a contaminant – this is called Mo-breakthrough. The higher the specific activity of molybdenum used, the less of it is required to provide the same overall radioactivity. Thus, higher specific activity molybdenum provides a sodium pertechnetate solution with less Mo-breakthrough [12]. Some procedures require very high purity pertechnetate, this necessitates that the molybdate be of high specific activity.

A large percentage of the Tc-99m is produced in the first week, therefore hospitals require a frequent delivery of generators [11]. This is typically done on a weekly basis. In order to retrieve the maximum amount of Tc-99m in a generator, several elutions must take place at specific time periods. This is due to the fact that Mo-99 and Tc-99m have different half-lives. The time period to achieve the maximum amount of Tc-99m from the generator is given by Eq. (5). Here m is known as the decay factor given by Eq. (6).

$$(t_{max})_{\text{Tc-99m}} = \frac{m}{m-1} \frac{\ln m}{\ln 2} (t_{1/2})_{\text{Mo-99}} = 23.1\text{h} \tag{5}$$

Figure 4: Cutaway of a typical Mo-99/Tc-99m generator [12].

$$m = \frac{(t_{1/2})_{\mathrm{D}}}{(t_{1/2})_{\mathrm{P}}} = \frac{\lambda_{\mathrm{P}}}{\lambda_{\mathrm{D}}} \tag{6}$$

If the specific activity of molybdenum is too low, then it is not feasible to use in standard alumina column generators. Work has been done in order to develop new types of generators that can use low specific activity molybdenum. These generators use a zirconium (poly)molybdate gel, which involves complex processing methods [14]. The steps involved in the production of gel generators can be viewed in Fig (5). These zirconium gel generators can be used with molybdenum sources of specific activities as low as $0.03 - 0.04$GBq/g [12]. Similar generators are also used for the alpha-emitters.

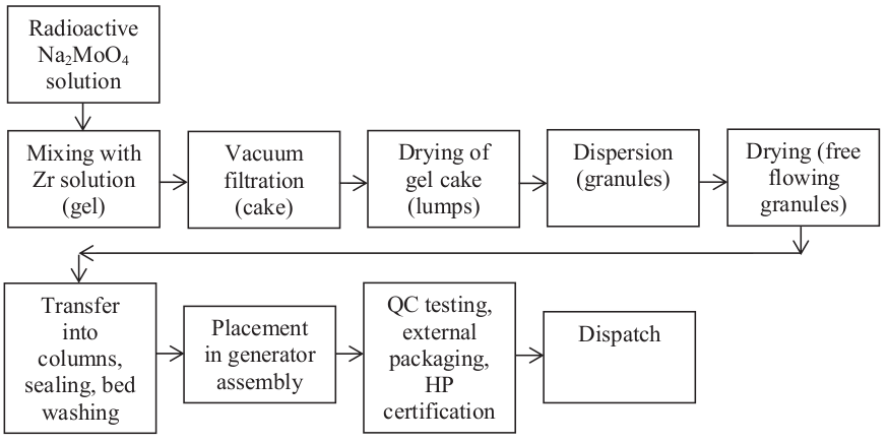

Figure 5: Flow chart of gel preparation and generator assembly [12].

2.5 Isotope Information

2.5.1 Mo-99

Molybdenum is the 42^{nd} element in the periodic table of elements where it is classified as a transition metal. Molybdenum is found in nature as molybdenite (MoS_2), wulfenite ($PbMoO_4$), and powellite ($CaMoO_4$) [15]. It is primarily produced as a byproduct of copper mining where it is found in the form of MoS_2 [15]. The world production was estimated at $258,000$t in 2013 [15]. It's principal use is in alloys where it acts as a hardening agent in metals such as steel, and cast iron [15]. When used as an alloying agent, molybdenum is often converted to either molybdic oxide (MoO_3, "MoX") or ferro-molybdenum (FeMo). The chemical conversion from molybdenite to metallic molybdenum is detailed in the chemical reactions described by Eqs. (7-10).

$$2\ MoS_2 + 7\ O_2 \rightarrow 2\ MoO_3 + 4\ SO_2 \tag{7}$$

$$MoO_3 + 2\ NH_3 + H_2O \rightarrow (NH_4)_2(MoO_4) \tag{8}$$

$$(NH_4)_2Mo_2O_7 \rightarrow 2\ MoO_3 + 2\ NH_3 + H_2O \tag{9}$$

$$MoO_3 + 3\ H_2 \rightarrow Mo + 3\ H_2O \tag{10}$$

The world demand for Mo-99 for medical procedures was $23,000$ six-day TBq/yr in 2012, though it has since dropped to approximately $18,500$ [2]. A $23,000$ six-day TBq/yr demand equates to about $167,000$TBq/yr that must be produced in the reactor in order to account for cooling, processing, and decay en route to the hospitals [2]. Mo-99 is used as a parent for Tc-99m, which is the most used radioisotope in medicine [2]. It is used in about 40 million procedures per year, and accounts for roughly 80% of

all nuclear medicine procedures [2]. There are several isotopes such as fluorine-18 (F-18), and thallium-201 (Tl-201), that can be used as an alternative to Tc-99m for certain procedures. F-18 is produced in a cyclotron as opposed to a reactor. However these isotopes come with their own set of problems that limit the degree to which they can be used in place of Tc-99m. There are also new treatments being developed that require the use of Tc-99m, and so the overall demand is likely to remain steady [16].

Prior to the shutdown of NRU, most of the Mo-99 produced in the world was done through fission of HEU. Due to the concerns of nuclear proliferation, a global initiative to use LEU for Mo-99 production was put forward by the International Atomic Energy Agency (IAEA). Mo-99 produced as a fission product can have specific activity as high as 185TBq/g [2]. The neutron capture method provides a much lower specific activity, on the order of $3.7 - 74$GBq/g though this can be increased with highly enriched Mo-98 targets as well as high neutron fluxes [12]. Typically, either MoO_3 or metallic molybdenum is used as a target for the neutron capture production method [12]. Metallic molybdenum tends to provide a higher activity but the post irradiation process is more difficult [12].

Four types of Mo-98 targets will be placed into the center pin of a 37-element fuel bundle for the DRAGON/DONJON simulations. Two samples of metallic molybdenum will be used. One with a natural composition of molybdenum isotopes, the other with highly enriched Mo-98. The two other targets will be composed of MoO_3, one with natural molybdenum and the other with highly enriched Mo-98. The total, elastic, and absorption cross-sections for Mo-98 can be viewed in Fig. (6).

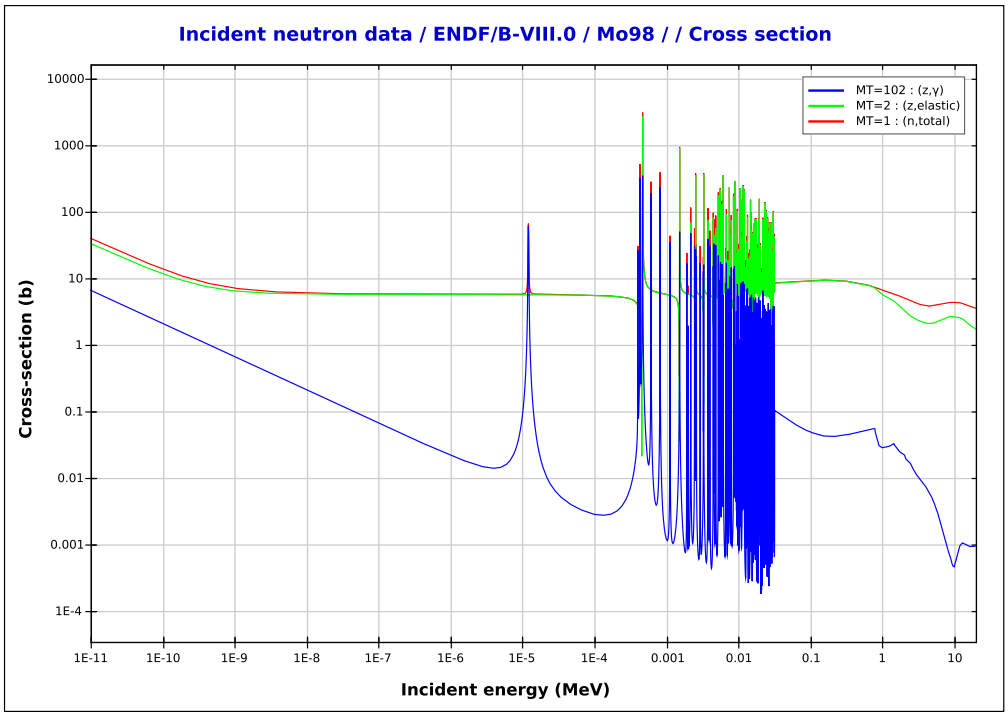

Figure 6: Incident neutron cross-section information for Mo-98.

2.5.2 Lu-177

Lutetium is the 71^{st} element on the periodic table of elements where it is classified as a lanthanide. It is the smallest atom of all the lanthanides, it also has the highest melting point, the highest density, and is the hardest [17]. There are two naturally occurring isotopes of lutetium, Lu-175, and Lu-176. The ratio of these isotopes found in nature is 97.5% Lu-175, and 2.5% Lu-176 [17]. Lutetium is a very scarce element, only found in trace amounts in minerals containing other lanthanides. This makes the element very expensive ($\$10,000$USD/kg) [17]. It is most commonly used as a catalyst in the petroleum industry [17].

In the nuclear medicine field, lutetium-177 is emerging as a very important radioisotope where it is used for targeted therapy [18]. A peptide containing Lu-177 is already being used to treat patients on a regular basis [18]. An important quality of Lu-177 is that it has a longer half-life of 6.64 days, this is long enough to be able to produce larger quantities without the need for generators such as with Tc-99m. There are two possible ways that Lu-177 can be produced. The first method uses either a natural, or enriched target of Lu_2O_3, and bombards it with neutrons until enough of them are absorbed to produce the required amount of Lu-177. The other method fires neutrons at a highly enriched target of $^{166}Yb_2O_3$, and relies on the short half-life of ytterbium-177 (Yb-177) to decay to Lu-177. These production paths can be viewed in Fig. (7).

Production of Lu-177 using Lu_2O_3 as a target leads to a lower specific activity ($925-1,295$GBq/mg) [18]. This method requires a medium to high flux and $2-4$ weeks of irradiation [18]. The second method produces targets of much higher specific activity. The major problem with this method is separating the Lu-177 from the ytterbium due to their chemical similarity. Commercially, the second method of production is thought to be impractical due to the large amount of enriched ytterbium required [18]. However, the second method of production may be required in cases where the chemical toxicity is high, and therefore requires a high specific activity [18].

Three types of targets will be used in the DRAGON/DONJON simulations for the production of Lu-177. A natural target of Lu_2O_3, an 82% enriched target of Lu_2O_3, and an highly enriched target of Yb_2O_3. The total, elastic, and absorption cross-sections for Lu-176 can be viewed in Fig. (8).

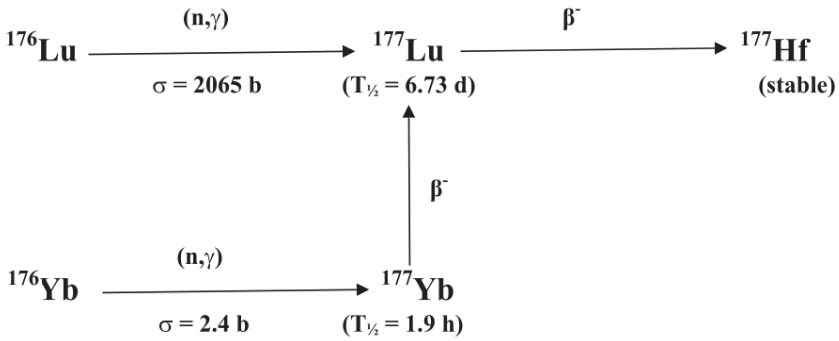

Figure 7: Schematic representation of Lu-177 production via neutron capture [18].

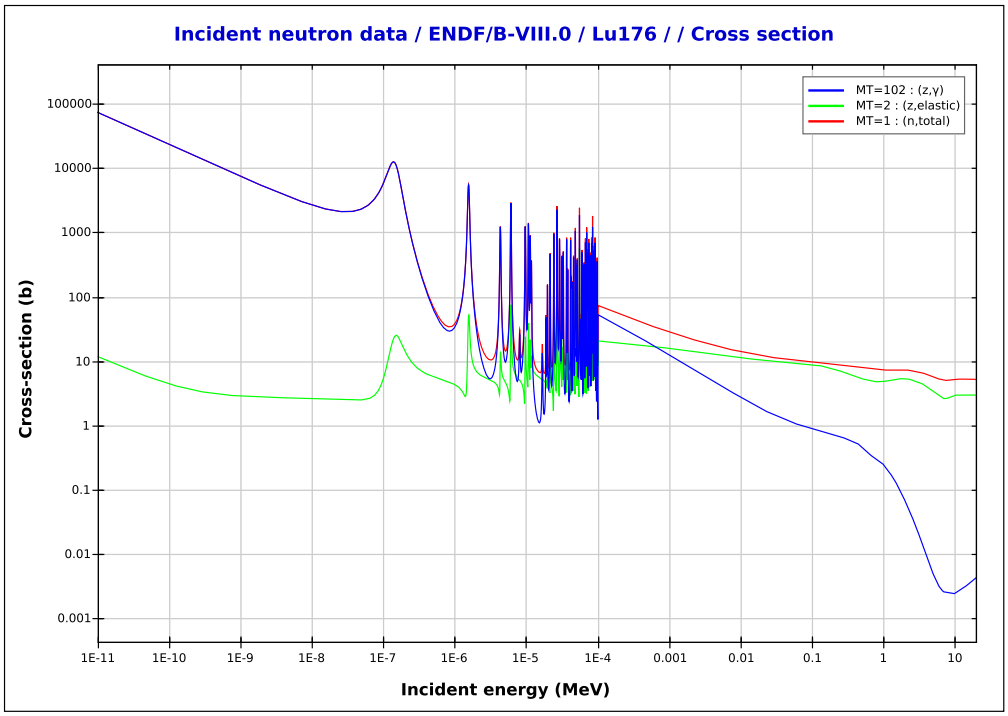

Figure 8: Incident neutron cross-section information for Lu-176.

2.5.3 Alpha-emitters

Alpha-emitters are at the forefront of targeted therapy. This is where a radionuclide is bonded to a molecule by a process known as chelation. The molecule, now called a chelate, is chosen for having an affinity to bind with a particular monoclonal antibody. The antibody then binds to a specific antigen receptor that happens to be over-expressed on the targeted cancer cell. Then when the radionuclide decays, the energy of it's emitted particle is likely to be deposited into the cancer cell. This energy is relatively high and is expected to kill the targeted cell by splicing the DNA helix. This type of systemic therapy is most efficacious where other traditional methods tend to fail, such as highly metastasized tumors. A representation of this process can be viewed in Fig. (9).

There are over 100 radionuclides that emit alpha particles [18]. However most of these have half-lives that are too long to be useful for therapeutic purposes [18]. Only the handful of alpha-emitters previously mentioned have been proposed for clinical radionuclide therapy [18]. This thesis will focus on three of these; Bi-212, Bi-213, and Ra-223. The reason that these three were chosen is because they can all potentially be produced by neutron bombardment of radium-226 (Ra-226).

Radium is the 88^{th} element on the periodic table where it is classified as an alkaline earth metal. It is a rare metal commonly found in trace amounts of uranium ores [20]. One ton of pitchblend contains approximately 150mg of radium [21]. Due to the chemical difficulty of extracting radium from uranium ore as well as it's scarcity, radium is an expensive element [20]. Radium-226 is the most abundant isotope of radium [21]. It has a half-life of $1,601$ years, and is produced naturally by the decay of uranium-238 [21]. Since uranium ore production is around $62,000$t per year (2016), a rough calculation estimates the amount of radium mined per year as a by-product to be 9kg per year [22].

Neutron bombardment of Ra-226 produces Ra-227 which has a half-life of 42 minutes [23]. Radium-227 beta-decays to actinium-227 (Ac-227), and eventually produces radium-223 (Ra-223), one of the primary alpha-emitting radioisotopes proposed for TAT. Ac-227 was first produced in 1945 by irradiating targets of radium carbonate ($RaCO_3$) [24]. This method of Ac-227 production also produces significant quantities of thorium-228 (Th-228), and thorium-229 (Th-229) as by-products [24]. Thorium-228 decays to produce the alpha-emitter bismuth-212 (Bi-212), and thorium-229 decays to produce bismuth-213 (Bi-213). The decay paths for Ac-227, Th-228, and Th-229 can be viewed in Figs. (11, 12, 13). So far, all of the Bi-213 used in clinical studies have been produced from neutron bombardment of thorium-232 (Th-232) [25].

A target of $RaCO_3$ will be placed in the center pin of a 37-element CANDU fuel bundle and irradiated for various lengths of time using the DRAGON and DONJON computer codes. The results will be analyzed to determined the amounts of Ac-227, Th-228, and Th-229 produced through this method in hopes of providing a viable alternative method of production. The total, elastic, and absorption cross-sections for Ra-226 can be viewed in Fig. (10).

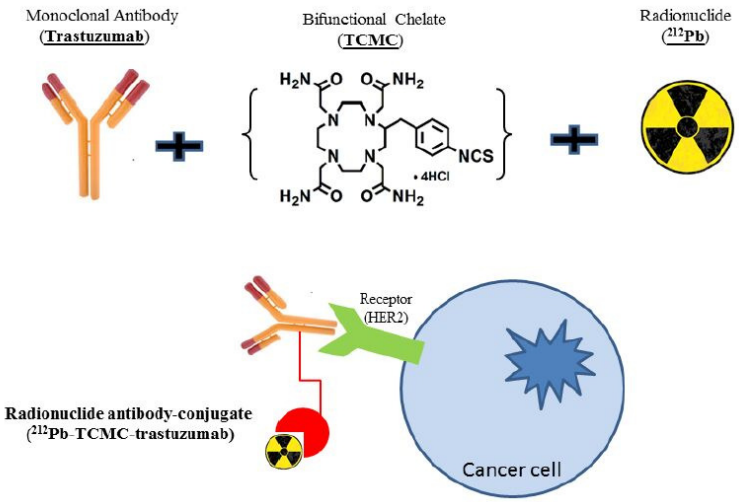

Figure 9: Schematic representation of the process of targeted alpha therapy [19].

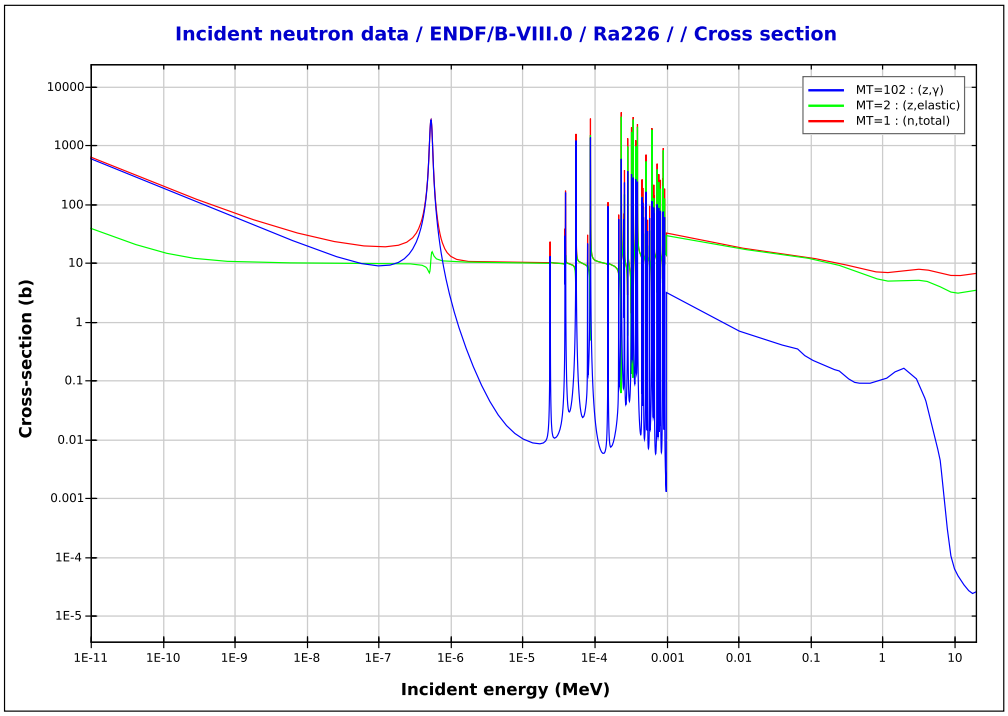

Figure 10: Incident neutron cross-section information for Ra-226.

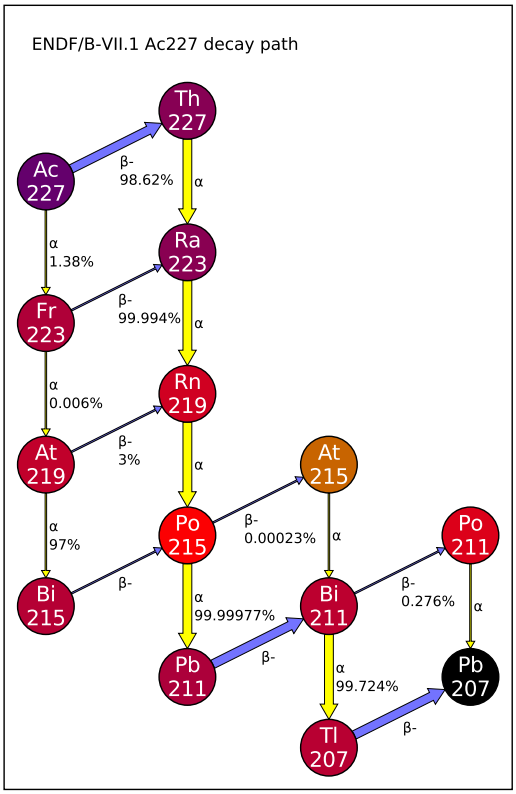

Figure 11: Schematic representation of the decay path for Ac-227

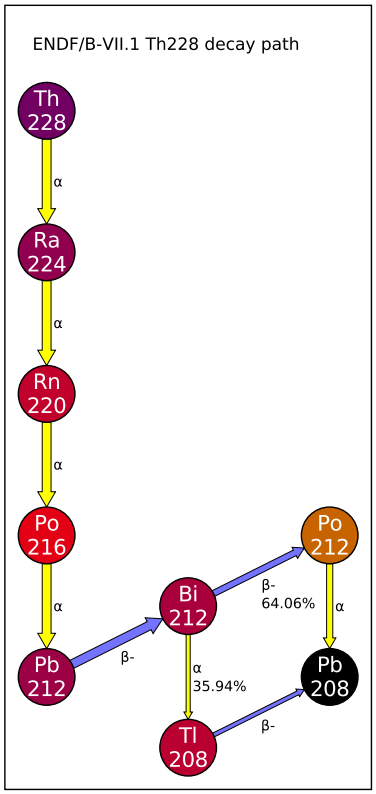

Figure 12: Schematic representation of the decay path for Th-228

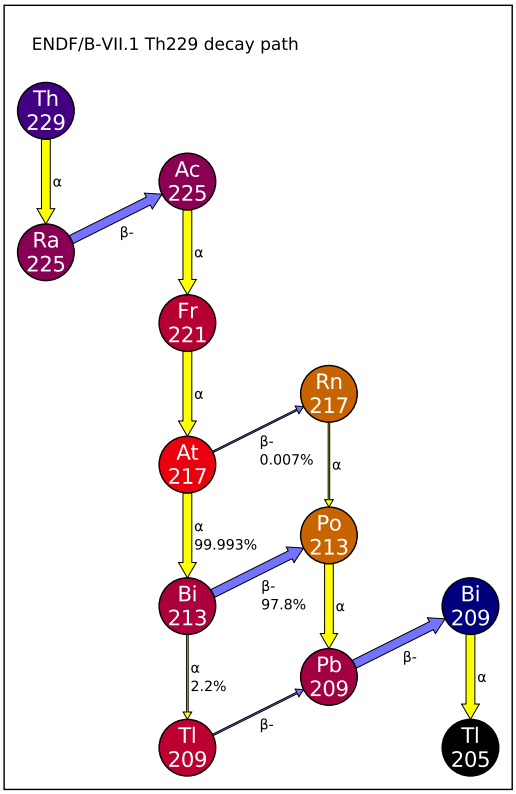

Figure 13: Schematic representation of the decay path for Th-229

2.6 CANDU Reactors

The CANDU[1] reactor is a pressurized heavy water reactor (PHWR). It stands for CANadian Deuterium Uranium. As of 2018, Canada has 19 PHWR reactors with a production capacity of $13,513$MWe [26]. Twelve of these are CANDU-9 reactors, all of which are located in Ontario. The heavy-water used in the CANDU reactor allows natural uranium to be used as a fission source. Natural uranium is composed of 0.711% uranium-235 (U-235), and 99.289% uranium-238 (U-238) [26]. Other light-water based reactors require enriched uranium to sustain the fission reactions. This is because the hydrogen in regular light water will absorb too many neutrons and so the chain-reaction will cease. The enrichment of uranium, increases the amount U-235 in the fuel. This leads to more fission reactions, and so more neutrons are produced. The over-absorption of neutrons is known as sub-criticality. The opposite case when not enough neutrons are being absorbed is called super-criticality, or excess-criticality. This leads to an increase in power and can be dangerous if not corrected.

The degree of criticality is known as the reactivity. The reactivity of a reactor is given by Eq. (11), where ρ is the reactivity, often measured in mk, and k_{eff} is the effective multiplication factor. This is the ratio of neutrons being produced to neutrons being absorbed or lost from one generation of fission reactions to the next. A reactor with zero reactivity ($\rho = 0$mk), or an effective multiplication factor of one ($k_{eff} = 1$) is said to be critical. Another term often used is the infinite multiplication factor (k_∞). This is, in essence, the same as the effective multiplication factor only applied to the infinite lattice. The infinite lattice is an idealized model of the reactor lattice where no neutron leakage takes place. In other words, it is as if the edges of the lattice were stretched out to infinity which implies that it would be impossible for neutrons to escape it's boundaries. This model is convenient to gain insight into the ratio of neutrons that are produced to neutrons that are absorbed in a lattice without worrying about the amount of neutrons leaving the system. In reality, however, there are always some neutrons that escape the system. The infinite lattice is important to gain insight into the material properties of the lattice as neutron leakage is dependent upon geometry.

Another important aspect of CANDU reactors is their ability to be refuelled on-line. The individual horizontal fuel channels pass through the reactor core, and can be refuelled at anytime without having to shut the reactor down. Traditional light-water reactors need to be completely shutdown before they can be refuelled. These fuel channels can be seen in a cutaway of a typical CANDU reactor in Fig. (14). The fuel channels are refuelled with a refuelling machine that pushes the fuel bundles through. This is often done in 4 or 8 bundle shifts. The nuclear operators are responsible for determining which of the channels are refuelled. They do so in way that ensures an optimal power profile for the reactor.

$$\rho = (1 - 1/k_{eff}) \cdot 1000\text{mk} \tag{11}$$

[1] CANDU is a registered trademark of Atomic Energy of Canada Limited in Canada.

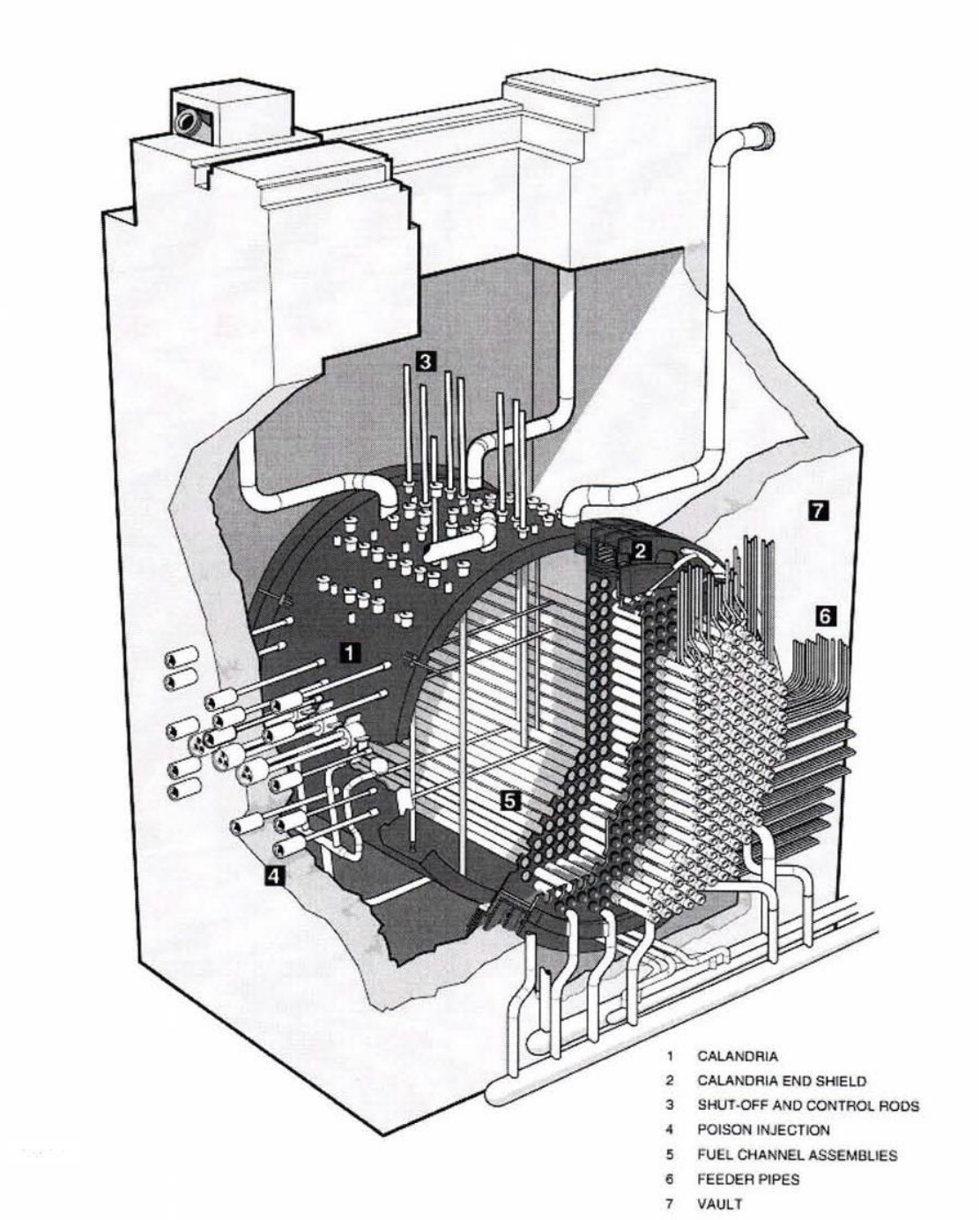

Figure 14: Cutaway view of a typical CANDU reactor vault and assembly [26]

2.6.1 Fuel Bundle Design

The fuel bundles in a CANDU-9 reactor are comprised of 37 elements. Inside these elements are uranium dioxide (UO_2) pellets that are sheathed in a Zircaloy-4 cladding [26]. The bundles are 49.5cm long and have a diameter of 10.24cm [26]. There are 13 bundles per channel, and 480 fuel channels in the reactor [26]. An image of a 37-element fuel bundle can be viewed in Fig. (15).

The bundles are shifted down the fuel channels as fresh bundles are pushed in. This is done when the fuel has been irradiated for a certain amount of time. The longer the fuel is in the core the more it is spent or burned. This is known as irradiation, and is described by Eq. (12). Here it can be seen that the irradiation (ω) is flux multiplied by time. Another more common way to measure how much fuel is spent is called burnup. This is the amount of fission energy that is released by the fuel over time per unit-mass of the fissionable material originally present in the fuel. Burnup is typically measured in megawatt days per tonne of uranium (MWd/Mg(U)).

$$\omega = \int \phi\left(t\right) dt \tag{12}$$

As seen by the end-view in the top left of Fig. (15), the configuration of the 37-elements, or pins as they are sometimes called, is done in three concentric circles surrounding a center pin. The center pin is partially blocked by the outer pins from neutrons coming in from the moderator. For this reason, the center pin contributes little to the power output of the fuel bundle at the beginning of its irradiation. The center starts to contribute to a greater degree once the U-235 in the outer rings becomes more and more depleted. This allows more neutrons to pass through the outer elements before becoming captured. This is the reason that it is thought that if the fuel from the center pin of the bundles from a few of the channels were replaced with non-fissile material, that the overall loss of power output of the reactor would negligible. The channels with the modified fuel bundles would simply have to be refueled with greater frequency. Additionally, the design of the fuel bundle apparatus lends itself for easy removal of the center-pin as it can be knocked out while the rest of the bundle remains intact.

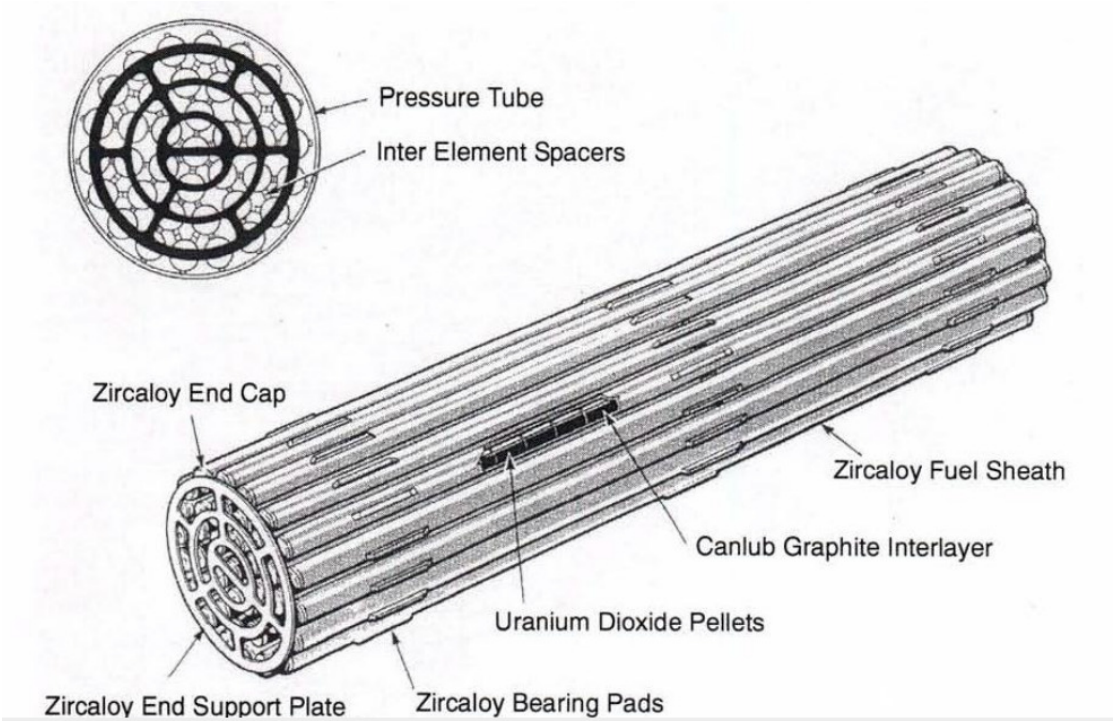

Figure 15: View of a 37-element CANDU fuel bundle [26]

3 Methodology

3.1 NJOY

A nuclear cross-section library is required in order to use the simulation software to analyze the production of these isotopes. A nuclear cross-section library contains detailed information about the individual isotopes. Various libraries have been produced, and are already available on-line. Most notable are the libraries generated in the WIMS Library Update Project (WLUP). These are libraries that have been generated in the Winfrith Improved Multigroup Scheme-D (WIMS-D) format. WIMS-D is the name for a family of public domain software packages that are used in many reactor lattice codes. The WLUP libraries are available for download from the IAEA, and have been used in countless nuclear lattice simulations. The problem with the WLUP libraries is that they only contain information for the most common isotopes involved in thermal nuclear reactors. This makes them incomplete for the purposes of this thesis.

In order to produce a new library, a nuclear data processing system called NJOY (2016 version) was used. At present the 2016 version of NJOY is the only version that is available without a license. All previous versions require a license from the Los Alamos National Laboratory (LANL). NJOY2016.0 is freely available and under the BSD license, and for this reason was the version that was used to produce new cross-section libraries. NJOY is essentially a computer software package that is used to translate information from nuclear data files into either pointwise or multigroup cross-section files. The nuclear

data files to be read by NJOY must be in the Evaluated Nuclear Data File (ENDF) format. The ENDF libraries are groups of files that contain vast amounts of information about the cross-section reactions for different isotopes. These libraries have been under continuous improvement since 1968 [27]. The ENDF libraries are the default for particle transport codes such as MCNP and SCALE, however they do not contain all of the necessary isotopes required for this thesis. Therefore, a combination of two separate data libraries were used. These were the Joint Evaluated Fission and Fusion File (JEFF) library version 3.2, and the TALYS Evaluated Nuclear Data Library (TENDL) version 2015. JEFF is an evaluated nuclear cross-section library produced through an international collaboration of Nuclear Energy Agency (NEA) members. TENDL is a computer simulated nuclear cross-section database produced with the TALYS software.

NJOY2016 is written in the Fortran-90/95/2003 computer code. It involves the use of several modules that manipulate the data from the provided nuclear cross-section library in various ways depending on the requirements of the final multigroup library. The isotopes are processed sequentially through the flow of modules and appended to a final data file. In order to automate this process the PyNJOY-2012 system was used. PyNJOY is a system provided by École Polytechnique de Montréal, that adds the DRAGR module to the NJOY data source files. PyNJOY also includes several Python scripts that can be used to easily produce a custom nuclear cross-section library in either ACELIB or DRAGLIB format. DRAGLIB is one of the formats used by DRAGON. The data flow through the NJOY modules from an ENDF library to a DRAGLIB library can be seen in Fig. (16). The PyNJOY-2012 system was developed to work in conjunction with NJOY-2012.0. Therefore, several minor modifications to the NJOY-2016 source code had to be made in order to render it compatible with the PyNJOY system. Further information about the PyNJOY system can be found in *A PyNJOY Tutorial* (Hébert, 2016)

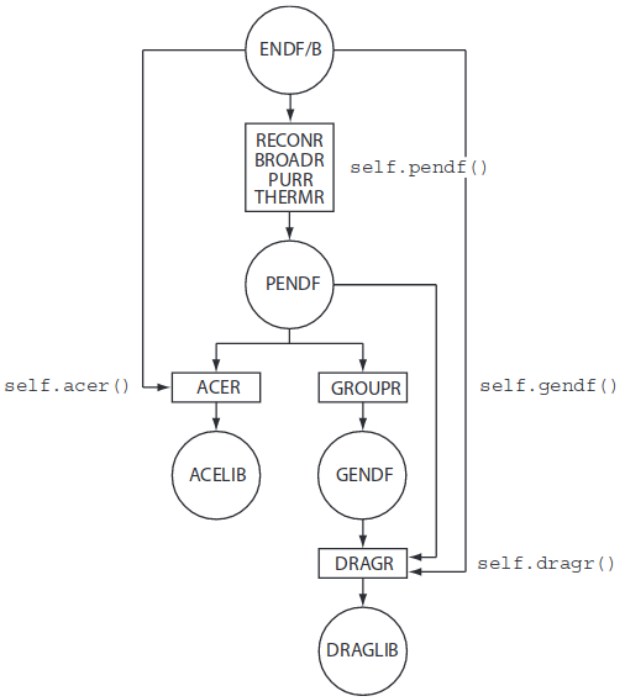

Figure 16: Flowchart for DRAGLIB/ACELIB production [28]

3.2 DRAGON Lattice Code

DRAGON is a computer code developed by École Polytechnique de Montréal [29]. It is a lattice code capable of using several different techniques to solve the neutron transport equation [29]. It is free to use and under the GNU Lesser General Public License as published by the Free Software Foundation [29]. DRAGON was specifically developed to analyze CANDU lattice calculations, though it has also been used to study other types of reactor lattices. DRAGON is divided into calculation modules that can be linked together using the GAN generalized driver [29]. The two most important components are the multigroup flux solver and the one-group collision probability (CP) tracking module [29]. DRAGON first generates the CP matrices for the lattice then solves the multigroup flux through the power iteration method where k_{eff} is obtained. DRAGON version 5.0.4 was used to perform all lattice simulations in this work.

3.2.1 Solution of the transport equation

The time-dependent neutron transport equation can be viewed in Eq. (13), this is known as the "integro-differential" form of the transport equation. This equation has seven independent variables ($\vec{r} = x, y, z; E; \hat{\Omega} = \theta, \phi; t$), and is thus quite difficult to solve. For a detailed derivation, the reader is invited to study *Nuclear Reactor Analysis* (Duderstadt & Hamilton, 1976). Due to the difficulty in solving Eq. (13), computer programs must use numerical methods to discretize the equation. One of the methods DRAGON uses to

solve the discretized form of the time-independent transport equation is the CP method. The discretized transport equation used by DRAGON can be viewed in Eq. (14), and the probability matrices in Eqs. (15-18). Of which, a full derivation can be studied in *DRAGON Theory Manual* (Marleau, 2001).

$$\begin{aligned}&\frac{\partial n}{\partial t}+v\hat{\Omega}\cdot\nabla n+v\Sigma_t n\left(\vec{r},E,\hat{\Omega},t\right)\\&=\int_{4\pi}d\hat{\Omega}'\int_0^\infty dE'v'\Sigma_S\left(E'\rightarrow E,\hat{\Omega}'\rightarrow\hat{\Omega}\right)n\left(\vec{r},E',\hat{\Omega}',t\right)+S\left(\vec{r},E,\hat{\Omega},t\right)\end{aligned}\tag{13}$$

$$\begin{aligned}\phi_i&=\sum_{\alpha=1}^{N_S}\sum_{\mu=0}^{N_\nu}p_{i\alpha}^{\mu}\phi_{-,\alpha}^{\mu}+\sum_{j=1}^{N_V}p_{ij}q_j\\\phi_{+,\alpha}^{\nu}&=\sum_{\beta=1}^{N_S}\sum_{\mu=0}^{N_\nu}p_{\alpha\beta}^{\nu\mu}\phi_{-,\beta}^{\mu}+\sum_{j=1}^{N_V}p_{\alpha j}^{\nu}q_j\end{aligned}\tag{14}$$

$$\tilde{p}_{ij}=V_ip_{ij}=\int_{V_i}\int_{V_j}\frac{e^{-\tau(R)}}{4\pi R^2}d^3r'd^3r\tag{15}$$

$$\tilde{p}_{i\alpha}^{\nu}=V_ip_{i\alpha}^{\nu}=\int_{V_i}\int_{S_\alpha}\frac{e^{-\tau(R_S)}}{4\pi R_S^2}\left(\hat{\Omega}\cdot\vec{N}_-\right)\psi^{\nu}\left(\hat{\Omega},\vec{N}_-\right)d^3r'd^2r\tag{16}$$

$$\tilde{p}_{\alpha i}^{\nu}=\frac{S_\alpha}{4}p_{\alpha i}^{\nu}=\int_{S_\alpha}\int_{V_i}\frac{e^{-\tau(R)}}{4\pi R^2}\left(\hat{\Omega}\cdot\vec{N}_+\right)\psi^{\nu}\left(\hat{\Omega},\vec{N}_+\right)d^2r'd^3r\tag{17}$$

$$\tilde{p}_{\alpha\beta}^{\nu\mu}=\frac{S_\alpha}{4}p_{\alpha\beta}^{\nu\mu}=\int_{S_\alpha}\int_{S_\beta}\frac{e^{-\tau(R_S)}}{4\pi R_S^2}\left(\hat{\Omega}\cdot\vec{N}_-\right)\psi^{\nu}\left(\hat{\Omega},\vec{N}_-\right)\left(\hat{\Omega}\cdot\vec{N}_+\right)\psi^{\mu}\left(\hat{\Omega},\vec{N}_+\right)d^2rd^2r'\tag{18}$$

3.2.2 CANDU-9 Lattice

A reactor lattice is a small section of a reactor that can be translated multiple times in order to produce a full reactor core. Often, only a two-dimensional (2-D) lattice calculation is performed as three-dimensional calculations can be computationally intensive. A 2-D lattice of a CANDU 37-element bundle as produced by DRAGON can be viewed in Fig. (18). Here, the different colours represent different regions in the standard fuel bundle. From 1 to 7, these regions are the moderator, coolant, pressure tube, gas gap, calandria tube, cladding, and fuel. The properties of the CANDU-9 lattice used in the DRAGON simulations are outlined in Tabs. (1, 2, 3). It is important to note that the properties used for the lattice calculations are approximations only. This is due to the proprietary nature of CANDU reactors. Thus, accurate comparisons of either the lattice or full-core calculations to real world data is not possible. Reference data must therefore come from previous academic work that uses similar tools and approximations.

The lattice simulation performed by DRAGON solves the transport equation for each burnup step. The calculations for each burnup step use the saved results from the previous step. DRAGON also determines the properties to be used in a two-group diffusion equation by a core code, such as DONJON. Once a complete set of calculations are performed for each burnup step by DRAGON, a cross-section

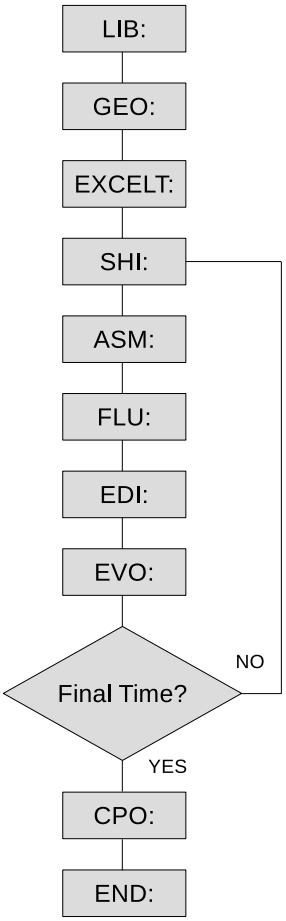

Figure 17: DRAGON calculation scheme.

database parameterized by burnup is saved to be used later by DONJON. DONJON can then be used to set up a 3-D grid of the lattices to perform a full core calculation.

The calculation scheme used to compute the lattice properties in DRAGON can be viewed in Fig. (17). The meshing, number of tracking lines and angles, and the burnup time steps used were the same as in *Development of the Micro-depletion Method in the Chain of Codes DRAGON4/DONJON4* (Guyot, 2011). Where an entire CANDU-6 with all reactivity devices, and detectors was modeled. This work was sponsored by Atomic Energy of Canada Limited (AECL) and done at École Polytechnique de Montréal where DRAGON and DONJON were developed [30]. The cross-section databases and input files for both DRAGON and DONJON that were used in the paper previously mentioned above are available from the École Polytechnique website. The input files were used as a basis for the input files in this work. The cross-section databases were used directly for the generation of the liquid zone controllers (LZCs) and adjuster rod properties.

The DRAGON modules perform the following tasks:

LIB: used to generate or modify a library that contains both microscopic and macroscopic cross-sections for all the isotopes to be used

GEO: used to generate of modify a geometry

EXCELT: used to track the geometry

SHI: used to perform self-shielding calculations on the library

ASM: used to generate the collision probability matrices

FLU: used to calculate the neutron flux, and multiplication factor

EDI: used to homogenize cross-sections and condense energy groups

EVO: used to calculate burnup and new isotope concentrations

CPO: used to generate burnup-dependent mono-parameter reactor database

END: used to terminate DRAGON

The DRAGON simulations were done in two sets. The first set of simulations were done to provide lattice parameters for each bundle to later be used by DONJON. In the first set, all of the bundles were burned at a constant bundle power of 31.971kW/kg for 500 days. Once the DONJON simulations were performed, a second set of DRAGON simulations were done given the information acquired from DONJON. For the second set, the average bundle power calculated by DONJON for a given channel is used to calculate the burnup steps at that particular power. DONJON also provides the refuelling rate for each individual channel. These refuelling rates can be used to determine the length of time that a bundle spends in the core. The simulations were performed for the approximate number of days given by the refuelling rate of that particular channel.

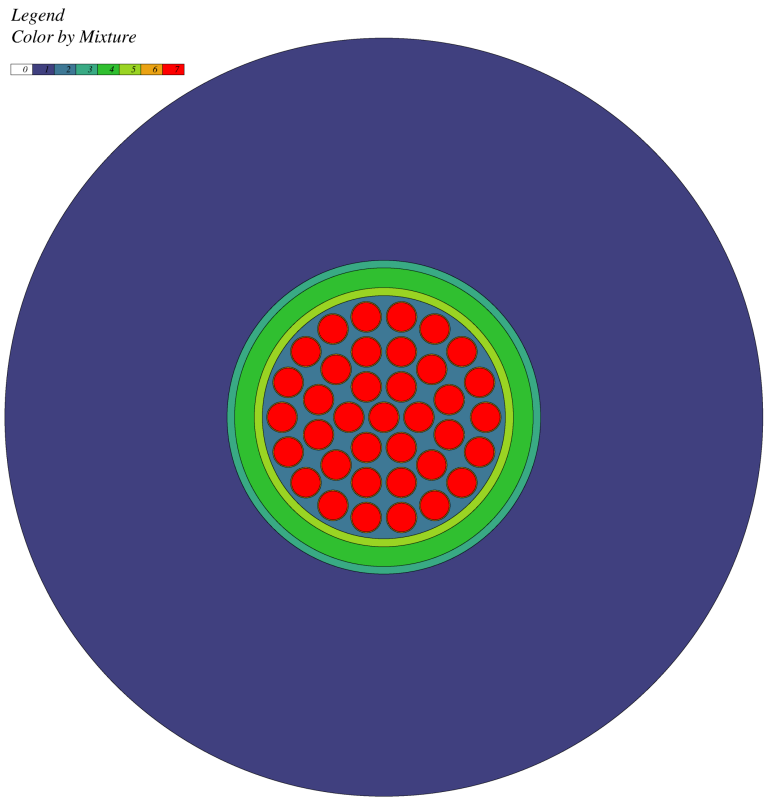

Figure 18: CANDU-9 lattice produced by DRAGON

Parameter	Value
Lattice pitch [cm]	28.575
Pitch radius [cm]	16.121
Fuel pellet diameter [mm]	12.24
Fuel pellet material	UO_2
Fuel density [g/cm^3]	10.4
Fuel enrichment, w/o	0.711
Cladding outside diameter [mm]	13.08
Cladding thickness [mm]	0.42
Cladding material	Zircaloy-4
Pressure tube material	Zr + 2.5% Nb alloy
Cladding density [g/cm^3]	6.44
Gap material	CO_2
Moderator material	D_2O
Moderator density [g/cm^3]	1.085

Table 1: CANDU-9 lattice parameters

Material	Nuclide	Percent weight
Zircaloy-4	Zr90	5.125e+1
	Zr91	1.116e+1
	Zr92	1.705e+1
	Zr94	1.744e+1
	Fe56	1.600e-1
	Ni58	6.000e-2
	Cr52	1.100e-1
	B10	6.138e-5
	B11	2.486e-4
Zr + 2.5%Nb alloy	Zr90	5.011e+1
	Zr91	1.092e+1
	Zr92	1.667e+1
	Zr94	1.706e+1
	Nb93	2.500
	B10	4.158e-5
	B11	1.684e-4
UO_2	O16	1.184e+1
	U235	6.271e-1
	U238	8.752e+1
Moderator	O16	7.988e-1
	H2_D2O	2.010e-1
	H1_H2O	8.960e-5

Table 2: CANDU-9 material compositions

Region	Temperature [K]
Fuel	960.15
Cladding	540.15
Coolant	540.15
Moderator	342.15

Table 3: CANDU-9 operating temperatures

3.2.3 CANDU-9 Lattice Benchmark Results

In order to track all of the isotopes of interest in the simulations, a new multi-group cross-section library had to be generated. This process has been previously outlined in Section (3.1). A lattice simulation was performed for a standard bundle with both the newly generated library as well as a commonly used library. The infinite lattice multiplication factors generated from the two libraries are presented in Fig. (19). Here it can be seen that there is initially a deviation between the two, though after 3000MWd/Mg(U) of burnup the two are identical. DRAGLIB is the name of the custom library generated with NJOY, while iaeagx is a validated WIMS-D formatted library available from the IAEA. Their group structures differ slightly, this may account for the initial discrepancy. DRAGLIB was generated with a XMAS 172-group structure, and iaeagx has a WIMS 172-group structure. The DRAGLIB library was generated from a combination of JEFF and TENDL libraries whereas iaeagx was generated from an ENDF library. The most likely source for the discrepancy between the two libraries though, is that the iaeagx library often uses cross-sections for an element that has been averaged over several isotopes that would occur in a natural abundance. The DRAGLIB on the other hand, stores all of the individual isotopes separately. Reference data taken from previous academic work entitled *Comparative Safety Evaluation of Thorium Fuel to Natural Uranium Fuel in a CANDU 6 Reactor* (Demers, 2017) is provided in Fig. (20) where it can be seen that a discrepancy in the k_∞ values among different libraries is common. The local minimum of approximately 1.06 during the first few burnup steps does, however, appear to be quite low. Nevertheless, the custom library was used for all subsequent simulations.

The reason for the rapid decline in reactivity at the earlier stages of burnup is due to the rapid increase in xenon-135 (Xe-135) within the fuel. Xenon is a strong neutron absorber. It is produced as a fission product, and is also produced from the decay of iodine-135 (I-135) which is also a fission product. The equations that can be used to determine the amount xenon present within the fuel can be viewed in Eqs. (19, 20). Here, γ is the yield from fission reactions, λ is the decay constant, Σ is the macroscopic cross-section, and ϕ is the flux. The subsequent rise in the multiplication constant is due to the initial high rate of plutonium-239 (Pu-239) production. This is known as the plutonium peak. The Pu-239 is produced from neutron capture reactions in uranium-238 (U-238). The plutonium continues to be produced however the U-235 decreases at a faster rate. This leads to the steady decline in the multiplication constant [35].

$$\frac{d\mathrm{I}}{dt} = \gamma_{\mathrm{I}}\Sigma_f\phi - \lambda_{\mathrm{I}}\mathrm{I} \tag{19}$$

$$\frac{d\mathrm{Xe}}{dt} = \lambda_{\mathrm{I}}\mathrm{I} + \gamma_{\mathrm{Xe}}\Sigma_f\phi - \lambda_{\mathrm{Xe}}\mathrm{Xe} - \sigma_{\mathrm{Xe}}\mathrm{Xe}\phi \tag{20}$$

The infinite multiplication factor of a standard 37-element CANDU lattice is compared to that of a modified bundle in Fig. (21). For the modified bundle, the fuel has been removed from the center pin and replaced with pure metallic Mo-98. Initially, the two are very similar and deviate gradually as burnup

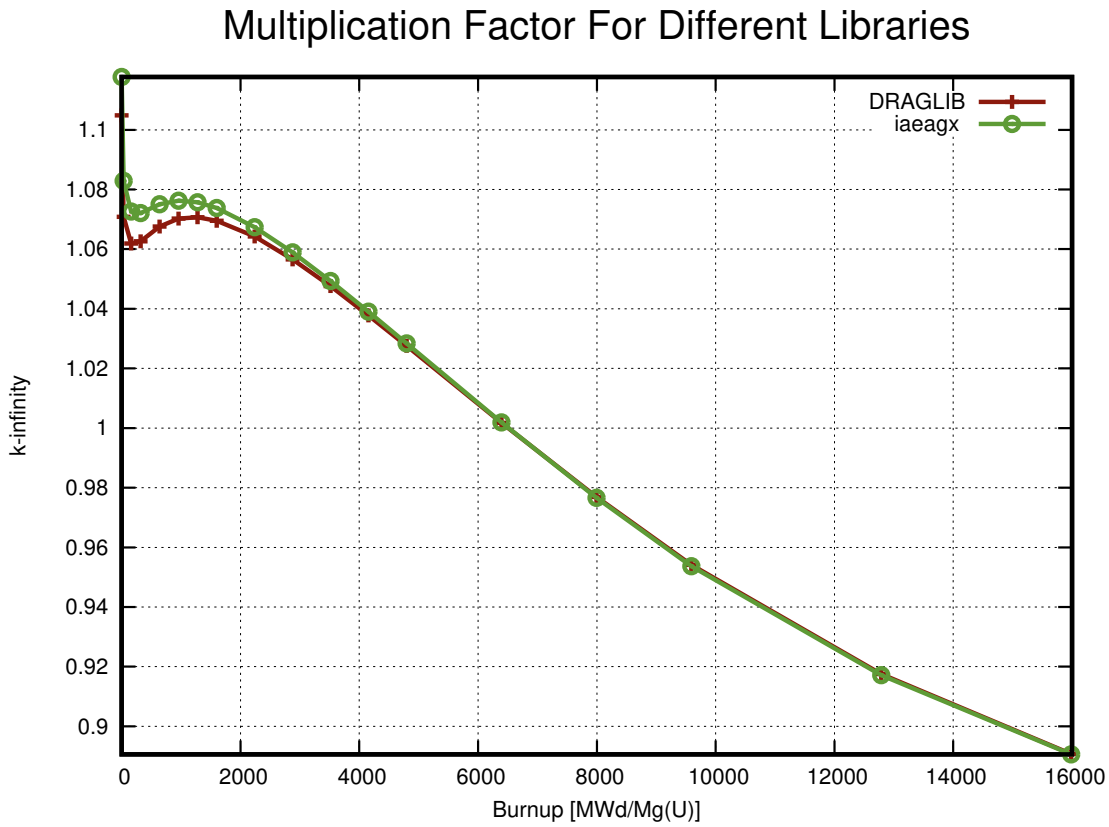

Figure 19: The infinite multiplication factor of a 37-element CANDU lattice for different multi-group cross-section libraries.

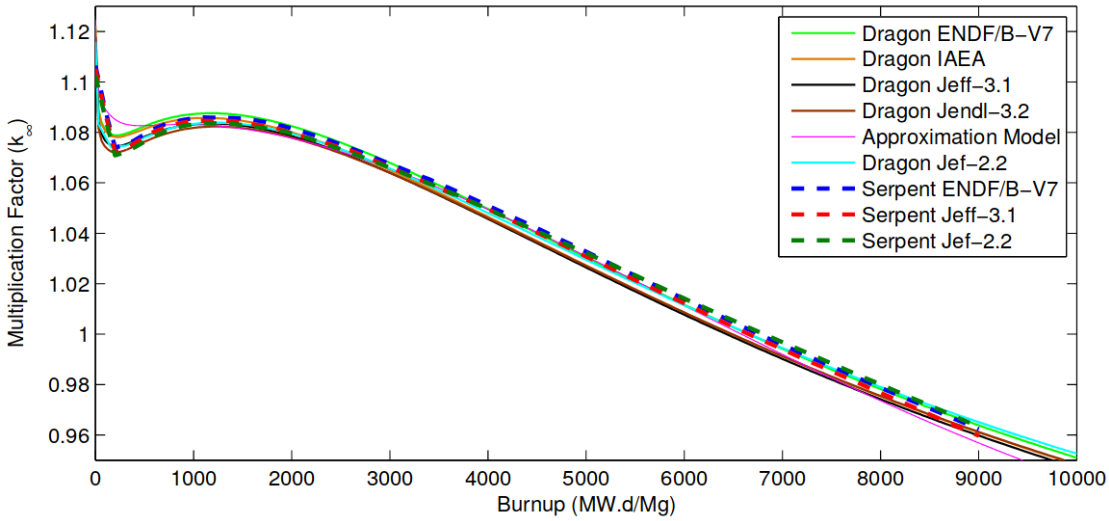

Figure 20: Reference data for the infinite multiplication factor produced with different libraries and codes [31].

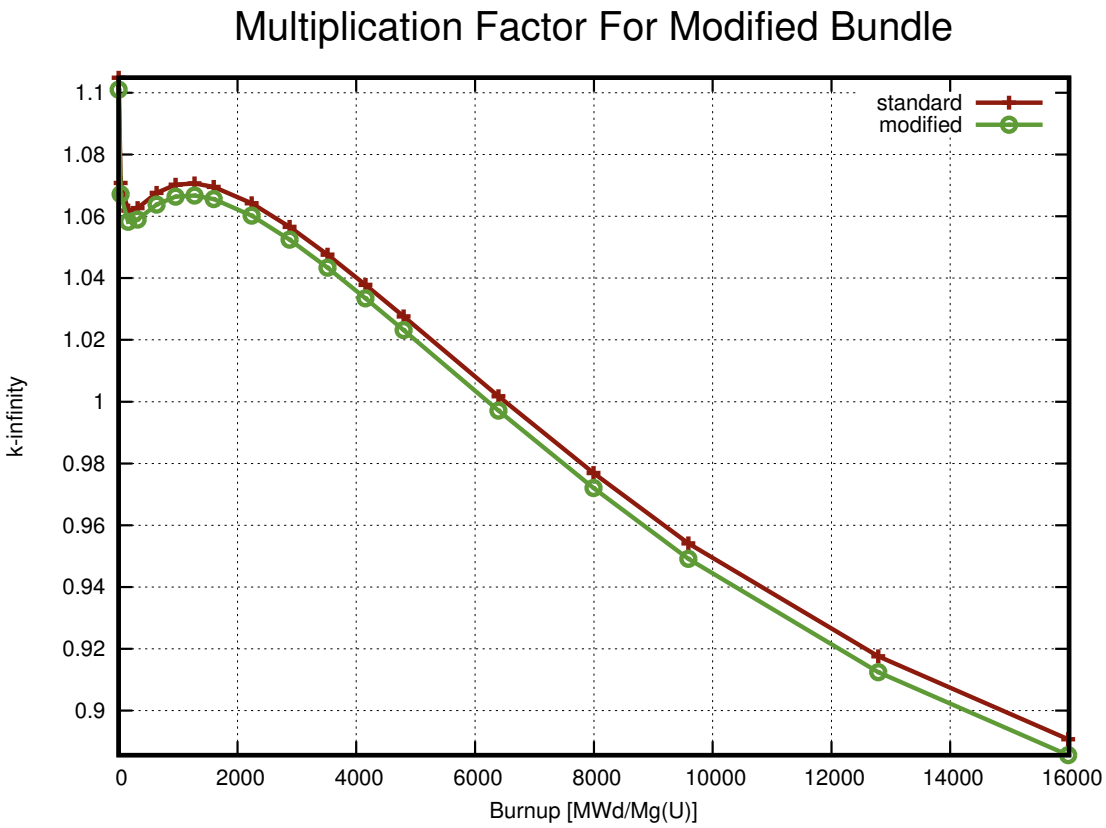

Figure 21: The reactivity of a 37-element CANDU lattice with a modified center pin. The center pin contains pure metallic Mo-98.

increases. At $16,000$MWd/Mg(U) the reactivity of the modified bundle is approximately 6.5mk less than the standard bundle.

3.3 DONJON Core Code

DONJON is a computer code developed by École Polytechnique de Montréal. It is a full-core modeling code designed around solution techniques of the neutron diffusion equation [32]. It is free to use and under the GNU Lesser General Public License as published by the Free Software Foundation [32]. DONJON was developed to analyze different types of nuclear reactors such as Pressurized Water Reactors (PWRs), legacy CANDU reactors, and Advanced CANDU Reactors (ACRs) [32]. It is divided into calculation modules, that can be linked together using the GAN generalized driver [32]. DONJON execution requires the use of DRAGON, which provides the macroscopic cross-section libraries and micro-depletion calculations [32]. The calculations performed by DONJON can be used to determine the power and normalized flux distributions over the reactor core [32]. DONJON version 5.0.4 was used to perform all full core simulations in this work.

3.3.1 Solution of the diffusion equation

The neutron transport equation used in lattice calculations is too computationally intensive to be used for an entire 3-D reactor core. The diffusion equation, Eq. (21), is instead used for this application. The diffusion equation takes much less computational effort to solve though it is less accurate than the transport equation, especially near the edge of the reactor or near an highly absorbing medium. The diffusion equation makes the assumption that the overall flow of neutrons in a reactor core behave similarly to molecules in a gas. Whereby the trajectory of the molecules can be predicted by the use of Fick's Law, which states that the motion of molecules in a gaseous medium will be proportional to the negative of the gradient of concentration of molecules within the medium. In a reactor, it is the neutron current density that is proportional to the negative of the gradient of neutron flux. The proportionality constant is known as the diffusion coefficient 'D', and is can be expressed in terms of transport theory terms and absorption cross-sections. Thus the solution to the neutron transport equation for a lattice must first be solved in order to provide the necessary information to solve the diffusion equation for the entire reactor. Also, the transport equation is solved in the number of groups that are provided by the multi-group library. In this case, the library provided is 172 groups. Typically, only two groups are required to perform a reactor analysis with the diffusion equation. The condensation from 172 groups to two groups is performed by DRAGON during the lattice computation. The two groups are known as the fast group, and the thermal group. The separation energy used is 0.625eV. This is the same separation energy used in *Analysis of Transuranic Mixed Oxide Fuel in a CANDU Nuclear Reactor* (Morreale, 2012) which used DRAGON, WIMS-AECL (transport lattice code), and RFSP (diffusion core code) to analyze alternative fuels for CANDU reactors.

$$\begin{aligned} S\left(\vec{r},E\right)+\chi\left(E\right)\int_{E}\nu\Sigma_{f}\left(\vec{r},E'\right)\phi\left(\vec{r},E'\right)dE'+\int_{E'}\Sigma_{S}\left(r,E'\rightarrow E\right)\phi\left(r,E'\right)dE' \\ -\Sigma_{t}\left(\vec{r},E\right)\phi\left(\vec{r},E\right)+\vec{\nabla}\cdot D\left(\vec{r},E\right)\nabla\phi\left(\vec{r},E\right)=0 \end{aligned} \tag{21}$$

As with the transport equation, the diffusion equation also needs to be discretized. DONJON uses the finite-difference method to solve the two-group diffusion equation, Eq. (22).

$$\begin{aligned} &-\nabla\cdot D_1(r)\nabla\phi_1(r)+(\Sigma_{a1}(r)+\Sigma_{1\rightarrow2}(r))\phi_1(r)-\frac{\nu\Sigma_{f2}(r)\phi_2(r)}{k_{\text{eff}}}=0 \\ &-\nabla\cdot D_2(r)\nabla\phi_2(r)+\Sigma_{a2}(r)\phi_2(r)-\Sigma_{1\rightarrow2}(r)\phi_1(r)=0 \end{aligned} \tag{22}$$

The finite-difference method solves for the flux at the midpoints of each cell. It assumes each cell is homogeneous; the properties for each cell are the same for every point within that cell. The flux leakage out of each cell also needs to be calculated. To do so, Eq. (23) is used where the superscripts 'C', and 'L' refer to the center cell, ie. the cell being solved for, and the the cell directly to it's left. 'CL' refers to the interface between cells 'C' and 'L'.

$$\phi_2^{CL} = \frac{D_2^L \phi_2^L \Delta x^C + D_2^C \phi_2^C \Delta x^L}{D_2^L \Delta x^C + D_2^C \Delta x^L} \tag{23}$$

The leakage out of C across CL is then found by Eq. (24).

$$Leakage\ out\ of\ C\ across\ CL = \frac{2 D_2^C D_2^L \Delta y^C}{D_2^L \Delta x^C + D_2^C \Delta x^L} \tag{24}$$

The total leakage out of cell 'C' can then be found with Eq. (25).

$$\begin{aligned} A_2^{CL}(\phi_2^C - \phi_2^L) + A_2^{CR}(\phi_2^C - \phi_2^R) + A_2^{CT}(\phi_2^C - \phi_2^T) + A_2^{CB}(\phi_2^C - \phi_2^B) \\ = A_2^C \phi_2^C - (A_2^{CL}\phi_2^L + A_2^{CR}\phi_2^R + A_2^{CT}\phi_2^T + A_2^{CB}\phi_2^B) \end{aligned} \tag{25}$$

Where $A_2^{CL} \equiv \frac{2 D_2^C D_2^L \Delta y^C}{D_2^L \Delta x^C + D_2^C \Delta x^L}$ and $A_2^C \equiv A_2^{CL} + A_2^{CR} + A_2^{CT} + A_2^{CB}$

By substituting back into Eq. (22), we have the finite-difference method of the two-group diffusion equation in Eq. (26).

$$\begin{aligned} & A_1^C \phi_1^C + (\Sigma_{a1}^C + \Sigma_{1\to 2}^C)\phi_1^C V^C - \frac{\nu \Sigma_{f2}^C \phi_2^C V^C}{k_{\text{eff}}} = A_1^{CL}\phi_1^L + A_1^{CR}\phi_1^R + A_1^{CT}\phi_1^T + A_1^{CB}\phi_1^B \\ & - \Sigma_{1\to 2}^C \phi_1^C V^C + A_2^C \phi_2^C + \Sigma_{a2}^C \phi_2^C V^C = A_2^{CL}\phi_2^L + A_2^{CR}\phi_2^R + A_2^{CT}\phi_2^T + A_2^{CB}\phi_2^B \end{aligned} \tag{26}$$

3.3.2 Time-average simulation

A CANDU reactor is being continuously refuelled online. Therefore, there is in essence no beginning and end time to simulate the reactor. In order to gain insight into the parameters of the core, a time-average model is used. This is where the lattice cross-sections are averaged over the residence time of the fuel at every point in the core. The cross-sections are averaged over the entrance and exit irradiation values required to maintain a critical reactor for a given bundle-shift. The target exit irradiations, or exit-burnup as well as the bundle-shift are provided by the user. DONJON then solves the diffusion equation normalized to a given total reactor power. The time-averaged solution determines the power distribution, the refuelling frequency, as well as the the exit burnup for all of the channels in the core [33]. The time-average calculation is performed in considering the bidirectional refuelling scheme of reactor channels and assuming that all channels have the same bundle-shift.

The calculation scheme used to compute the reactor core properties in DONJON can be viewed in Fig. (22). A 2x2x2 coarse mesh was used for the full core simulations as coarse-meshing has been shown to provide more accurate results than fine-meshing in CANDU-type reactor simulations [34]. The time-average calculation is an iterative process that repeats all the steps required to compute the axial power-shape. The process is repeated until the relative error between two successive axial power-shape calculations reaches a requested convergence. In this case the requested convergence was 1.0×10^{-05}.

The DONJON modules perform the following tasks:

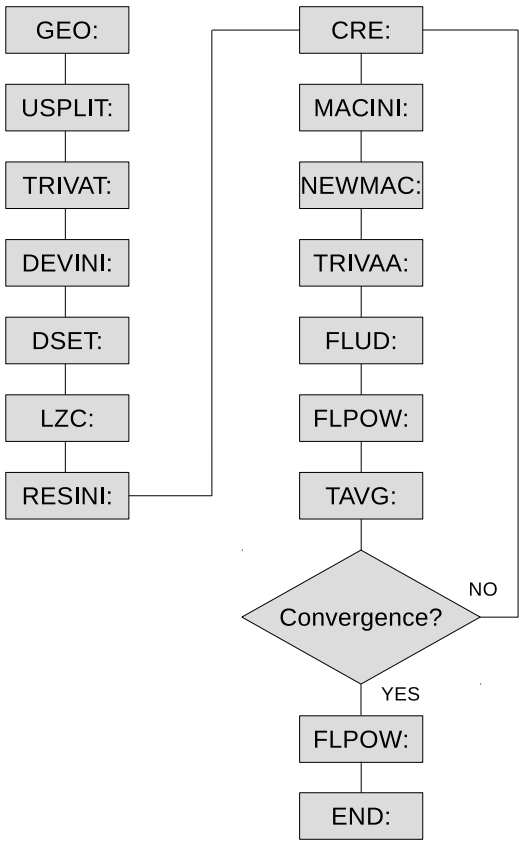

Figure 22: DONJON calculation scheme.

GEO: used to generate core geometry

USPLIT: used to perform mesh splitting and to determine mixture indices

TRIVAT: used to perform TRIVAC-type tracking on the geometry

DEVINI: used to model 3-D rod-type devices in the reactor core

DSET: used to set new device parameters

LZC: used to model 3-D liquid zone controllers in the reactor core

RESINI: used to define the fuel lattice, to generate a fuel-map, and set local and global parameters

CRE: used to generate a library containing the material properties by interpolating the nuclear properties from a mono-parameter database produced by DRAGON

MACINI: used to generate an extended library where the properties per material region over the entire reactor core are stored

NEWMAC: used to generate an extended library that contains updated material properties computed with respect to the device locations

TRIVAA: used to generate systems matrices which are necessary to perform flux calculations

FLUD: used to determine the flux distribution in the reactor core

FLPOW: used to compute and print powers and normalized fluxes over the reactor core

TAVG: used to perform burnup calculations according to the time-average model. Computes burnup integration limits, core-average exit burnup, axial power-shapes and channel refuelling rates

END: used to terminate DONJON

There are 480 channels in a CANDU-9 reactor. The channel numbering scheme as well as the alphanumeric channel naming scheme are provided in Fig. (23). This is a face view of the reactor. Here it can be seen that channel number 1 corresponds to channel A8. DONJON requires a target exit-burnup for every region in the core. For the following time-average simulations the core was divided into three separate regions: outer, middle, and center. With a greater number of regions, more accurate control over the reactor parameters can be obtained. Doing so requires more input from the user and adds to the complexity of fine tuning the exit-burnups to achieve a critical reactor. The time-average calculation scheme shown above had to be repeated many times while adjusting the exit-burnups and liquid zone controller levels until an acceptable multiplication factor and power profile was achieved. The power profile is expressed through form factors that are detailed in Section (3.3.4). The exit-burnups used in

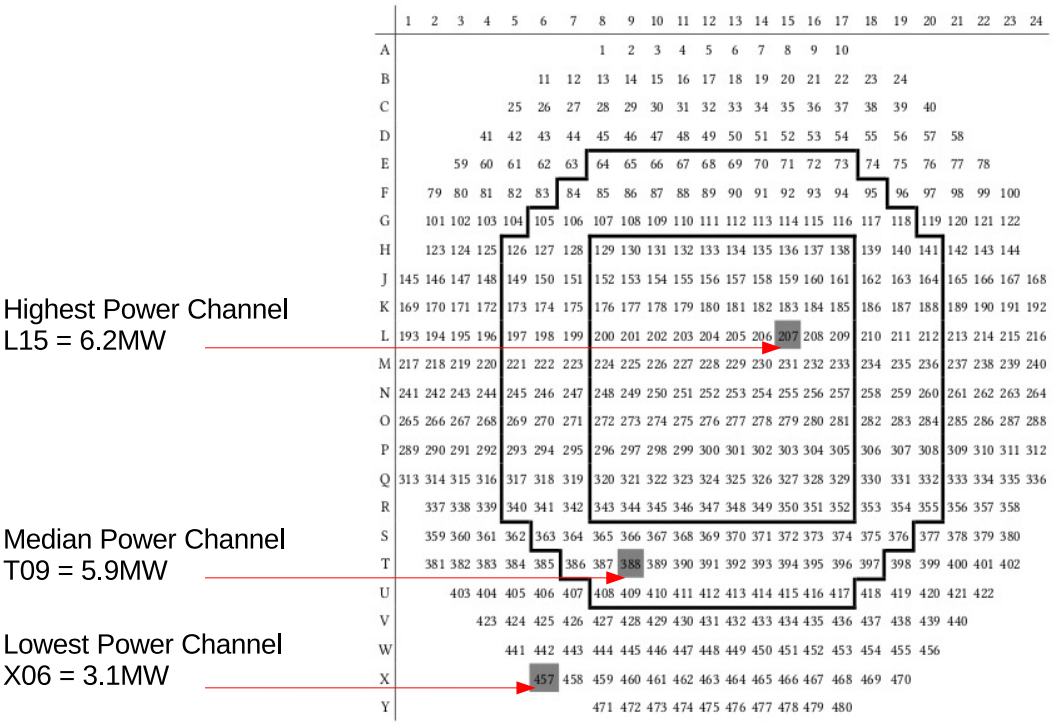

Figure 23: Face view of the reactor showing channel numbers and naming system.

the time-average simulations are provided in Tab. (4). A four-bundle-shift was used for every channel and the flux was normalized to a total reactor power of $2,600$MW.

The three highlighted channels in Fig. (23) refer to the channels that were chosen to be loaded with the modified bundles. In the initial time-average simulation all 480 channels were loaded with standard bundles. These were the channels with the maximum, minimum, and median power output. These channels, ranging from lowest to highest power, were chosen to be loaded with the modified bundles in subsequent simulations. This was done to analyze the effect of radioisotope production when placed in different regions of the core as well as the overall effect on the core itself by placing modified bundles in different channels.

Region	Burnup [MWd/Mg(U)]
Outer	8685.0
Middle	7585.0
Center	7510.0

Table 4: Exit-burnups provided for the different regions of the core.

3.3.3 Reactivity Devices

CANDU-9 reactors contain several reactivity control, and safety devices. There are two spatially and functionally separate special shutdown systems (SDS) [35]. The first system (SDS-1) consists of 32 cadmium shutoff rods that fall into the core from above [35]. The second system (SDS-2) consists of six horizontal high-pressure injection nozzles, that inject poison into the moderator [35]. The poison is a gadolinium solution. Cadmium and gadolinium have large neutron absorption cross-sections. Each system can insert over 50mk of negative reactivity into the core in approximately one second [35]. These safety devices were not modelled in this work as only steady-state reactor conditions were of interest.

There are four reactivity control devices. These are the liquid zone controllers, adjuster rods, mechanical control absorbers, and moderator poison. There are 14 liquid zone controllers. These contain variable amounts of light water that, as previously mentioned, absorbs neutrons at a greater rate than heavy water and thus represents a negative reactivity insertion. The water levels in the LZCs can be set individually so that the power distribution in the core can be finely tuned to counter any reactivity insertions such as fresh fuel into the core. When all of the LZCs are filled they have a total negative reactivity worth of $6 - 7$mk [35]. There are 24 adjuster rods. These are typically constructed of stainless steel, though some contain cobalt in order to produce Co-60. The adjuster rods are normally fully inserted into the reactor core and only driven out when positive reactivity is required [35]. Their total negative reactivity worth is approximately 17mk [35]. The adjuster rods and LZCs also help to flatten the power distribution. Doing so allows a higher total reactor power to be produced without exceeding bundle or channel power limits [35]. The mechanical control absorbers, and moderator poison are not typically in use during steady-state conditions and so they were not modelled in this work. The locations in the core of the various reactivity control devices can be viewed in Figs. (24, 25, 26).

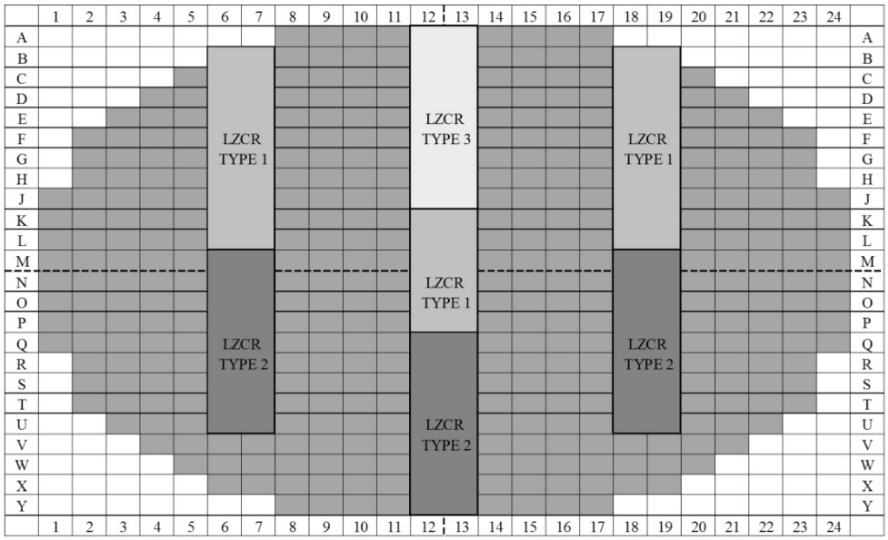

Figure 24: Face view of CANDU-9 liquid zone controller locations [36].

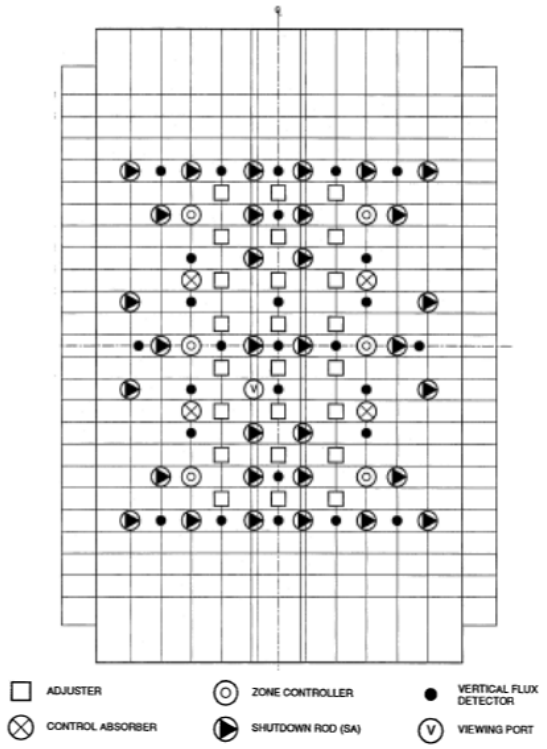

Figure 25: Top view of CANDU-9 reactivity control device locations [35]

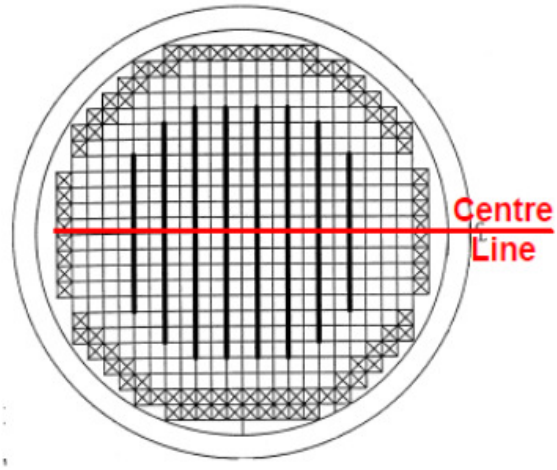

Figure 26: Face view of CANDU-9 adjuster rod locations [35]

3.3.4 CANDU-9 Core Benchmark Results

An initial time-average simulation was done with standard bundles throughout the entire core to establish a benchmark. The results are shown in Fig. (27), which gives a face few of the reactor displaying the channel powers. Fig. (28) is a surface plot showing the channel powers. From these figures it is apparent that the flux has been flatted by the adjuster rods, and liquid zone controllers. The same core was also modeled with the LZCs and adjuster rods removed and can be viewed in Fig. (29).

The maximum, minimum, and median power channels were chosen as candidates for the modified bundles. These channels were 457 (X06), 388 (T09), and 207 (L15), and their powers were $3,077.3$kW, $5,884.5$kW, and $6,168.6$kW respectively. Three subsequent time-average simulations were performed placing modified bundles in one of the three channels in order to analyze any deviations in the cores parameters from the benchmark. The modified bundles in these cases had the fuel from the center pin replaced with enriched metallic molybdenum. The parameters have been recorded and placed in Tab. (5). As can be seen from the results, the modified bundles alter the parameters of the core only marginally. The change in reactivity of the core is on the order of -0.01mk from the benchmark to the case where the modified bundles are placed in the highest power channel (324). The form factors are various parameters of interest that give power ratios within the core. The radial form factor is the average channel power divided by the maximum channel power. The axial form factor is the maximum channel power divided by the product of the maximum bundle power with the number of bundles in a channel. The overall form factor is the average bundle power divided by the maximum bundle power. These factors depict the various elements of the power profile of the core, and are important when attempting to attain an optimal power distribution.

The data presented in Tab. (6) is taken from previous academic work entitled *Analysis of Transuranic Mixed Oxide Fuel in a CANDU Nuclear Reactor* (Morreale, 2012) where a CANDU-9 reactor was modeled with both standard 37-element fuel bundles and modified bundles containing transuranic mixed oxide

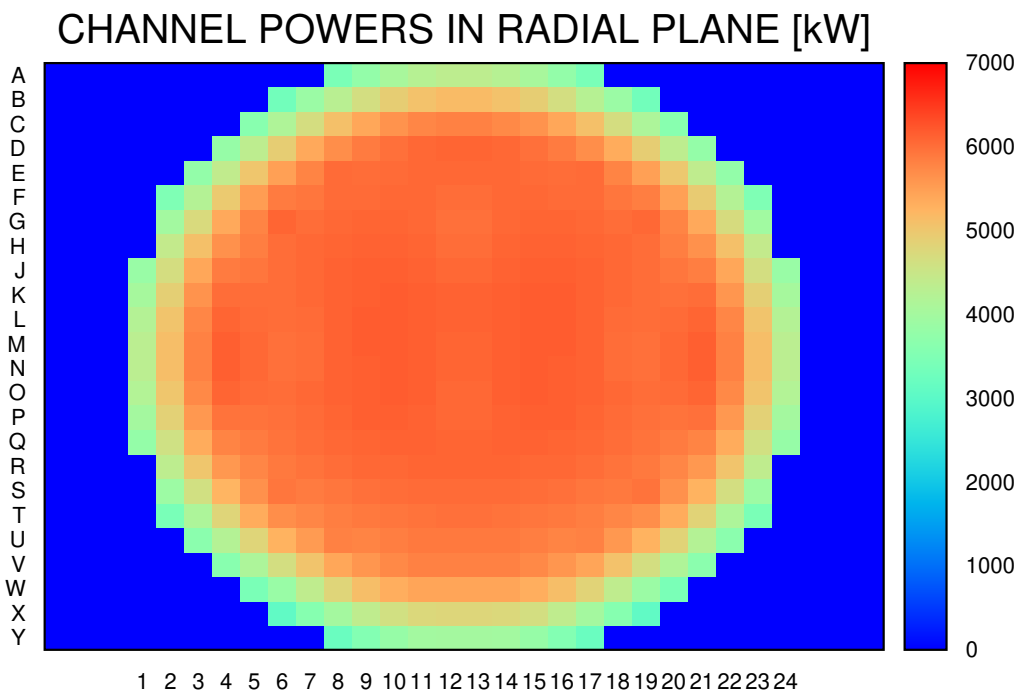

Figure 27: Face view of the reactor showing the channel powers in kilowatts.

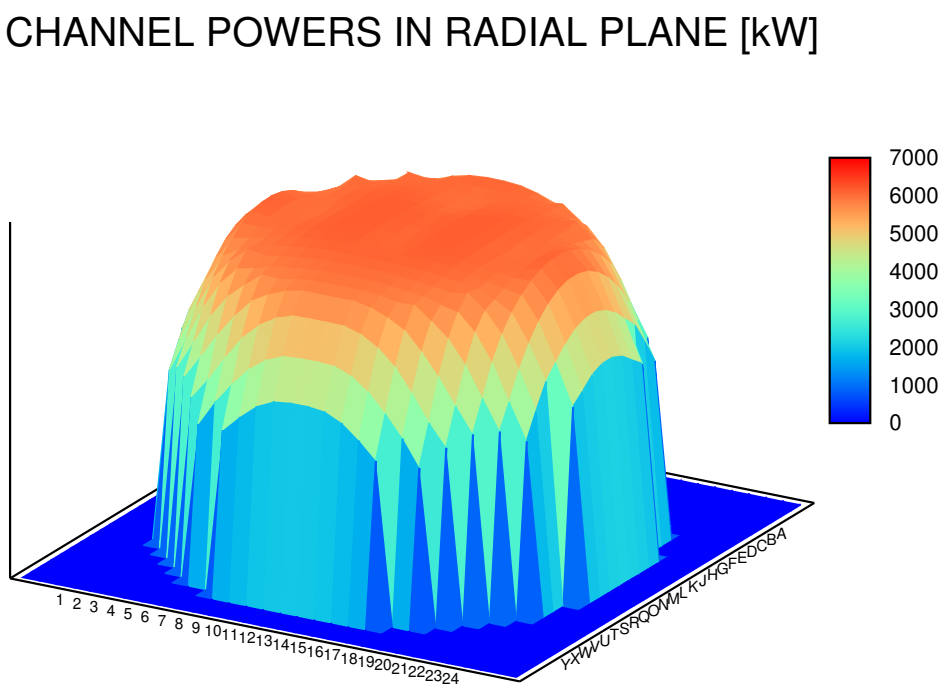

Figure 28: Surface plot of the reactor showing the channel powers in kilowatts.

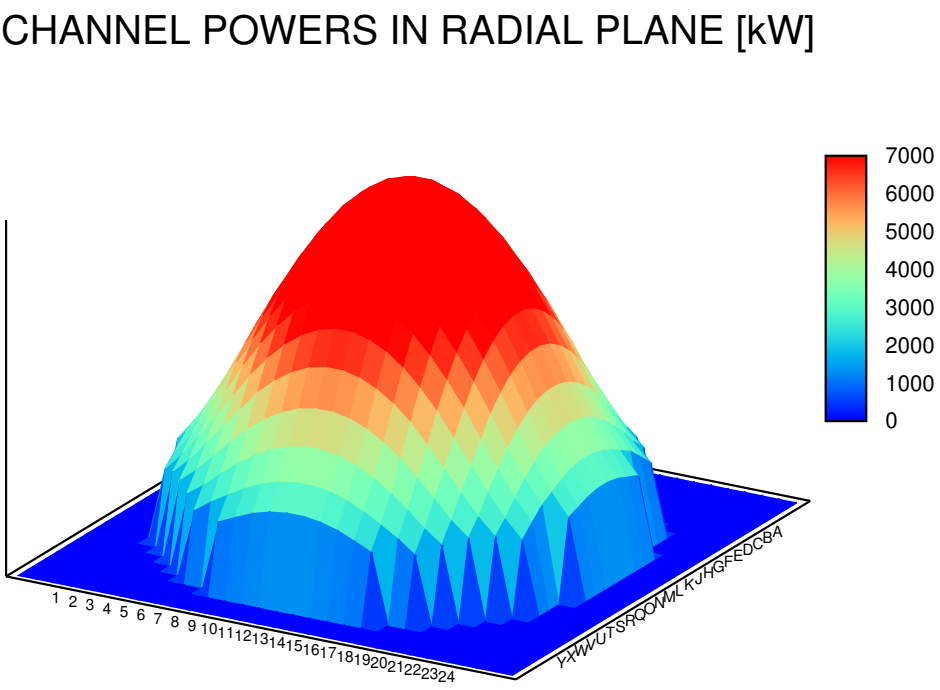

Figure 29: Surface plot of the reactor without reactivity devices.

Parameter	Unit	Standard Bundle		Modified Bundle		
		no devices	with devices	X06	T09	L15
k_{eff}		1.026e+00	1.000e+00	1.000e+00	9.999e-01	9.999e-01
Reactivity	mk	2.607e+01	5.364e-03	2.264e-03	-6.079e-03	-7.152e-03
Core-Average Exit Burnup	MWd/Mg(U)	7.880e+03	8.036e+03	8.035e+03	8.036e+03	8.036e+03
Maximum Bundle Power	kW	1.334e+03	8.790e+02	8.793e+02	8.794e+02	8.780e+02
Maximum Channel Power	kW	1.024e+04	6.168e+03	6.170e+03	6.175e+03	6.166e+03
Minimum Channel Power	kW	1.976e+03	3.077e+03	3.019e+03	3.064e+03	3.081e+03
Radial Form Factor		5.284e-01	8.780e-01	8.777e-01	8.771e-01	8.783e-01
Axial Form Factor		5.905e-01	5.398e-01	5.397e-01	5.401e-01	5.402e-01
Overall Form Factor		3.121e-01	4.739e-01	4.737e-01	4.737e-01	4.744e-01

Table 5: Core parameters showing the results of the benchmark simulation using all standard bundles, and subsequent simulations using modified bundles in selected channels.

(TRUMOX) fuel. When comparing the core parameters for a reactor loaded with standard 37-element bundles, it can be seen that both models show similar results for the reactivity, maximum channel power, and radial form factor. However, the core-average exit burnup, maximum bundle power, axial form factor, and overall form factor differ. The nature of the discrepancy is unclear as there are several factors to consider. The lattice and core codes WIMS-AECL and RFSP were used to produce the data in Tab. (6). Whereas DRAGON and DONJON were used in this work. There, the cross-sections of the reactivity control devices were modeled in a 3-D lattice using DRAGON. Here, the databases were borrowed from previous work that modeled a CANDU-6. There, the reactor was subdivided into seven irradiation regions, while only three regions were used here. Finally, Morreale used an 89-group ENDF/B-VI multi-group library while here, a custom 172-group JEFF/TENDL multi-group library was used. As previously shown, there can be some significant difference in results when different codes or different multi-group libraries are used. This work only uses the full core calculations to provide insight into the range of channel powers and bundle irradiation times to later simulate isotope production in a lattice calculation. Therefore, it is assumed that the relatively minor discrepancy is some of the core parameters between two models is non-critical.

Parameter	Unit	TRUMOX	Standard
k-effective		0.999	~ 1
Core-Average Exit Burnup	MWd/Mg(U)	2.998e+04	9.1e+03
Maximum Bundle Power	kW	7.78e+02	$\sim$ 7.5e+02
Maximum Channel Power	kW	6.32e+03	$\sim$ 6.5e+03
Radial Form Factor		0.874	$\sim$ 0.85
Axial Form Factor		0.625	0.625
Overall Form Factor		0.546	0.54

Table 6: Reference CANDU-9 core parameters from previous academic work [36].

3.4 Sensitivity to Uncertain Inputs

There always exists some uncertainty when modeling a system. Uncertainties arise as approximations are performed in order to simplify the system being modeled. These approximations are done to reduce the complexity and therefore, the computation time of the model. The uncertainty is the degree to which the approximation causes a deviation in the results of the model compared to actual results. Uncertainties also arise due to input data errors. In some cases, precise input data is not available and thus estimations are required. A balance must be made in order to minimize the uncertainty in a model without making the computation time absurdly long. There have been several approximations made in this work that were mentioned earlier. The 2-D lattice calculation performed by DRAGON is an approximation to a 3-D calculation. In this case the 2-D calculation takes much less computation time yet provides relatively accurate results. The equations used to track the neutrons in the lattice and full core calculations are themselves approximations.

The validity of any model relies on the accuracy and reliability of its output. The uncertainty due to modeling approximations using DRAGON/DONJON to model the multiplication factor and various other safety parameters is largely known and considered acceptable as DRAGON is an industry standard tool. It is commonly used in industry to perform safety analyses on CANDU reactors. Since the very same approximations used in previous work to model the lattice and reactor were also used in this work the uncertainty in these approximations are considered acceptable and ignored. However, the uncertainty in isotope production is less well known. Thus, a sensitivity analysis to uncertain inputs has been performed.

A sensitivity analysis attempts to determine which sources of input uncertainty have the largest effect on output uncertainty. This is often done by rerunning a model under different assumptions to determine what impact a certain variable will have on the output. The isotopic density of Mo-99 produced from an enriched metallic molybdenum target placed in channel X06 for 800 days was used to perform the sensitivity analysis. The tornado chart in Fig. (30) displays the sensitivity of uncertain inputs as the percent of relative difference from a benchmark case. The benchmark case uses all the

same assumptions that were used in the original lattice calculations. The isotopic density of Mo-99 in the benchmark case was $3.749 \times 10^{-07} atoms \cdot \mathrm{b}^{-1}\mathrm{cm}^{-1}$.

The time step category displays the sensitivity of the model to the amount of burnup calculations performed. Here the green portion represents a doubling of the amount of burnup calculations up to 800 days. The red portion represents dividing the amount of burnup calculations by a factor of two. The output is much more sensitive to the reduction in the number of burnup calculations than an increase.

In the density category the green portion represents a 10% increase in target density, and the red portion represents a 10% decrease in target density. The reason that this case was tested is because the density of a ceramic is largely a product of the sintering process and so the densities of all the ceramic targets should be considered estimations [37]. Here it can be seen that as the density increases so does the amount of Mo-99 produced.

The Eigenvalue category represents which fission source eigenvalue problem is to be treated when solving the linear system of multigroup collision probabilities. For the green portion (benchmark), the eigenvalue is the effective multiplication factor with a fixed buckling. For the red portion, the eigenvalue is the critical buckling with a fixed effective multiplication factor [29]. Here it can be seen that if the eigenvalue is the critical buckling then the there is slightly less Mo-99 produced.

The tracking category represents the angular quadrature and the density of integration lines used to track the geometry of the lattice cell. The green portion represents a doubling of both of these parameters, while the red portion represents a halving. Here it can be seen that increasing these parameters has next to no effect on the output. However, decreasing these parameters reduces the amount of Mo-99 produced.

The geometry category represents whether an annular or Cartesian cell was used. As can be seen, the geometry of lattice has no effect on the output.

The meshing category represents the amount of regions in the center pin used to compute the collision probability matrices. Here, the green portion represents a doubling of the amount of regions, while the red portion represents a division by a factor of two. Here, using finer meshing decreases the amount of Mo-99 produced. Coarser meshing increases the amount of Mo-99 produced by approximately the same amount, although in both cases the deviation from the benchmark case is marginal.

The output is most sensitive to the amount of burnup calculations although, increasing the amount of calculations beyond the benchmark case produces little benefit at the cost of greater computation time. The time step, tracking, geometry, and meshing categories have been optimized in previous work. It is therefore not surprising to find that increasing any of the parameters provides little benefit at the cost of computation time. For this reason, the benchmark parameters for all these categories were used for all of the subsequent lattice calculations. The input with the greatest amount of uncertainty is therefore the density of the ceramic targets.

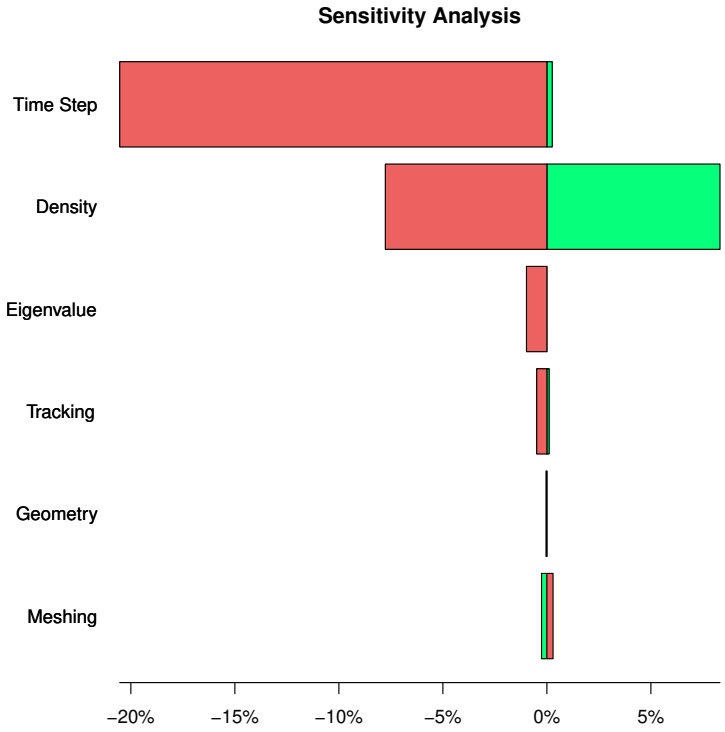

Figure 30: Sensitivity analysis of various input parameters.

4 Results and Discussion

The results for the various simulations are grouped into the first set of DRAGON simulations, and the second set of DRAGON simulations. In the first set, the isotopic densities of the various radioisotopes of interest are presented. The second set is further subdivided into three groups. These groups present the results for Mo-99, Lu-177, and the alpha-emitters respectively. In the second set, the isotopic densities, mass, and specific activity of these isotopes are presented. It is important to note that isotopic density of an isotope is a parameter that is tracked by DRAGON, and so these figures are taken directly from the DRAGON results. The reason for the odd units can be explained by viewing Eqs. (27,28). Where Σ is the macroscopic cross-section, N is the atomic density, and σ is the microscopic cross-section. The mass and specific activity are not tracked by DRAGON directly. These results are calculated based off of the isotopic densities. The calculations used to determine the mass, and specific activity of the isotopes are outlined in Appendix A.

$$\Sigma \equiv N\sigma \tag{27}$$

$$[\Sigma] = cm^{-1}, \quad [\sigma] = b = cm^{-24} \tag{28}$$

4.1 First Set of DRAGON Simulations

There are various possible targets that could be used to produce Mo-99 by the neutron capture method. Metallic molybdenum, and molybdic oxide were chosen as these are common targets that are already used. Metallic molybdenum generally leads to greater specific activity Mo-99, though the post irradiation processing is considered more difficult. Enrichment of the targets in terms of Mo-98 content also increases specific activity. In Fig. (31) the isotopic density of Mo-99 for different targets is shown. Here the Mo-98 targets use 100% Mo-98. The natural targets use the isotopic concentration of molybdenum found in nature. Here it can be seen that the enrichment of Mo-98 increases the amount of Mo-99 produced.

The metallic targets produce greater amounts of Mo-99 than the oxide of equivalent enrichment. It should be noted however, that the density is calculated over the entire mixture. Since the metallic molybdenum does not include oxygen, there is more molybdenum present in the pin. It is therefore difficult to determine what type of target actually produces the most Mo-99 as a percentage of molybdenum initially present. A further analysis would have to be performed in order to determine whether the cost of enrichment or processing is worth the additional Mo-99 produced. It should also be noted that there is little benefit of burning the bundle anymore than $1,000$MWd/Mg(U) as the amount of Mo-99 produced past this point is relatively small, especially for the natural MoO_3 target. If an emphasis is placed on Mo-99 production then that particular channel could be fuel at a higher frequency, though this would also increase the reactivity in the area surrounding the channel. This could be mitigated by reducing the refuelling frequency of the surrounding channels. In this scenario, a target of highly enriched metallic molybdenum might be preferable. If, on the other hand, the emphasis is placed on maintaining benchmark reactor parameters, then a natural MoO_3 may be preferable.

For the Lu-177 simulations there are two commonly used targets, Lu_2O_3, and Yb_2O_3. Here enriched signifies an 82% enrichment of Lu-176, and not 100%. This is due to the fact that 82% enrichment is the highest level of enrichment commercially available. For Yb_2O_3, enriched signifies 100% Yb-166. As with molybdenum, natural Lu_2O_3 refers to the isotopic concentration of lutetium found in nature. As can be seen in Fig. (32) the enriched lutetium target produces the most Lu-177, while the ytterbium target produces the least. The natural lutetium target produces a peak at $1,000$MWd/Mg(U). This is due to the fact that Lu-177 has a half-life of 6.65 days. Natural lutetium is composed of 97.5% Lu-175, and 2.5% Lu-176. Initially Lu-177 is produced directly from this amount of Lu-176. Later, Lu-177 is produced from Lu-176 that was produced from Lu-175 after it has captured a neutron. The rate of production of Lu-177 slows once the initial amount of Lu-176 has been depleted. The same is true for the enriched lutetium target though it is not as significant in this case, as there is much more Lu-176 to begin with. Once all of the initial Lu-176 has be depleted, the production and decay of Lu-177 reaches an equilibrium. Due to the high cost of lutetium, especially the enriched targets, it is conceivable that a higher refuelling rate be adopted so that less of the target is consumed to produce the same amount of Lu-177. It should be noted that the amount of Lu-177 produced is two orders of magnitude greater than the amount of

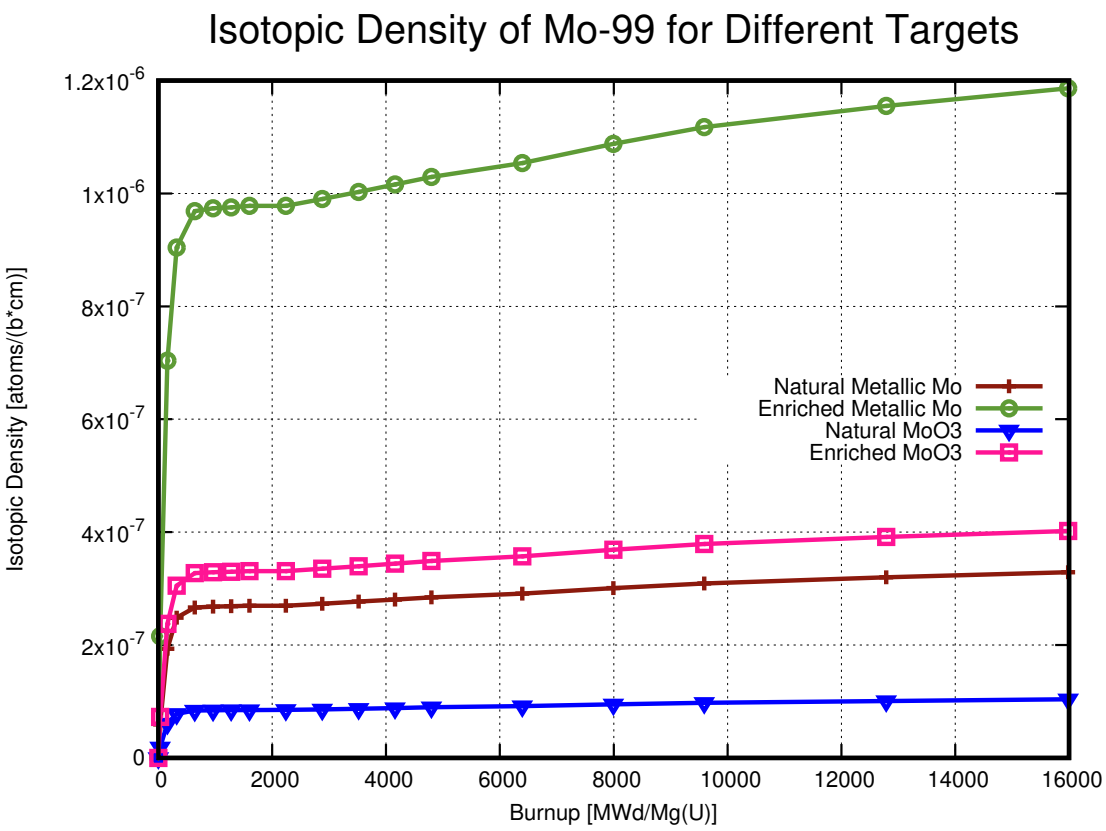

Figure 31: DRAGON lattice simulation with burnup showing the isotopic density of Mo-99. Different targets were placed in the center pin of a 37-element CANDU bundle.

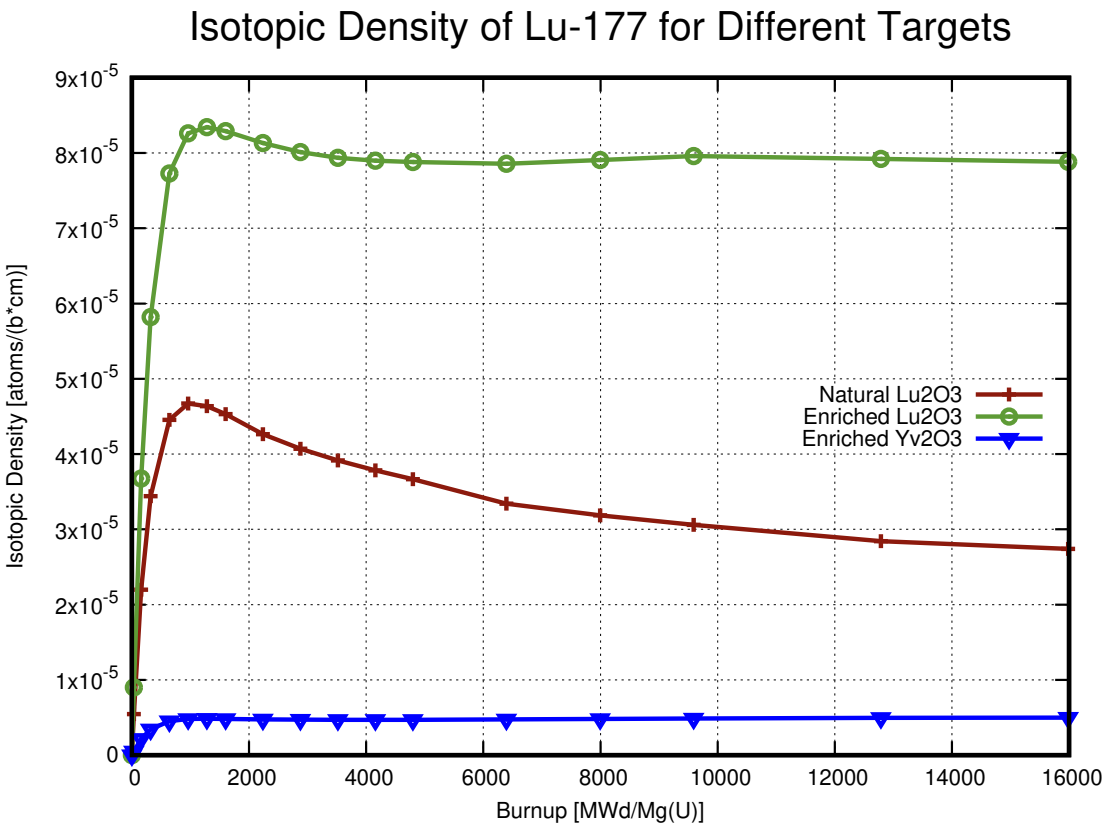

Figure 32: DRAGON lattice simulation with burnup showing the isotopic density of Lu-177. Different targets were placed in the center pin of a 37-element CANDU bundle.

Mo-99 produced.

For the alpha-emitters, only one target has been chosen, $RaCO_3$. In this case the radium is 100% Ra-226. Radium carbonate has been chosen for the target as this was the target that was used in the first synthesis of Ac-227. Here, the information is divided into two graphs. The first graph shows the production of Ac-227, Th-228, and Th-229. The second graph shows the production of Th-227, Ra-224, and Ac-225. The second set of isotopes are mostly produced from the decay of the first set of isotopes. They are therefore termed the secondary isotopes, whereas the first set are termed the primary isotopes. Ultimately the goal is to produce significant quantities of the alpha-emitters: Ra-224, Bi-212, and Bi-213. The primary set of isotopes decay into the secondary set of isotopes that are used in generators to produce the final alpha-emitters. Therefore, all six radioisotopes presented are of interest. As an aside Ra-224 does not produce Bi-212 directly in a generator. It instead produces Pb-212, a beta-emitter that is used as an intermediary, and is itself used as an *in vivo* generator of sorts.

In Fig. (33) it can be seen that significant quantities of all the primary isotopes are produced. Here, the amount of each isotope continues to increase with burnup in contrast to the Mo-99 and Lu-177, which reached equilibrium early on. Only Ac-227 appears to be reaching equilibrium toward the 16, 000MWd/Mg(U) mark. In Fig. (34), all of the secondary isotopes increase with burnup as do the

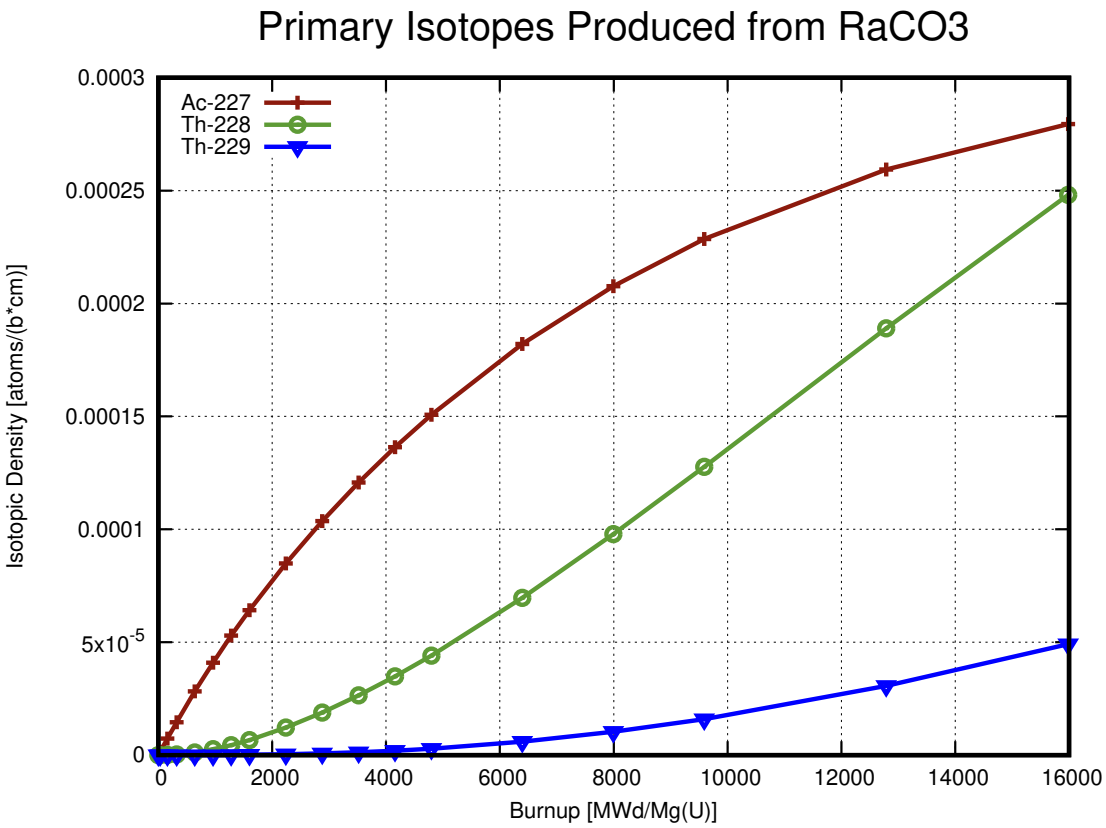

Figure 33: DRAGON lattice simulation with burnup showing the isotopic density of Ac-227, Th-228, and Th-229. A target of $RaCO_3$ was placed in the center pin of a 37-element CANDU bundle.

primary isotopes although the secondary isotopes are produced to a lesser degree than the primary ones. It should be noted that the production of secondary isotopes is on the same order of magnitude as Mo-99 produced in previous simulations while the primary isotopes are produced to the same degree as Lu-177. Here the best course of action would mostly likely be to let the bundles reside in the core as long as possible as none of the six isotopes of interest reaches equilibrium earlier than $16,000$MWd/Mg(U) of burnup.

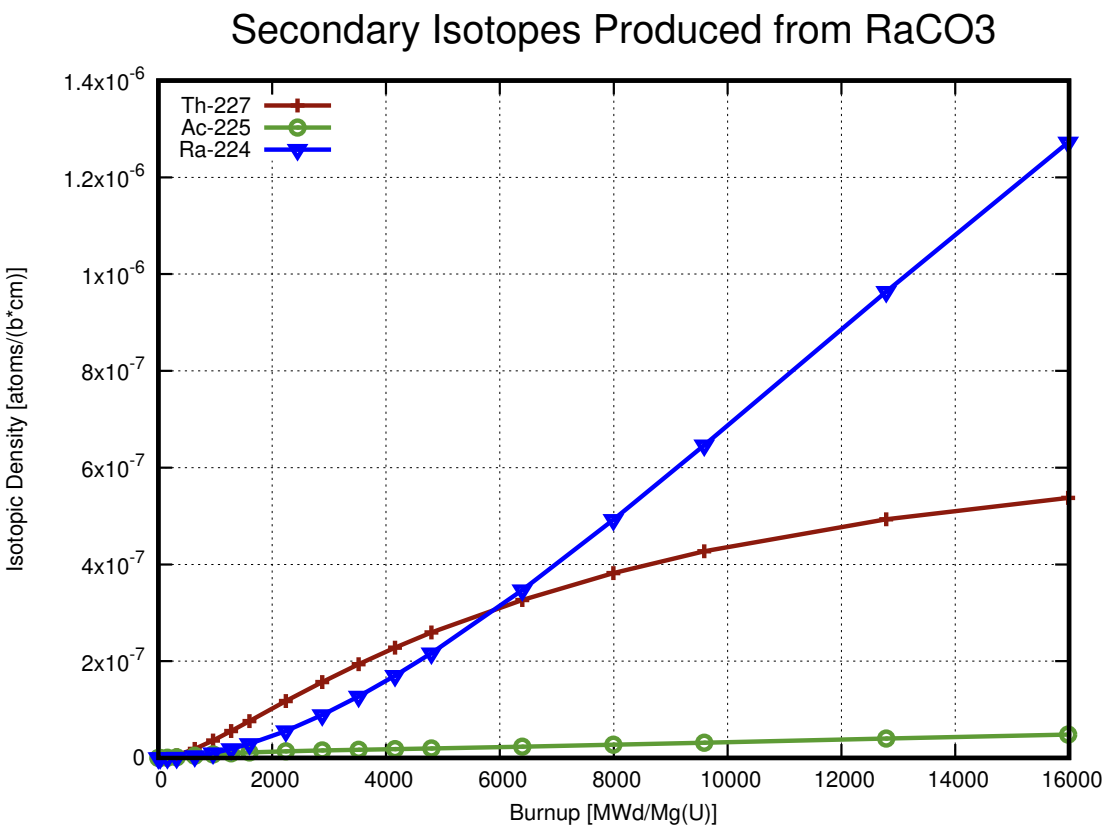

Figure 34: DRAGON lattice simulation with burnup showing the isotopic density of Th-227, Ra-224, and Ac-225. A target of $RaCO_3$ was placed in the center pin of a 37-element CANDU bundle.

4.2 Second Set of DRAGON Simulations

In the second set of DRAGON simulations, the burnup steps are calculated using the average bundle power for the channel that was loaded with that particular modified bundle. The amount of time that the burnup steps are calculated corresponds to the refuelling rate given by DONJON. The refuelling rate is the expected amount of fuel per channel that is loaded per day required to maintain criticality. This result has been converted to express the amount of time that a bundle resides in the fuel channel. The equation used to convert the refuelling rate is outlined in Appendix A. Therefore, in these DRAGON simulations all targets are burned at different power levels and for different amounts of time, depending on which channel that they are being loaded into. This is in contrast to the first set of simulations that used 31.971kW/kg for 500 days for each target. All of the specific activity, and mass calculations were done for the final data point for all simulations.

4.2.1 Mo-98

In Figs. (35-38) the amount of Mo-99 produced from each of the four molybdenum targets are shown when placed in channels X06, T09, and L15. In all cases channel, L15 produces the greatest amount of Mo-99, except for the enriched metallic target, which produces the same amount in channel L15 as it does in channel T09. This is expected as it is the channel with the highest average bundle power. When the targets are placed in channel L15, the results are similar to the first set of DRAGON simulations for all targets. Channel T09 produces slightly less Mo-99 in all cases, except for the enriched metallic target. Channel X06 produces approximately half the Mo-99 that channel T09 produces.

In Figs. (39-41) the amount of Mo-99 produced from different molybdenum targets is shown for each individual channel. For all three channels the enriched metallic molybdenum target produces the highest amount of Mo-99. The natural MoO_3 target produces the least amount of Mo-99 in each case, approximately an eighth compared to the enriched metallic molybdenum. Enrichment of the target produces more Mo-99 in each case, as do the metallic targets. More Mo-99 is also produced in channels with higher average bundle power.

In Fig. (42), the estimated specific activity of Mo-99 produced from different targets when placed in different channels is shown. In each case, channel L15 produces Mo-99 with a higher specific activity. Again, in each case, the enriched targets produce more than their natural counterparts with the enriched MoO_3 target producing the highest specific activity. The specific activity has greater dependence on enrichment than it does for the target material. The lowest specific activity achieved was approximately 30GBq/g for the natural metallic molybdenum target in channel X06. This is very similar to the results obtained by bombardment of natural MoO_3 targets placed in research reactors.

In Fig. (43), the amount of Mo-99 produced from different targets when placed in different channels is shown. Here, the most amount of Mo-99 produced is from the target of enriched metallic molybdenum. It produces approximately 7mg when placed in channel L15, but only 3.5mg when placed in channel

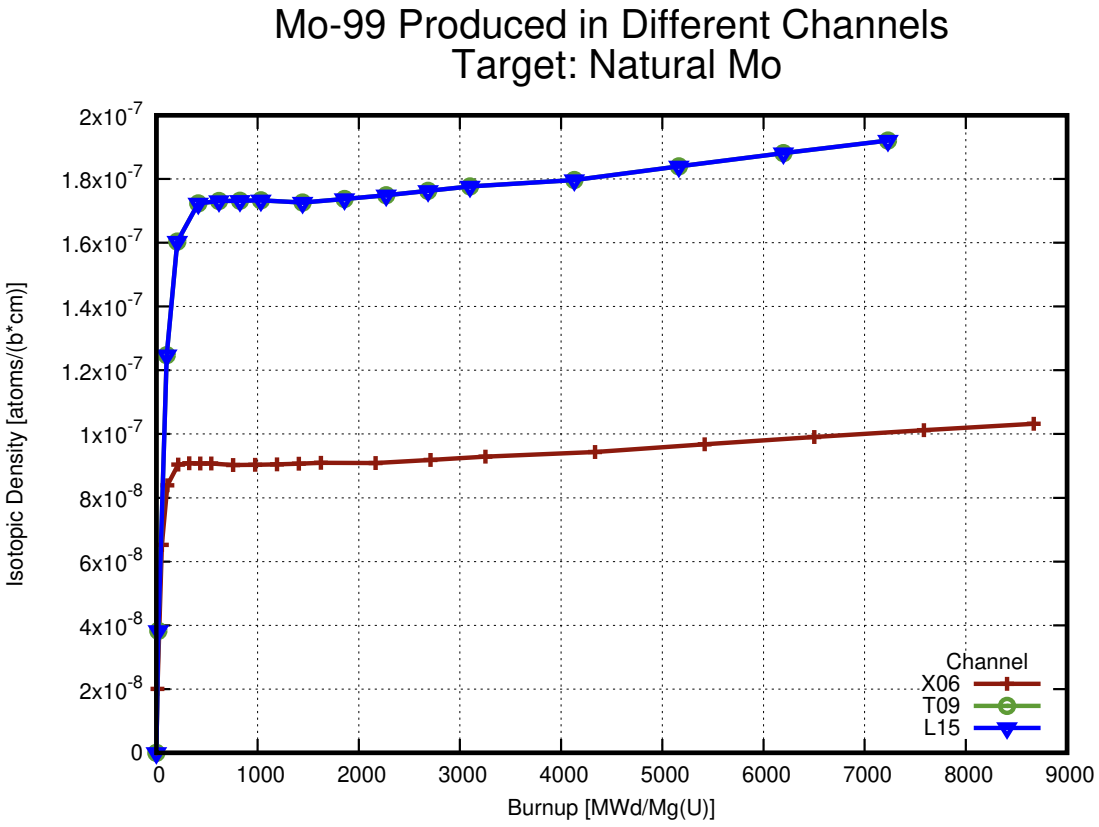

Figure 35: Natural metallic molybdenum placed in different channels.

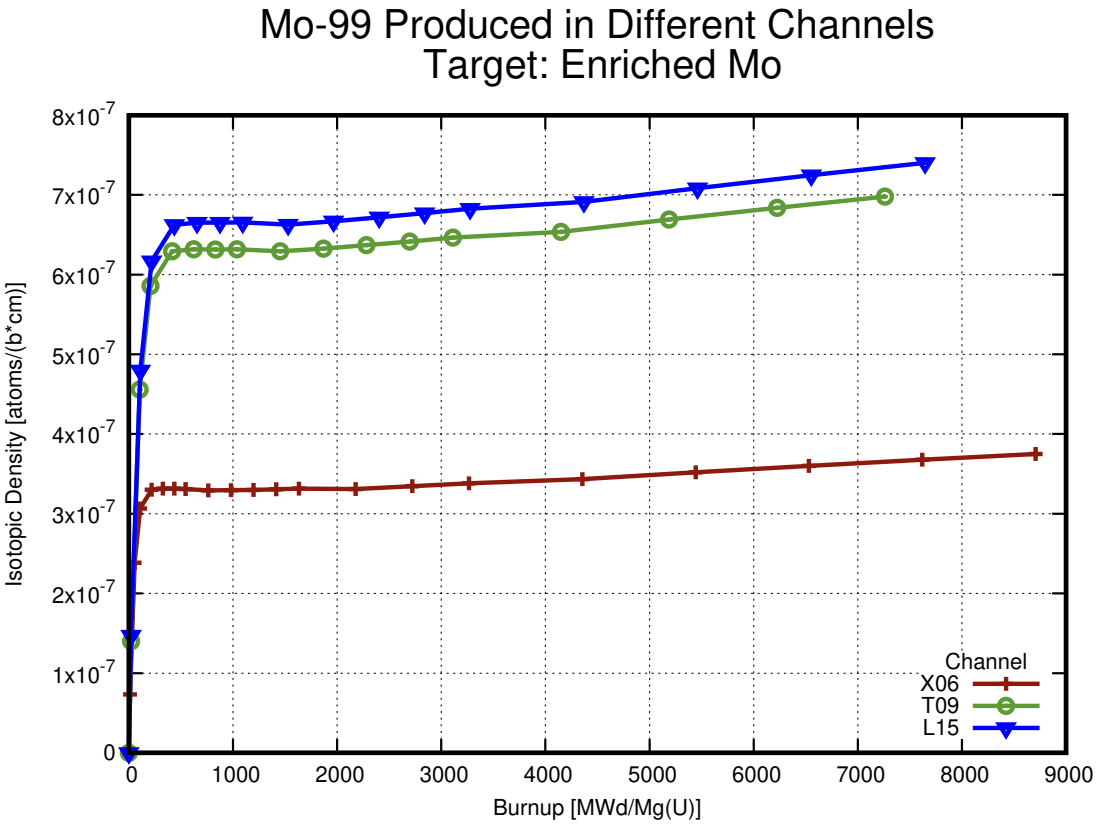

Figure 36: Enriched metallic molybdenum placed in different channels.

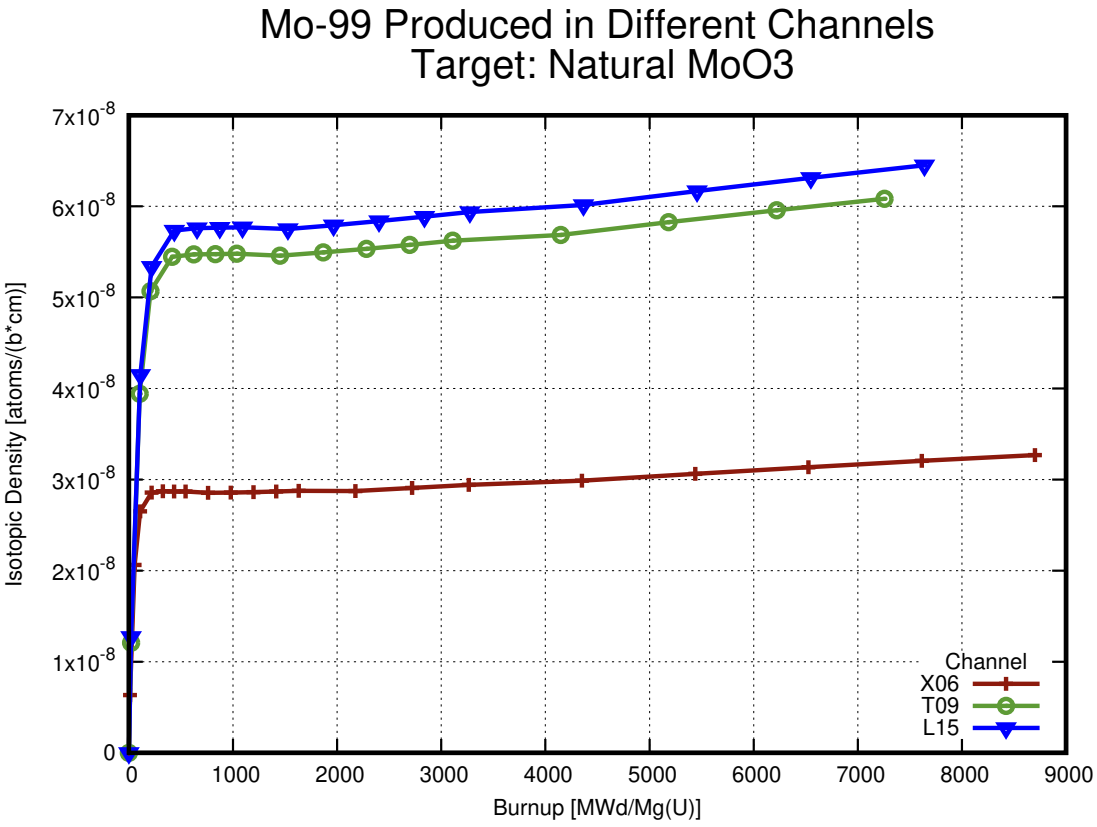

Figure 37: Natural molybdic oxide placed in different channels.

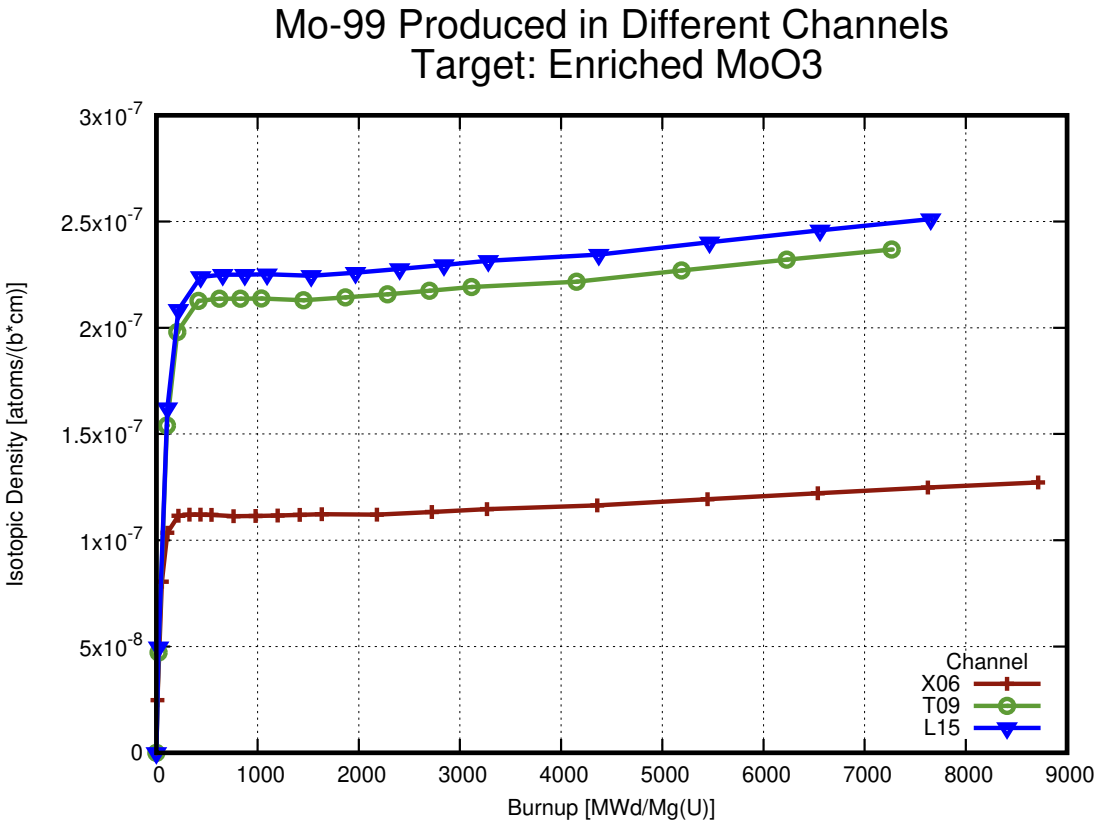

Figure 38: Enriched molybdic oxide placed in different channels.

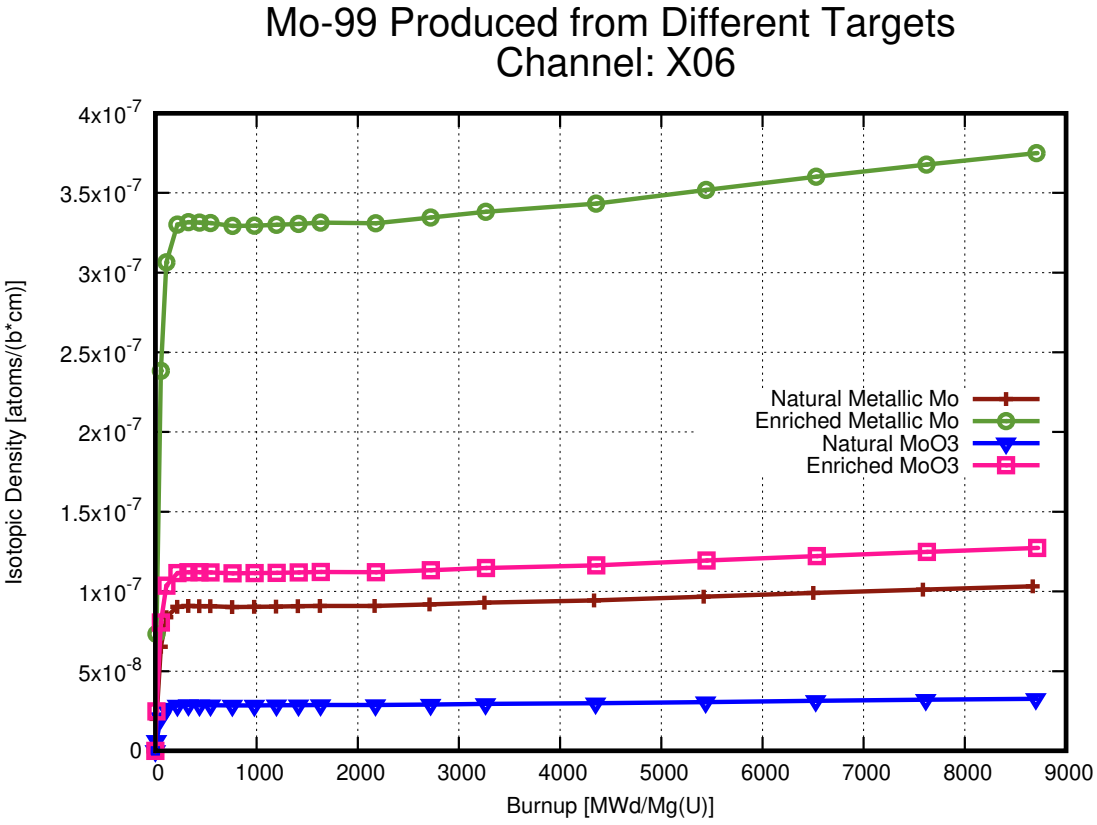

Figure 39: Amount of Mo-99 produced from different targets of molybdenum placed in channel X06.

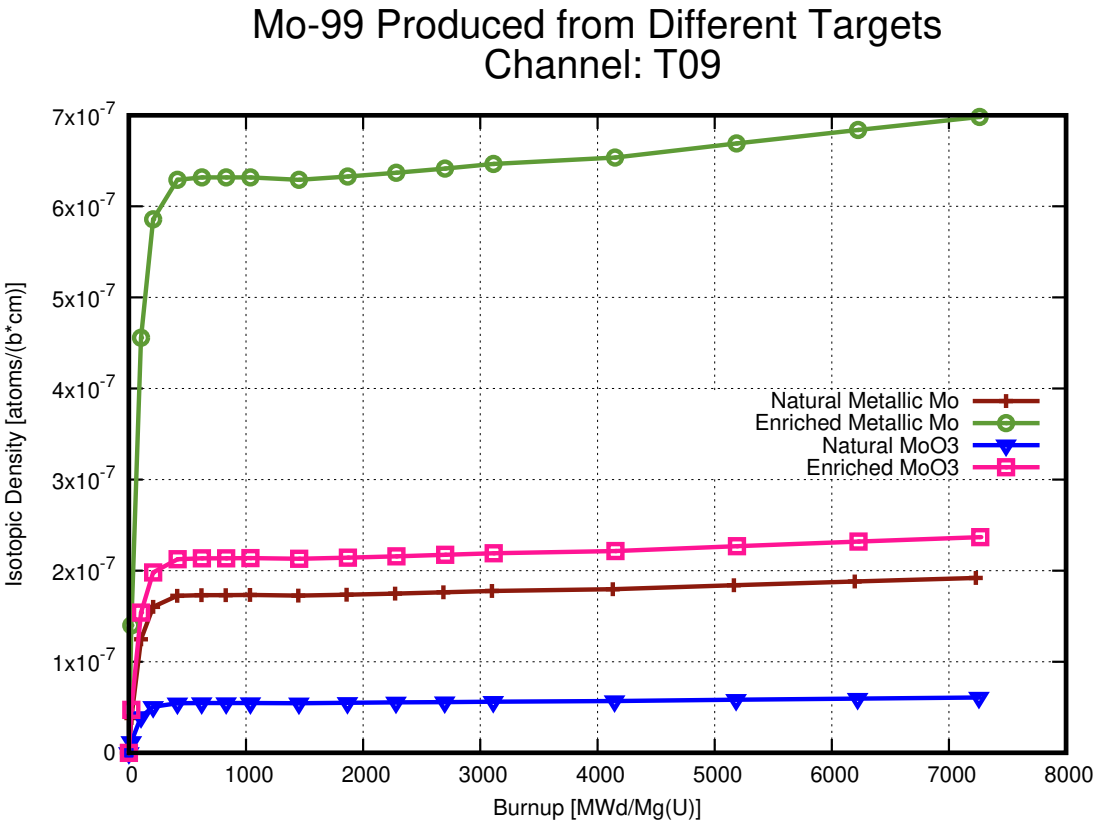

Figure 40: Amount of Mo-99 produced from different targets of molybdenum placed in channel T09.

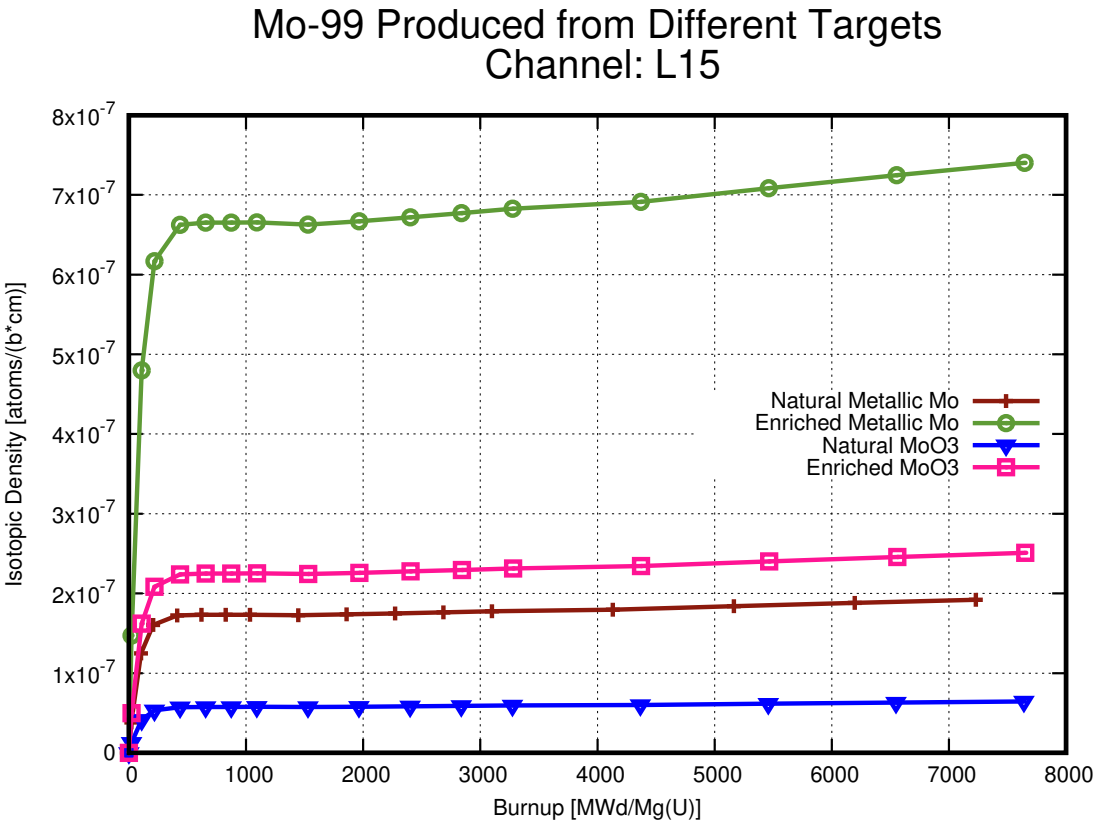

Figure 41: Amount of Mo-99 produced from different targets of molybdenum placed in channel L15.

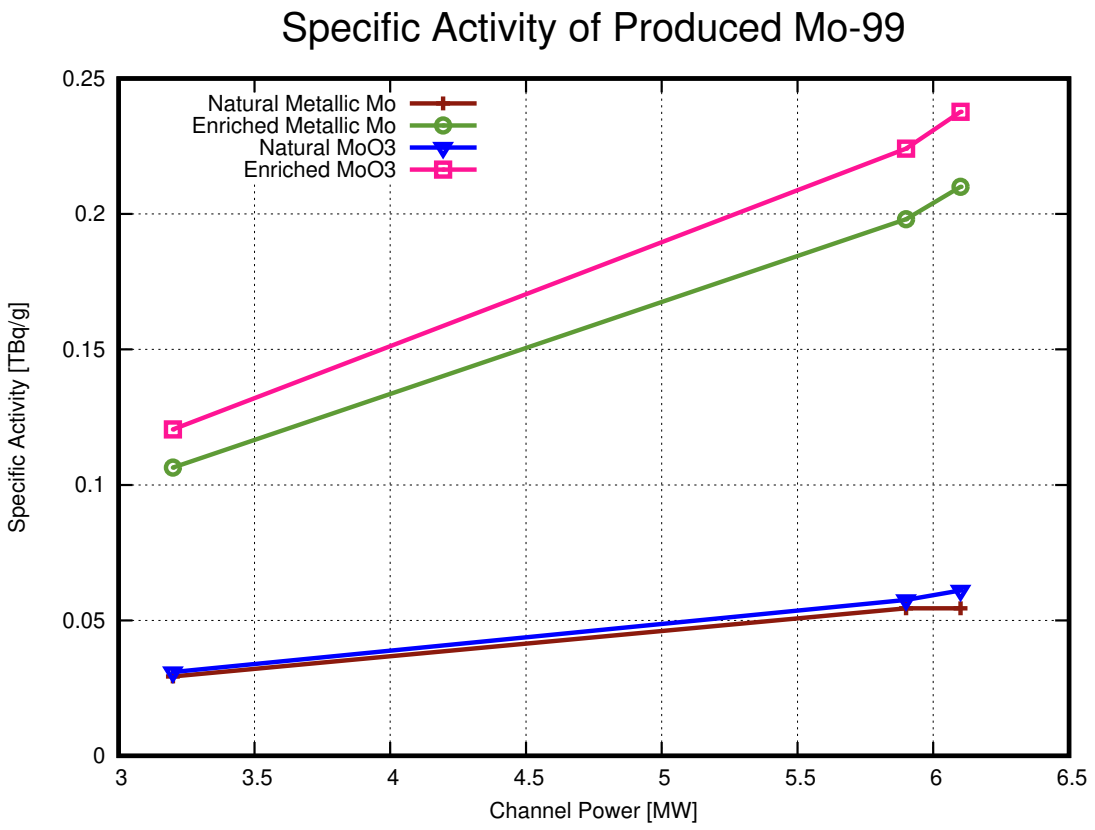

Figure 42: Specific activity of Mo-99 produced from different targets when placed in different channels.

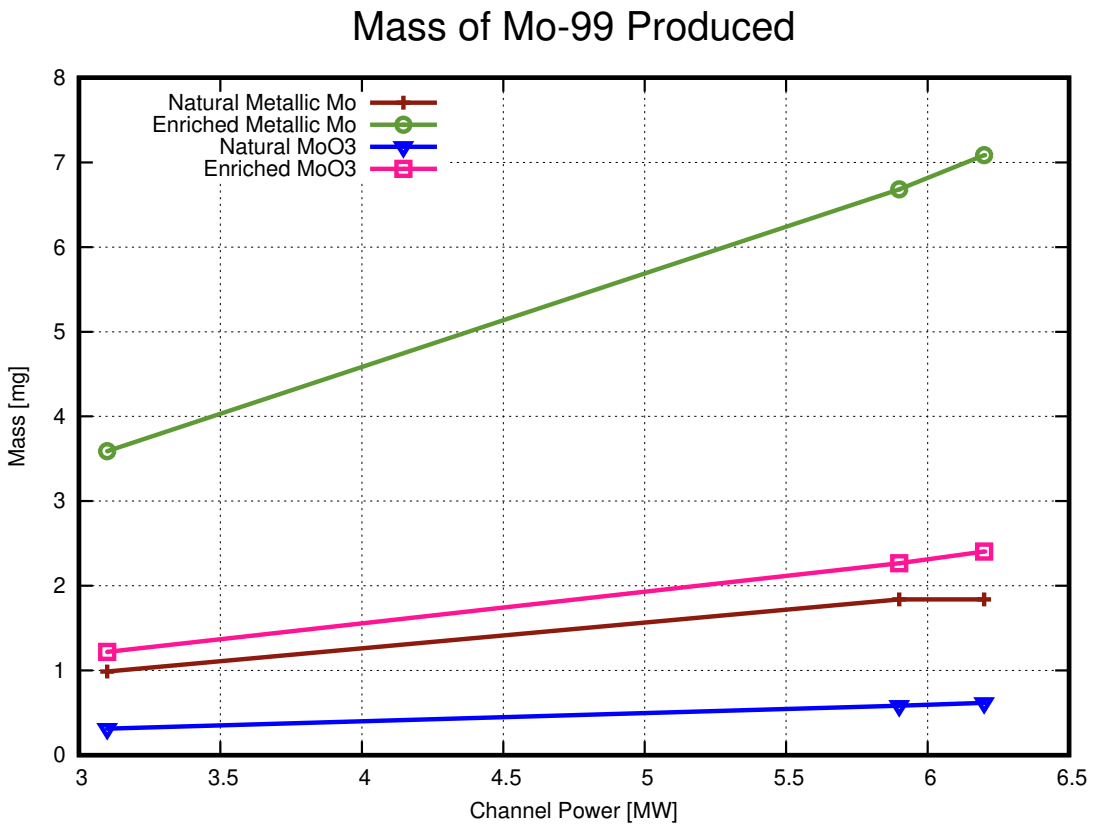

Figure 43: Amount of Mo-99 produced from different targets when placed in different channels.

X06. The natural MoO_3 target produces the least amount of Mo-99. It produces approximately 0.6mg when placed in channel L15, and 0.3mg when placed in channel X06. The world demand for Mo-99 in 2012 was $23,000$ six-day TBq/yr. This amount equates to approximately $167,000$TBq/yr that must be produced in a reactor. For the enriched metallic molybdenum target placed in channel L15, 7mg of Mo-99 at 240GBq/g provides 0.001TBq/yr per bundle assuming each bundle remains in the core for 350 days. Therefore, if the highest power channel is used to produce Mo-99 the greatest amount that can be expected equates to approximately $1.3 \times 10^{-5}\%$ of yearly global demand for the entire channel which would require nearly 8kg of pure Mo-98 metallic molybdenum as a target. This would prove to be an highly inefficient method for producing Mo-99.

4.2.2 Lu-177

In Figs. (44-46), the amount of Lu-177 produced from each of the three targets are shown when placed in channels X06, T09, and L15. In all cases channel L15 produces the most Lu-177, and channel X06 produces the least. Both of the enriched targets reach equilibrium Lu-177 production at around the $3,000$MWd/Mg(U) mark in all three channels. On the other hand, the natural target only begins to reach equilibrium towards the end of irradiation where the amount of Lu-177 has decreased by as much as a third from peak production at around 800MWd/Mg(U). The enriched Lu_2O_3 target in channel L15

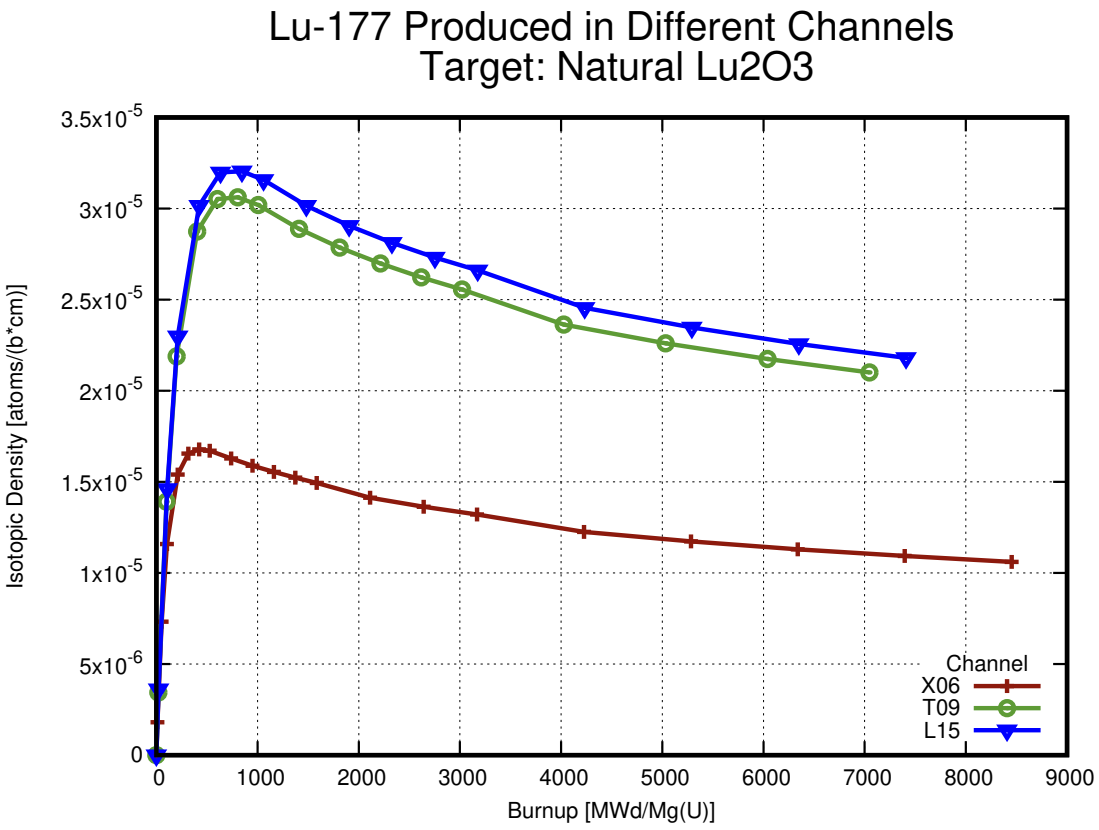

Figure 44: Natural Lu_2O_3 placed in different channels.

produces the most Lu-177, whereas the enriched Yb_2O_3 target in channel X06 produces the least. These trends mirror those of the first set of simulations. As in the Mo-99 simulations, Lu-177 production increases with channel power and enrichment.

In Figs. (47-49), the amount of Lu-177 produced from different targets is shown for each individual channel. For all three, channels the enriched lutetium target produces the most Lu-177 while the ytterbium target produces the least.

In Fig. (50), the estimated specific activity of Lu-177 produced from different targets when placed in different channels is shown. For both lutetium targets, the specific activity increases with channel power. The highest level produced was 8.2TBq/g for the enriched target placed in channel L15. Whereas the natural target produced 3.3TBq/g when placed in the same channel. The ytterbium target produced much higher specific activity than the lutetium targets. The highest level produced was $3,625$TBq/g when placed in channel T09. Surprisingly, the specific activity of Lu-177 produced from the ytterbium target decreases slightly from channels T09 to L15, though the reason for this is unclear.

In Fig. (51), the amount of Lu-177 produced from different targets when placed in different channels is shown. Here, the most amount of Lu-177 produced in 0.9g from the enriched lutetium target placed in channel L15. The natural lutetium target provides approximately a third of enriched target. The least amount produced was 29mg from the ytterbium target placed in channel X06. In all cases, the amount

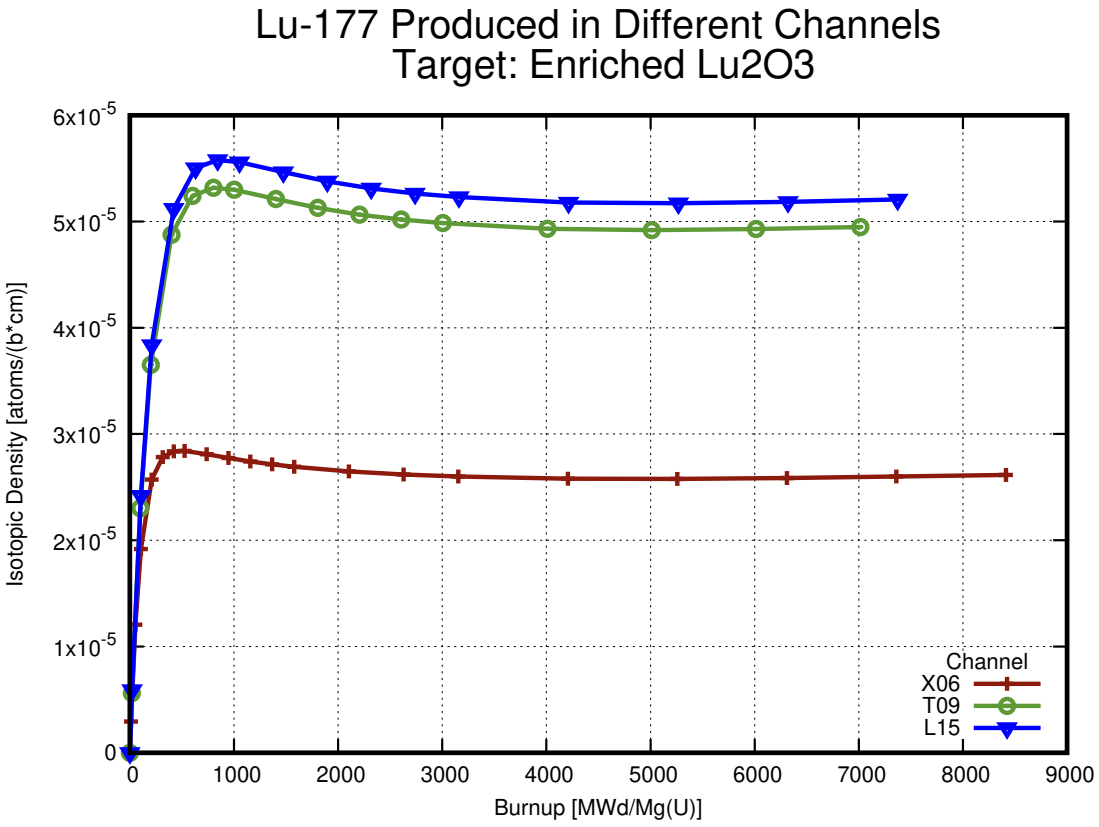

Figure 45: Enriched Lu_2O_3 placed in different channels.

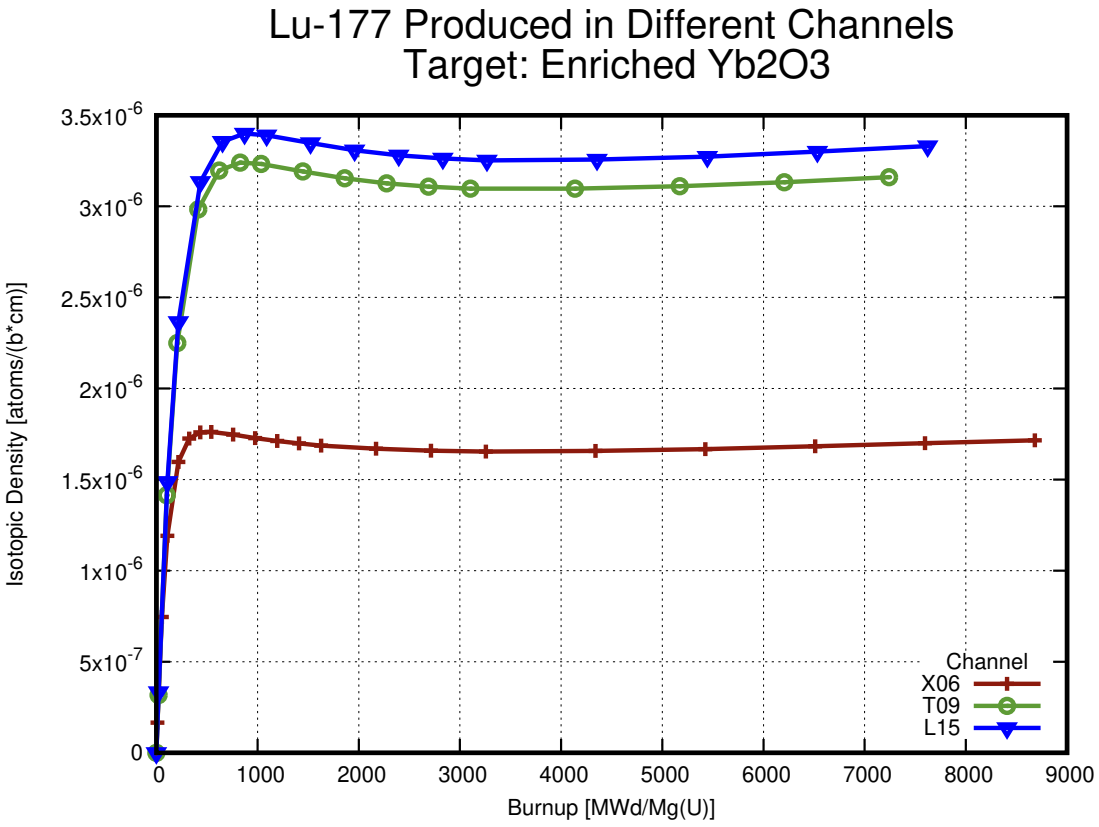

Figure 46: Enriched Yb_2O_3 placed in different channels.

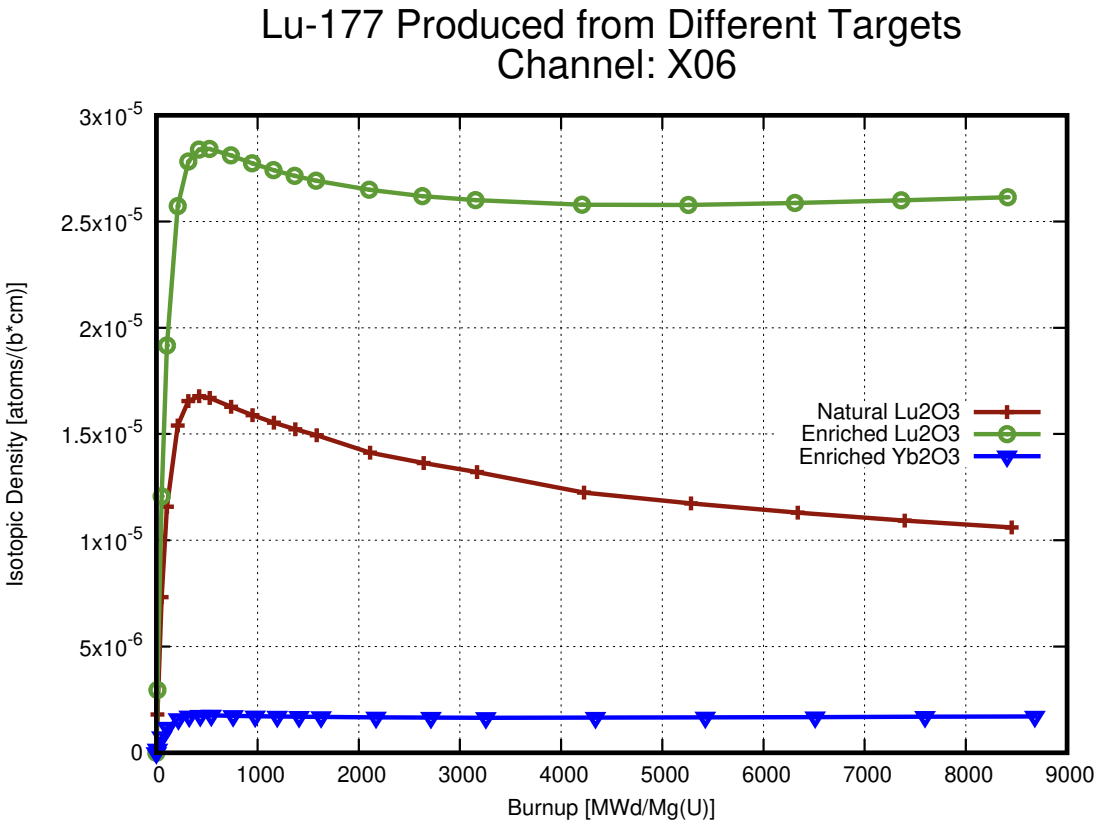

Figure 47: Amount of Lu-177 produced from different targets placed in channel X06

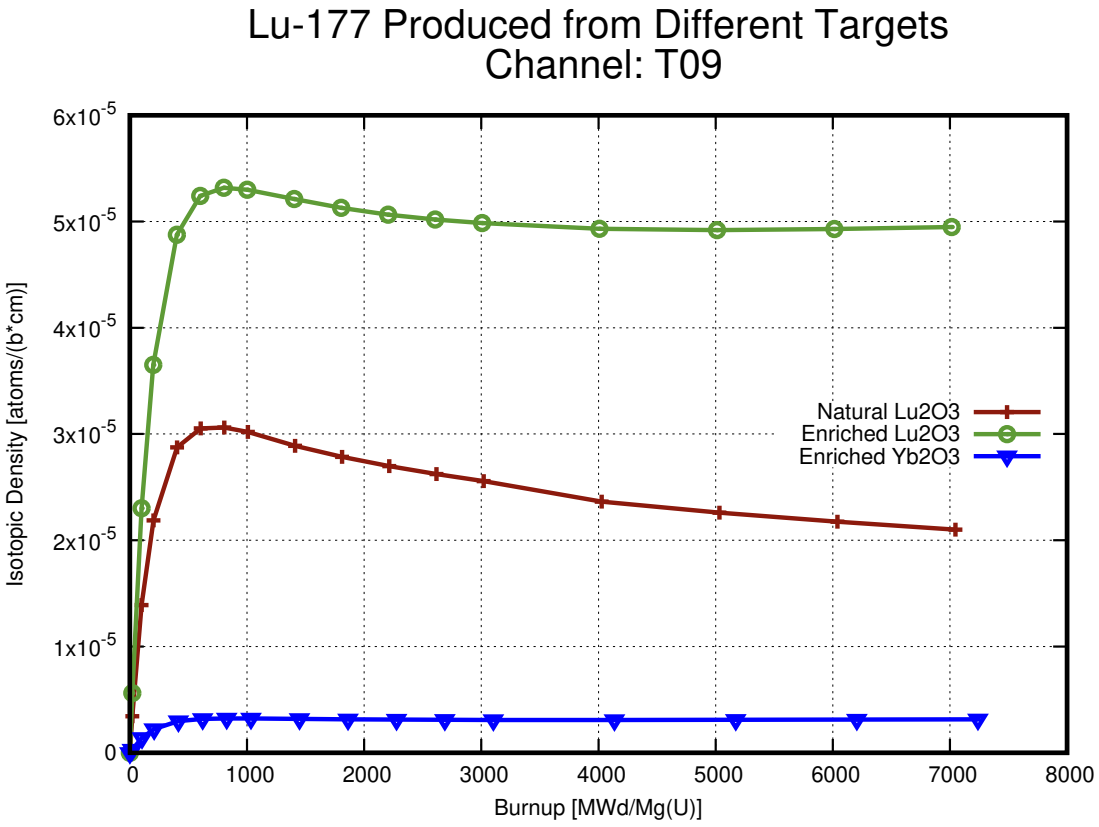

Figure 48: Amount of Lu-177 produced from different targets placed in channel T09

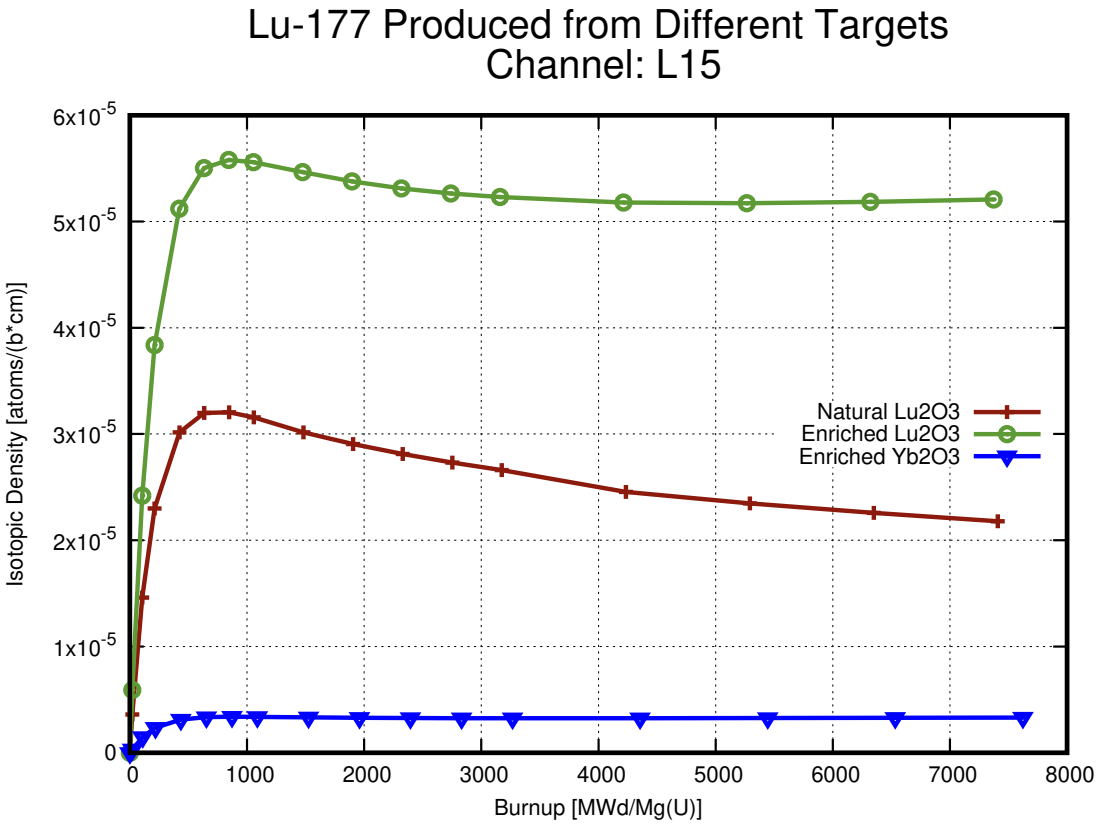

Figure 49: Amount of Lu-177 produced from different targets placed in channel L15

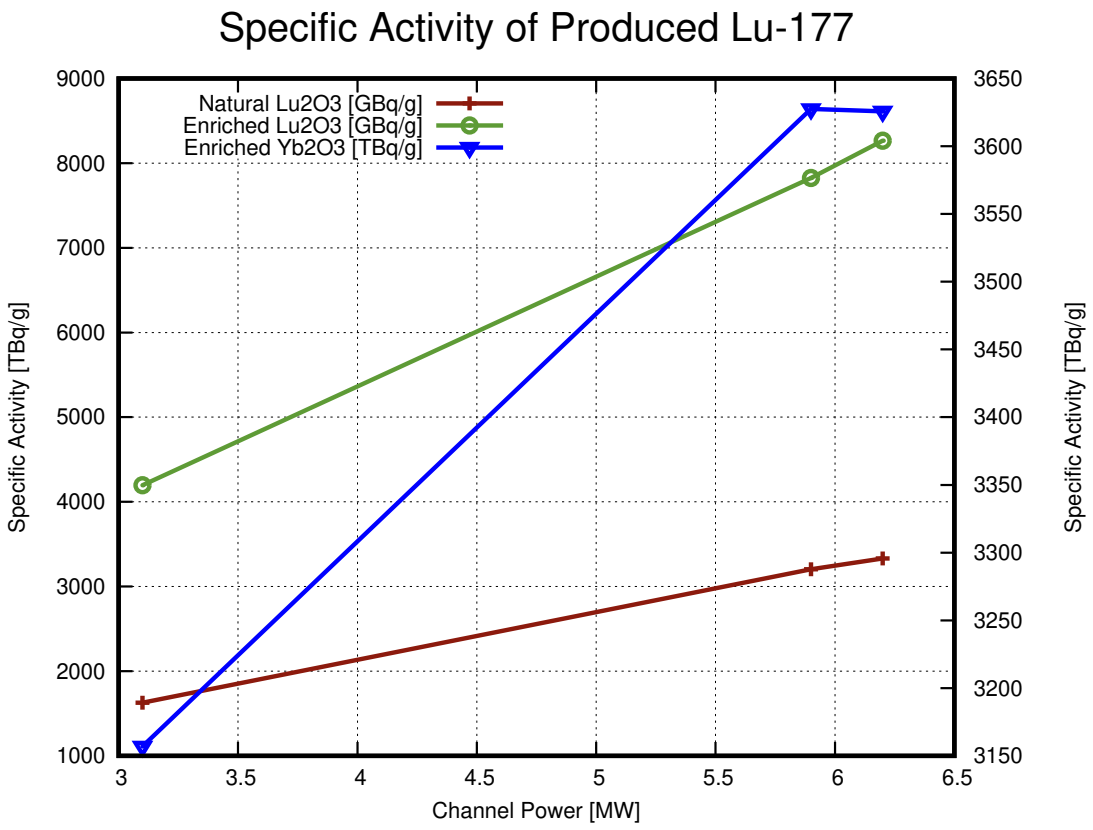

Figure 50: Specific activity of Lu-177 produced from different targets when placed in different channels

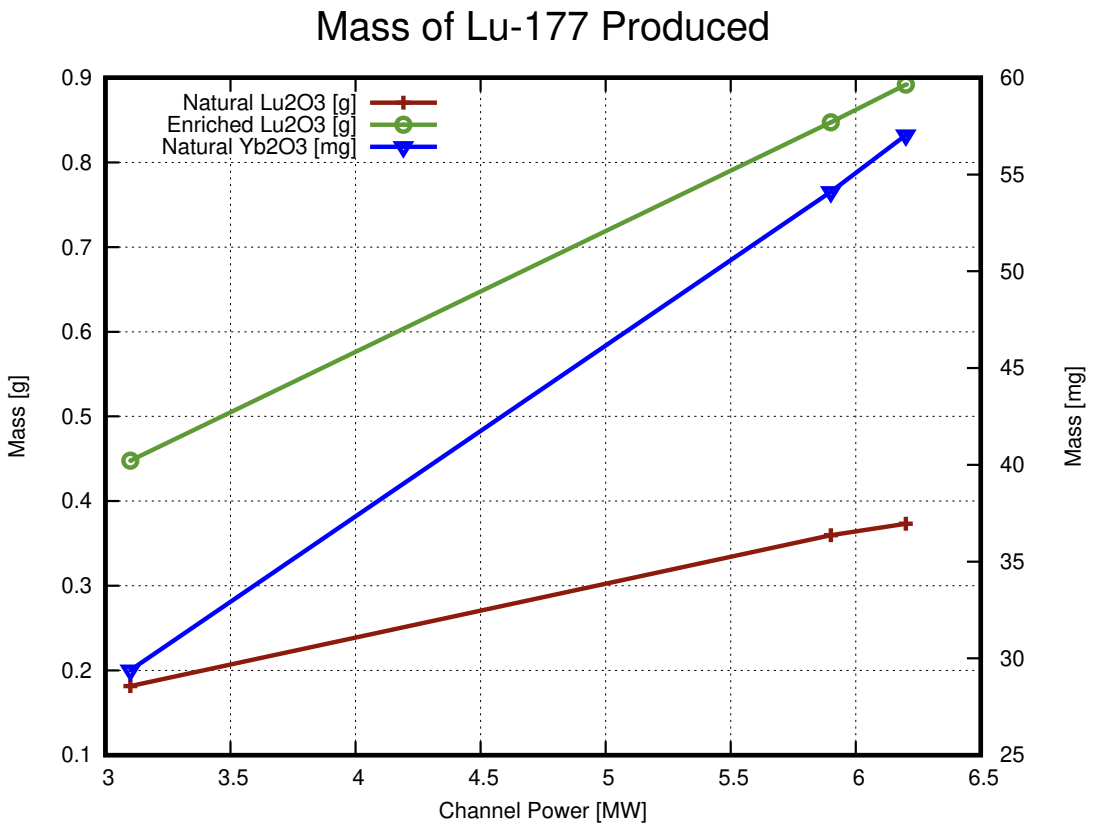

Figure 51: Amount of Lu-177 produced from different targets when placed in different channels.

of Lu-177 increases with channel power. The ytterbium, target while producing the least amount of Lu-177, still produces ten times as much as the molybdenum targets produce Mo-99. Therefore Lu-177 production through this method is much more feasible than Mo-99 production, especially if natural lutetium targets are used.

4.2.3 Alpha-emitters

In Figs. (52, 53), the amount of primary and secondary isotopes produced from a target of $RaCO_3$ are shown when placed in channels X06, T09, and L15. In all cases, the amount of isotopes of interest produced is very similar for each isotope irrespective of whichever channel the target was placed in though the secondary amounts display a slightly greater degree of disparity between channels than do the primary isotopes.

In Figs. (54, 55), the estimated specific activity of primary and secondary isotopes produced from a target of $RaCO_3$ when placed in different channels can be viewed. The specific activity of the primary isotopes is relatively constant regardless of which channel is used. Th-228 displays the highest level of specific activity at 27TBq/g. Th-229 display the lowest amount at 0.7GBq/g though the specific activity of the primary isotopes is not of any great importance. It is the secondary isotopes, those that are placed into generators, that must of high specific activity. For these, Th-227 displays the highest level of specific

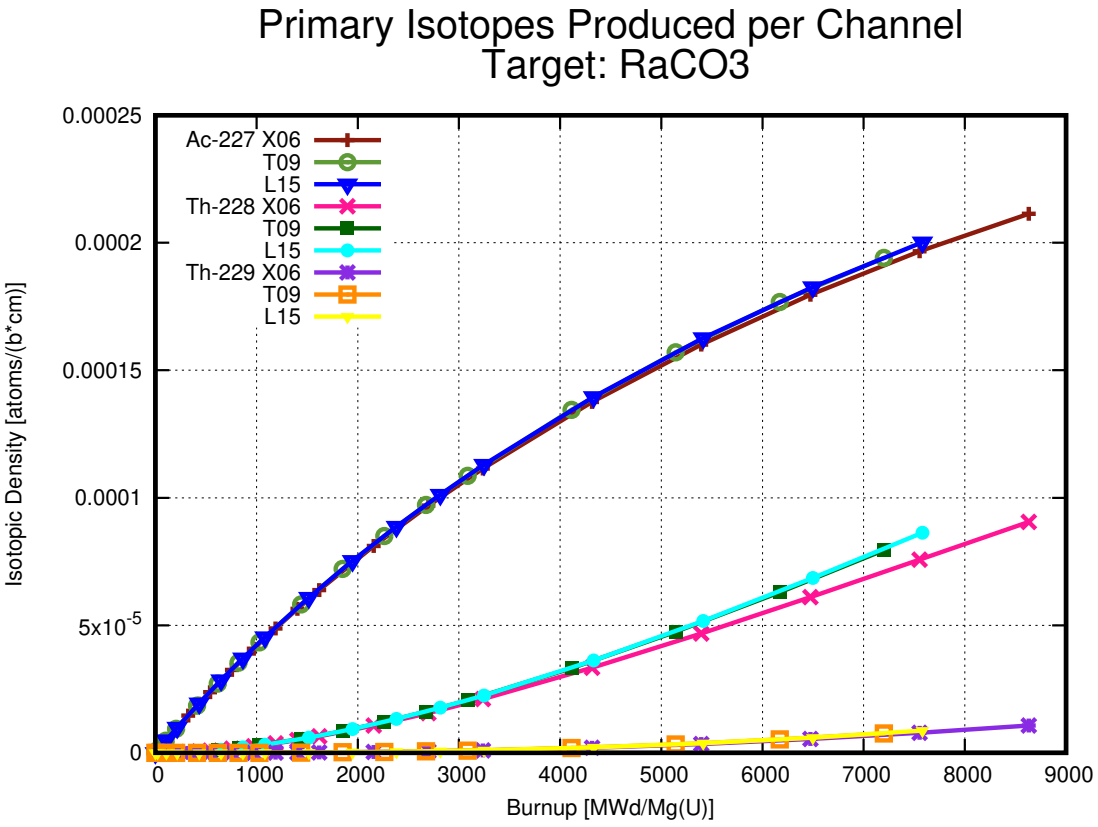

Figure 52: Primary isotopes produced from $RaCO_3$ placed in different channels

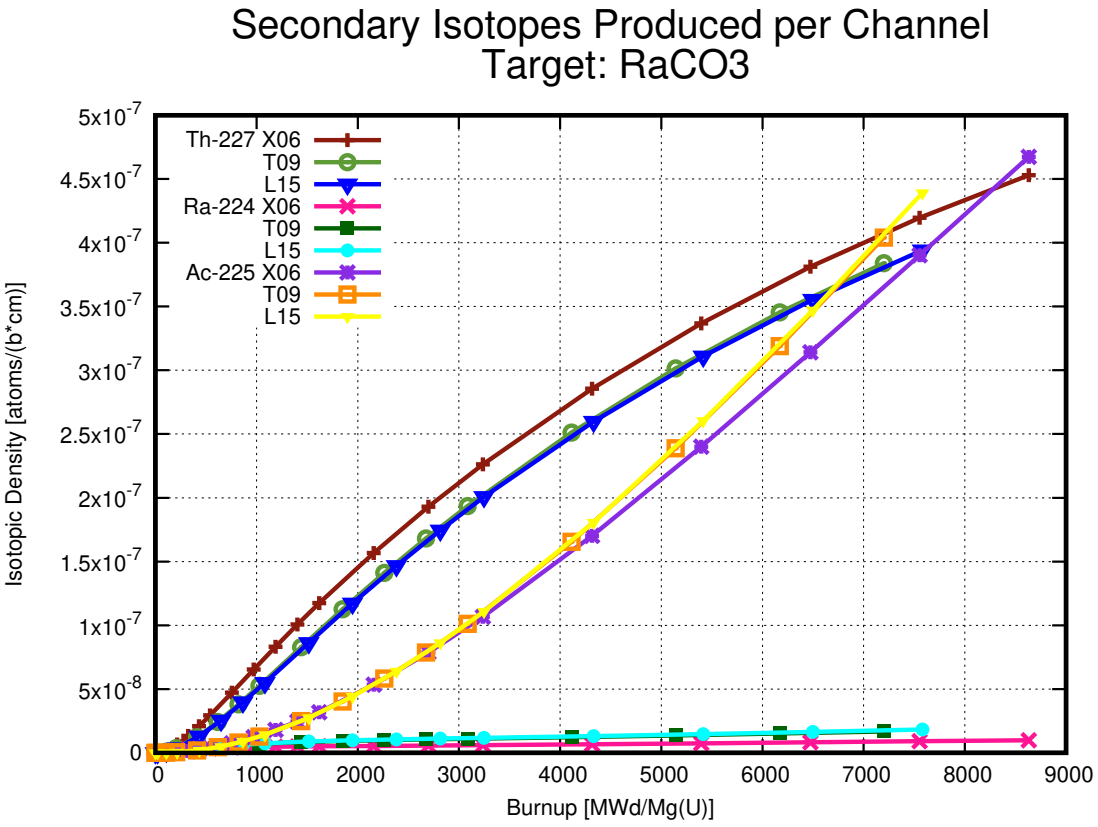

Figure 53: Secondary isotopes produced from $RaCO_3$ placed in different channels

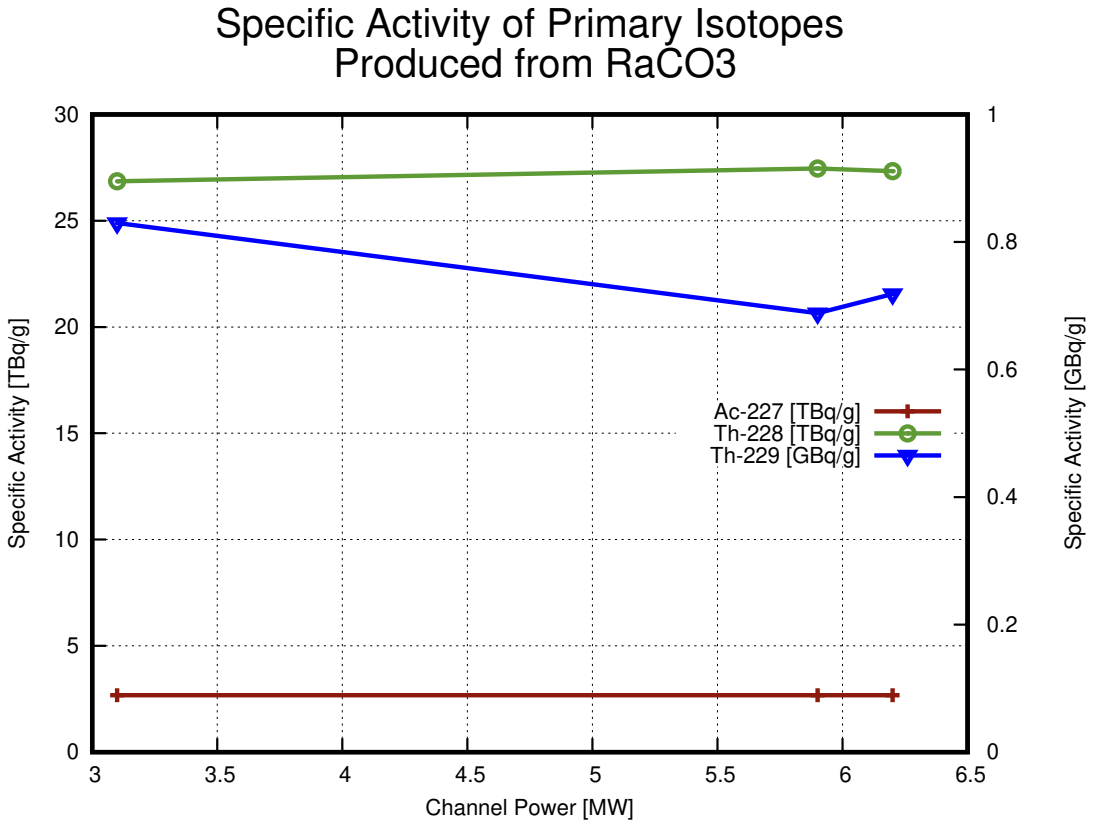

Figure 54: Specific activity of primary isotopes produced from $RaCO_3$ placed in different channels

activity at 5TBq/g when $RaCO_3$ is placed in channel X06. Curiously, this number falls to 4.7TBq/g for channel L15. Ra-224 displays the least amount of specific activity at 0.3TBq/g regardless of whichever channel the target is placed in.

In Figs. (56, 57), the amount of primary and secondary isotopes produced from a $RaCO_3$ target when placed in different channels is shown. Here, a significant amount of primary isotopes are produced. Similar to the amounts of Lu-177 produced from lutetium targets. The approximate amounts of the primary isotopes produced are 4.5, 2, and 0.3g, for Ac-227, Th-228, and Th-229 respectively. The amount of these isotopes that is produced is more or less constant, regardless of which channel the target of $RaCO_3$ was placed in. Much less quantities of the secondary isotopes are produced. About the same amount as Mo-99 was produced from the molybdenum targets. The most amount of the secondary isotopes that was produced was 10mg of Ra-224 from a target placed in channel X06. The least amount produced was 0.2mg of Ac-225 from a target placed in channel X06.

The specific activity and mass of all of the isotopes produced by each target in the three channels of interest as well as their respective theoretical specific activities have been compiled into Tab. (B).

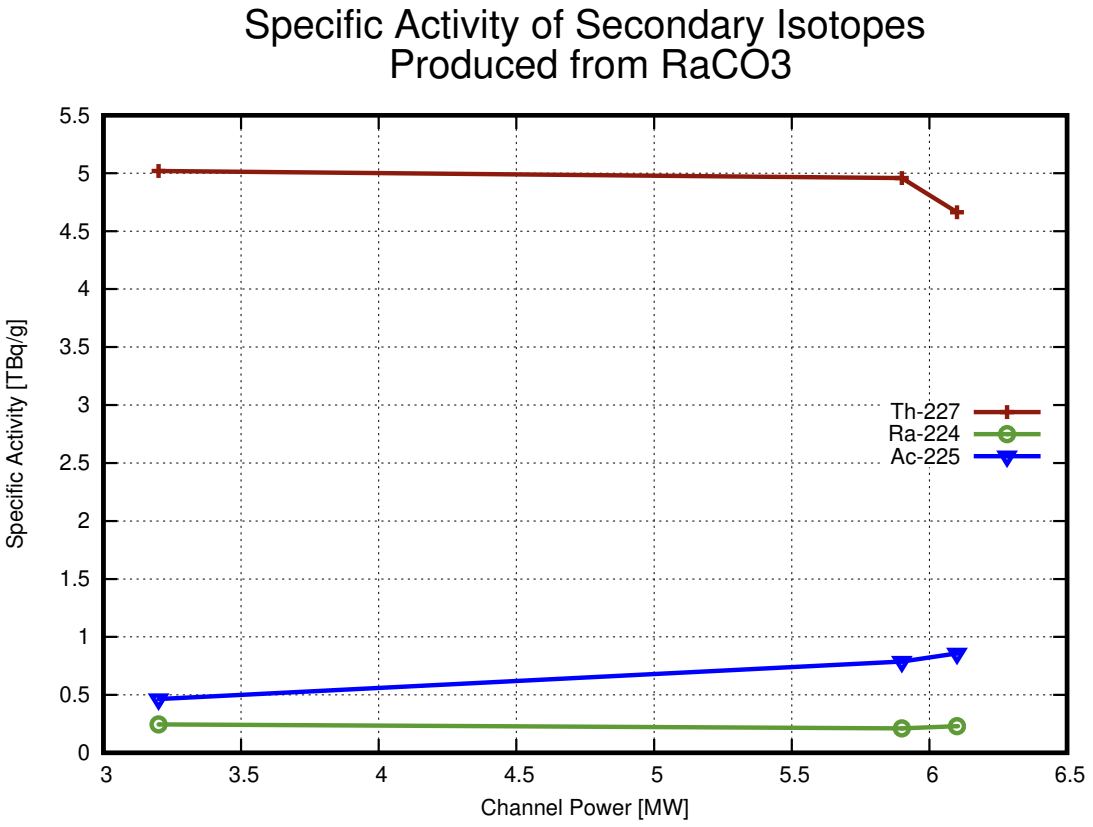

Figure 55: Specific activity of secondary isotopes produced from $RaCO_3$ placed in different channels

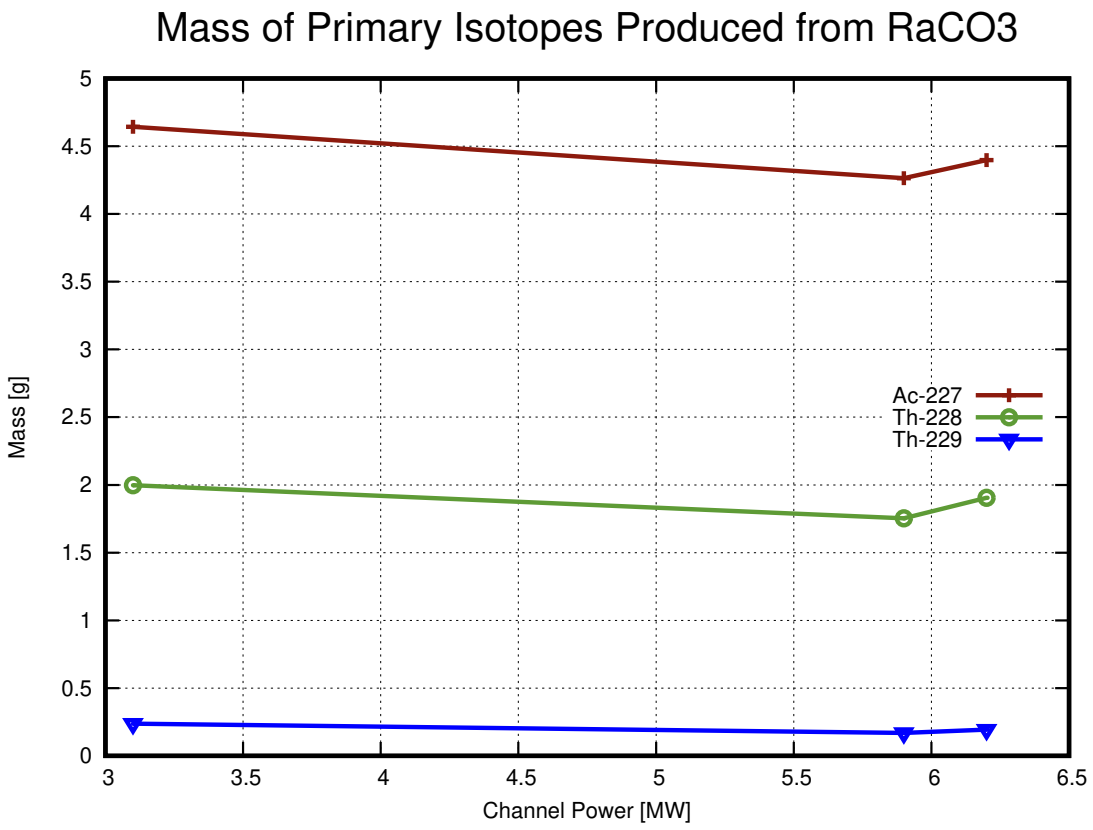

Figure 56: Amount of primary isotopes produced $RaCO_3$ when placed in different channels

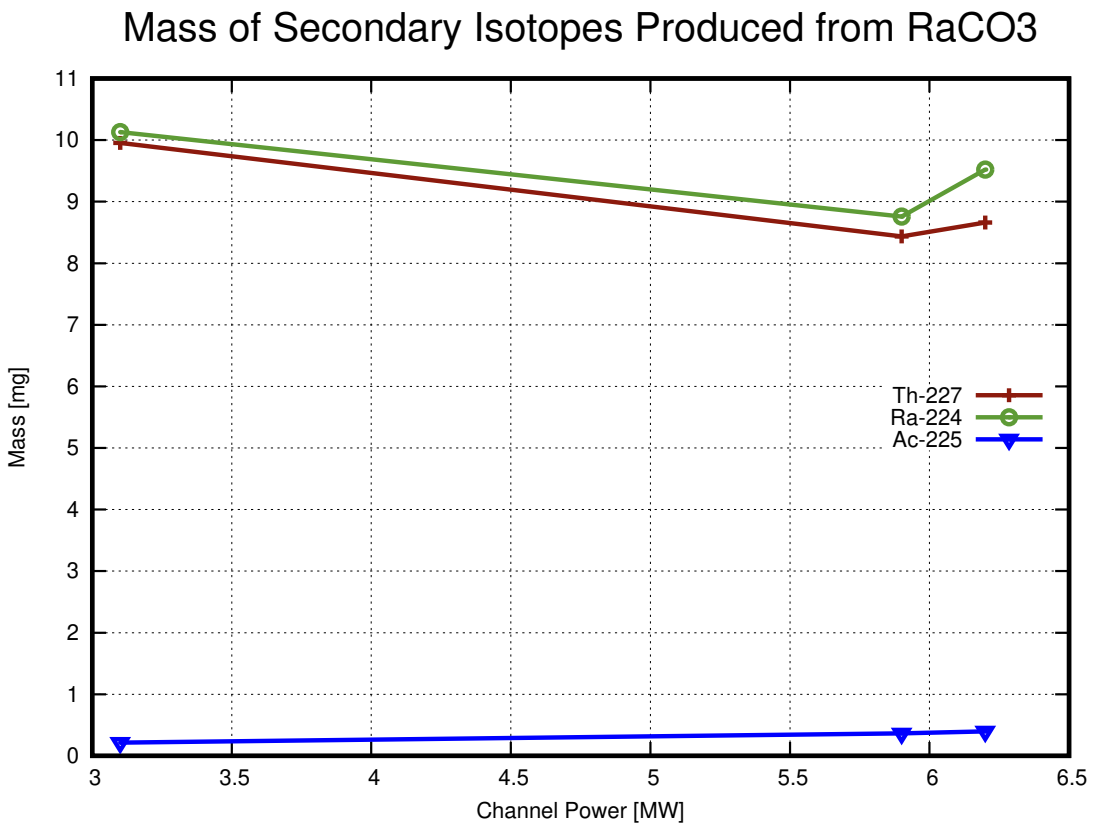

Figure 57: Amount of secondary isotopes produced $RaCO_3$ when placed in different channels

5 Concluding Remarks and Future Work

The objective of this thesis was to provide a detailed analysis of the viability of producing several different medical radioisotopes in CANDU reactors by replacing the fuel in the center pin of 37-element fuel bundle with non-fissile material. To perform the analysis, the computer codes DRAGON and DONJON were used. The DRAGON simulations required the generation of a customized multi-group cross-section library. This was done using the NJOY and PyNJOY computer codes, and the JEFF and TENDL nuclear cross-section libraries. Lattice calculations were performed with custom library and a WIMS-D validated library provided by the IAEA. It was found that the two libraries deviated substantially in terms of the reactivity of lattice prior to about $3,000$MWd/Mg(U) of burnup, where the custom library displayed lower reactivity, on the order of 10mk. After $3,000$MWd/Mg(U) both libraries behaved identically. Whether this initial deviation is due to the use of the different nuclear data libraries, the different energy mesh schemes, or whether the use of averaged isotopic cross-sections is the primary cause remains undetermined. Despite the initial deviation in reactivity, the custom library was used for all subsequent simulations.

A simulation was done for a lattice where the fuel from the center pin was replaced with enriched metallic molybdenum. The reactivity of this lattice over a burnup period of $16,000$MWd/Mg(U) was juxtaposed with that of a standard bundle. The two lattices displayed very similar reactivity initially and diverged gradually until the end of the burnup calculation where the modified bundle displayed approximately 6.5mk lower reactivity. This confirmed the assumption that the center pin of a 37-element bundle contributes very little to the overall power output of a fuel bundle.

Full core simulations of a CANDU-9 reactor were performed with DONJON. The reactivity of the core using only standard fuel bundles was found to be 5.364×10^{-03}mk. The core-average exit burnup was found to be 8.036×10^{03}MWd/Mg(U). The maximum bundle power, maximum channel power, and minimum channel power were found to be 8.790×10^{02}, 6.168×10^{03}, and 3.077×10^{03}kW respectively. Three channels were selected as candidates to hold the modified fuel bundles. These were: channel X06, channel T09, and channel L15. Channel X06 provided the lowest power output, channel L15 provided the highest power output, and channel T09 provided a power output somewhere between these two values. Subsequent simulations were performed by placing modified bundles into one of three selected channels. The modified bundles had the fuel in their center pins replaced with pure metallic Mo-98. The reactivity of the core when the bundles were placed into channel X06 fell to 2.264×10^{-03}mk. The reactivity was -6.079×10^{-03}mk when channel T09 was used, and -7.152×10^{-03}mk for channel L15. Therefore, the largest change in reactivity when the highest power channel used modified bundles was -0.007mk when compared to a core using only standard bundles. Additional DONJON simulations were performed for modified fuel bundles containing all of the aforementioned targets, once the refuelling rates and average bundle powers per channel were determined. This information was then used to perform DRAGON simulations to determine the amount and specific activity of each radioisotope of

interest.

In the DRAGON simulations it was found for all of the molybdenum and lutetium targets that the amount and specific activity of Mo-99 and Lu-177 produced depended on the power output of the channel. The most Mo-99 produced was done so in the the highest output channel where approximately 7mg of Mo-99 was produced from the enriched metallic target. This represents a 1.182×10^{-03}%-yield from the amount of molybdenum that was used in the target. The Mo-99 had a specific activity of 2.4×10^{-01}TBq/g, well within the acceptable range for use in a generator. However, since such minute amounts of Mo-99 were generated, the method of production using the center pin of fuel bundles is most likely unfeasible. The results for lutetium fared better. Here, 0.9g of Lu-177 were produced from the enriched lutetium target. This represents a 1.871×10^{-01}%-yield from the amount of lutetium that was used in the target. The Lu-177 had a specific activity of 8.3TBq/g. The enriched ytterbium target produced much less Lu-177 at 56mg. However, the specific activity of the Lu-177 produced was much higher at 3.625×10^{03}TBq/g. The isotopes produced from the radium carbonate target depended much less on which channel was used. When placed in channel X06 4.5, 2, and 0.3g of Ac-227, Th-228, Th-229 were produced respectively. Their specific activities were 2.5, 27, and 7×10^{-04}TBq/g respectively.

It should be noted that the criteria for the feasibility of production is taken as a measure of the percentage of global demand for Mo-99. This was done because the global demand for the other isotopes was not available at this time. Since the global demand of the other radioisotopes would be different, it is entirely possibly that minute amounts of Ac-225 that were produced represent a significant amount of global demand for that particular radioisotope.

In the end, it was found that the method of replacing the fuel in the center pin of a 37-element fuel bundle with non-fissile targets for the purpose of producing medical radioisotopes is feasible for Lu-177, and the parent isotopes of the alpha-emitters Bi-212, and Ra-224. The production of Mo-99, and the parent isotope of the alpha-emitter Bi-213 proved to be highly inefficient as only a few milligrams would be produced per year for an entire channel. The deviation of core parameters by the inclusion of these modified bundles in any one channel was found to be negligible.

In future work, reactor response to quicker refuelling of modified bundles should be explored. The use of depleted uranium to offset the positive reactivity insertion of quicker refuelling should also be investigated. The effects on the reactor when multiple channels are used should be explored. Here, only one channel was used at a time for each simulation. If, for instance, 10 or 20 channels could be used then the production capacity would be much greater. Disassembly of the bundle procedure should also be reviewed. Finally further modification of the bundle should be investigated where a greater number of fuels pins are replaced with target material. It may even be possible to remove all of the fuel from the bundle and produce radioisotopes in an inert channel. This would allow a high frequency refuelling rate without the cost of increased reactivity.

References

[1] I. R. Radiological Society of North America, "General nuclear medicine — radiology info for patients." https://www.radiologyinfo.org/en/info.cfm?pg=gennuclear, 2018. [Online; accessed 5-March-2018].

[2] W. N. Association, "Radioisotopes in medicine." http://www.world-nuclear.org/information-library/non-power-nuclear-applications/radioisotopes-research/radioisotopes-in-medicine.aspx, 2018. [Online; accessed 5-March-2018].

[3] N. E. Agency, "Medical radioisotopes." https://www.oecd-nea.org/med-radio/, 2017. [Online; accessed 5-March-2018].

[4] J. Haroon, "Development of a 37-element fuel bundle for the production of molybdenum-99 in candu power reactors," Master's thesis, University of Ontario Institute of Technology, 2014.

[5] C. Brown, "Will new isotope sources be ready in time?," 2016.

[6] Cision, "University of missouri research reactor files for nrc approval to start u.s. production of medical isotopes." https://www.newswire.ca/news-releases/..., 2017. [Online; accessed 6-March-2018].

[7] A. Dash, M. R. A. Pillai, and F. F. Knapp, "Production of 177lu for targeted radionuclide therapy: available options," *Nuclear medicine and molecular imaging*, vol. 49, no. 2, pp. 85–107, 2015.

[8] E. Britannica, "Radioactive isotope." https://www.britannica.com/science/radioactive-isotope, 2018. [Online; accessed 5-March-2018].

[9] J. R. Lamarsh, "Introduction to nuclear engineering," 1975.

[10] W. Wolf and J. Shani, "Criteria for the selection of the most desirable radionuclide for radiolabeling monoclonal antibodies," *International Journal of Radiation Applications and Instrumentation. Part B. Nuclear Medicine and Biology*, vol. 13, no. 4, pp. 319–24, 1986.

[11] E. B. Podgorsak, *Radiation physics for medical physicists*. Springer Science & Business Media, 2010.

[12] I. A. E. Agency, *Feasibility of Producing Molybdenum-99 on a Small Scale Using Fission of Low Enriched Uranium Or Neutron Activation of Natural Molybdenum*. Iaea Technical Reports Series, International Atomic Energy Agency, 2015.

[13] W. H. Cooper, "Method of producing radioisotopes using a heavy water type nuclear power plant," 2016. Canadian Patent CA2895622A1.

[14] M. Ahmad, "Medical isotope production: Can enriched molybdenum-98 replace enriched uranium?," *Nonproliferation Review*, vol. 16, no. 2, pp. 285–292, 2009.

[15] D. E. Polyak, "2013 minerals yearbook," tech. rep.

[16] INTERNATIONAL ATOMIC ENERGY AGENCY, *Feasibility of Producing Molybdenum-99 on a Small Scale Using Fission of Low Enriched Uranium or Neutron Activation of Natural Molybdenum.* No. 478 in Technical Reports Series, Vienna: INTERNATIONAL ATOMIC ENERGY AGENCY, 2015.

[17] Softschools, "Lutetium facts." `http://www.softschools.com/facts/periodic\_table/lutetium\_facts/345/`, 2018. [Online; accessed 5-March-2018].

[18] T. Das and P. Mra, "Options to meet the future global demand of radionuclides for radionuclide therapy," vol. 40, 10 2012.

[19] M. B. Kwon Yong, "Application of pb-212 for targeted alpha-particle therapy (tat): Pre-clinical and mechanistic understanding through to clinical translation," *AIMS Medical Science*, vol. 2, p. 228, 2015.

[20] T. C. E. Encyclopedia, "Ra-226." `https://encyclopedia2.thefreedictionary.com/Ra-226`, 2018. [Online; accessed 5-March-2018].

[21] Softschools, "Radium facts." `http://www.softschools.com/facts/periodic_table/radium_facts/360/`, 2018. [Online; accessed 5-March-2018].

[22] W. N. Association, "Uranium, from mine to mill." `www.world-nuclear.org/getmedia/968bc601-efbb-40e0-b3aa-1cd66fca4860/Pocket-Guide-Uranium.pdf.aspx`, 2017. [Online; accessed 5-March-2018].

[23] N. D. C. at KAERI, "Table of nuclides." `http://atom.kaeri.re.kr/nuchart/`, 2018. [Online; accessed 5-March-2018].

[24] Z. Karalova, R. Ivanov, B. Myasoedov, L. Rodionova, Z. Pyzhova, S. Kalebin, and V. Y. Gabeskiriya, "Production of ac 227 and th 228 isotopes by irradiation of radium in the sm-2 reactor," *Soviet Atomic Energy*, vol. 32, no. 2, pp. 133–136, 1972.

[25] M. Chérel and J. Barbet, "Alpha emitting radionuclides and radiopharmaceuticals for therapy," tech. rep., 2013.

[26] W. Garland, "The essential candu, a textbook on the candu nuclear power plant technology," *Chap*, vol. 17, p. 12, 2015.

[27] B. N. Laboratory, "Endf/b-viii.0 evaluated nuclear data library." `http://www.nndc.bnl.gov/endf/b8.0/index.html`, 2018. [Online; accessed 5-March-2018].

[28] A. Hebert, "A pynjoy tutorial," *École Polytechnique de Montréal Montréal QC, Canada, Tech. Rep. IGE-305*, 2016.

[29] G. Marleau, A. Hébert, and R. Roy, "A user guide for dragon version 4," *IGE-294, Ecole Polytechnique de Montréal, Institut de génie nucléaire Département de génie mécanique (Aug. 26, 2016)*, 2011.

[30] M. Guyot, "Development of the micro-depletion method in the chain of codes dragon4/donjon4," Master's thesis, École Polytechnique de Montréal, 2011.

[31] Z. Demers, "Comparative safety evaluation of thorium fuel to natural uranium fuel in a candu 6 reactor," Master's thesis, 2017.

[32] A. Hébert, D. Sekki, and R. Chambon, "A user guide for donjon version4," *École Polytechnique de Montréal Montréal QC, Canada, Tech. Rep. IGE-300*, 2013.

[33] M. J. Driscoll, T. J. Downar, and E. E. Pilat, *The linear reactivity model for nuclear fuel management*. Amer Nuclear Society, 1990.

[34] W. Shen, "On the better performance of the coarse-mesh finite-difference method for candu-type reactors," *Annals of Nuclear Energy*, vol. 46, pp. 169–178, 2012.

[35] B. Rouben, "Introduction to reactor physics," *Atomic Energy of Canada Ltd*, 2002.

[36] A. Morreale, *Analysis of Transuranic Mixed Oxide Fuel in a CANDU Nuclear Reactor*. PhD thesis, McMaster University, 2012.

[37] W. G. Fahrenholtz, "Ceramic engineering 111 sintering."

A Equations

The following equations were used to calculate the mass and the specific activity of the produced isotopes. Eq. (29) shows the equation used to obtain the mass of the produced isotope. Here, m is the total mass of the isotope in grams, ρ_{Iso} is the isotopic density given in atoms/(barn·cm), m_a is the atomic mass of the isotope given in grams/mole, $V = 58.282\text{cm}^3$ is the volume of the center pin, $N_A = 6.022 \times 10^{23}$atoms/mole is Avogadro's constant, and $b = 1 \times 10^{-24}\text{cm}^2$ is one barn. The dimensional analysis is provided in Eq. (30).

$$m = \frac{\rho_{Iso} m_a V}{N_A b} \tag{29}$$

$$[m] = g = \frac{atoms}{b \cdot cm} \frac{g}{mol} \frac{cm^3}{1} \frac{mol}{atoms} \frac{b}{cm^2} \tag{30}$$

Eq. (31) shows the equation used to obtain the specific activity of the isotope produced. Here, a_{th} is the theoretical specific activity of the isotope given by Eq. (1), m_i is the mass of the isotope, and m_N is the total mass of all the isotopes of the same element.

$$a = \frac{a_{th} m_i}{m_N} \tag{31}$$

Eq. (32) shows the equation used to obtain the length of time that each modified bundle would spend in a channel. Here, t is the time that a bundle spends in the core given in days, m is the mass of the fuel in a bundle, R is the refuelling rate calculated by DONJON given in kg/day. This the amount of fuel in kg that is loaded into the channel everyday. A dimensional analysis is provided in Eq. (33)

$$t = \frac{m}{R} \cdot 13 \tag{32}$$

$$[t] = days = \frac{kg}{bundle} \frac{days}{kg} \cdot 13 bundle \tag{33}$$

B Results

A compilation of all the specific activities and masses of the isotopes produced can be seen in Tab. (B). Here it should be noted that the mass of the target is the mass of the targeted element and not the entire target. In other words, the mass provided for MoO_3 is the mass of the molybdenum in the target. The %-yield is the mass of the produced isotope displayed as a ratio of the mass of the targeted element.

Isotope	Target	Channel	Estimated [TBq/g]	Mass [g]	%-Yield
Theoretical [TBq/g]	Mass [g]				

Mo-99	Nat. Mo	X06	2.926e-02	9.877e-04	1.648e-04
1.776e+04	5.991e+02	T09	5.445e-02	1.838e-03	3.068e-04
		L15	5.445e-02	1.838e-03	3.068e-04
	Enr. Mo	X06	1.064e-01	3.589e-03	5.991e-04
	5.991e+02	T09	1.980e-01	6.681e-03	1.111e-03
		L15	2.100e-01	7.084e-03	1.182e-03
	Nat. MoO_3	X06	3.094e-02	3.129e-04	5.223e-05
	1.795e+02	T09	5.757-02	5.822e-04	9.718e-05
		L15	6.105e-02	6.174e-04	1.030e-04
	Enr. MoO_3	X06	1.204e-01	1.217e-03	2.032e-04
	1.796e+02	T09	2.241e-01	2.266e-03	3.783e-04
		L15	2.376e-01	2.403e-03	4.012e-03
Lu-177	Nat. Lu_2O_3	X06	1.627e+00	1.815e-01	3.809e-02
4.107e+03	4.766e+02	T09	3.204e+00	3.596e-01	7.546e-02
		L15	3.330e+00	3.732e-01	7.831e-02
	Enr. Lu_2O_3	X06	4.157e+00	4.477e-01	9.393e-02
	4.753e+02	T09	7.825e+00	8.473e-01	1.777e-01
		L15	8.265e+00	8.918e-01	1.871e-01
	Enr. Yb_2O_3	X06	3.157e+03	2.938e-02	6.261e-03
	4.693e+02	T09	3.627e+03	5.411e-02	1.152e-02
		L15	3.625e+03	5.704e-02	1.215e-02
Ac-227	$RaCO_3$	X06	2.676e+00	4.643e+00	1.833
2.677e+00	2.532e+02	T09	2.674e+00	4.264e+00	1.683
		L15	2.674e+00	4.397e+00	1.736
Th-228	$RaCO_3$	X06	2.685e+01	1.997e+00	7.887e-01
3.036e+01	2.532e+02	T09	2.745e+01	1.753e+00	6.920e-01
		L15	2.733e+01	1.905e+00	7.521e-01
Th-229	$RaCO_3$	X06	8.297e-04	2.380e-01	9.399e-02
7.872e-03	2.532e+02	T09	6.881e-04	1.694e-01	6.690e-02
		L15	7.183e-04	1.930e-01	7.622e-02
Th-227	$RaCO_3$	X06	5.019e+00	9.953e-03	3.929e-03
1.139e+03	2.532e+02	T09	4.957e+00	8.435e-03	3.330e-03
		L15	4.662e+00	8.660e-03	3.419e-03
Ra-224	$RaCO_3$	X06	2.451e-01	1.013e-02	3.999e-03
5.938e+03	2.532e+02	T09	2.108e-01	8.759e-03	3.458e-03
		L15	2.294e-01	9.518e-03	3.758e-03

Ac-225	$RaCO_3$	X06	4.639e-01	2.160e-04	8.531e-05
2.147e+03	2.532e+02	T09	7.876e-01	3.668e-04	1.448e-04
		L15	8.573e-01	3.993e-04	1.576e-04

Table 7: Table compiling all of the estimated specific activities and masses of the isotopes produced.